Macrogels, Microgels and Microparticles

Au^{3+}-mediated cross-linking for constructing protein-based materials

Laura M.I. Schijven

Propositions

1. Au^{3+} ions provide a dual functionality to the design of protein-based materials by cross-linking proteins and formation of AuNPs.
   (this thesis)

2. Protein-protein and protein-template interactions determine the final structure of the protein-based materials.
   (this thesis)

3. A uniform scientific writing style will facilitate multidisciplinary collaborations.

4. Fundamental research is as beneficial as applied research.

5. Environmental taxes do not effectively reduce fossil-based emissions.

6. Equality comes with acknowledging differences.

Propositions belonging to the thesis, entitled

"Macrogels, microgels and microparticles: Au^{3+}-mediated cross-linking for constructing protein-based materials"

Laura M.I. Schijven

Wageningen, 5 October 2022

Macrogels, Microgels and Microparticles

Au^{3+}-mediated cross-linking for constructing protein-based materials

Laura M.I. Schijven

Thesis committee

Promotors
Prof. Dr J.H. Bitter
Professor of Biobased Chemistry and Technology
Wageningen University & Research

Prof. Dr A.H. Velders
Professor of BioNanoTechnology
Wageningen University & Research

Co-promotors
Dr C.V. Nikiforidis
Associate professor, Biobased Chemistry and Technology Group
Wageningen University & Research

Dr V Saggiomo
Assistant professor, BioNanoTechnology Group
Wageningen University & Research

Other members
Prof. Dr C.G.P.H. Schroën, Wageningen University & Research
Dr E. Scholten, Wageningen University & Research
Dr J. Paulusse, University of Twente
Dr I. Lykakis, Aristotle University of Thessaloniki, Greece

This research was conducted under the auspices of the Graduate School VLAG (Advanced studies in Food Technology, Agrobiotechnology, Nutrition and Health Sciences).

Macrogels, Microgels and Microparticles

Au^{3+}-mediated cross-linking for constructing protein-based materials

Laura M.I. Schijven

Thesis

submitted in fulfilment of the requirements for the degree of doctor
at Wageningen University
by the authority of the Rector Magnificus,
Prof. Dr A.P.J. Mol,
in the presence of the
Thesis Committee appointed by the Academic Board
to be defended in public
on Wednesday 5 October 2022
at 01:30 p.m. in the Omnia Auditorium.

Laura M.I. Schijven
Macrogels, Microgels and Microparticles: Au^{3+}-mediated cross-linking for constructing protein-based materials
124 pages

PhD thesis, Wageningen University, Wageningen, the Netherlands (2022)
With references, with summary in English

ISBN 978-94-6447-343-8
DOI https://doi.org/10.18174/574604

Macrogels, Microgels and Microparticles

Au^{3+}-mediated cross-linking for constructing protein-based materials

Table of Contents:

Chapter 1

General Introduction

1.1 Polymers

Polymers have a great impact on our daily life, as they are applied as e.g. plastics, elastomers, fibers, protective coatings on surfaces, adhesives.[1] Additionally, polymers are often present in many consumer or industrial formulations, including detergents, pharmaceuticals, and cosmetics.[2] The basic structure of a polymeric consists of a backbone with connected repeating subunits (monomers) and residual side groups. Polymers can be cross-linked through interactions of their residual side groups between neighboring polymers, such as physical and chemical cross-links, and form polymeric networks or gels. Physical cross-links are reversible, non-covalent interactions, such as ionic bonds, hydrogen bonds, and hydrophobic effects. Chemical cross-links are permanent, covalent bonds.[3]

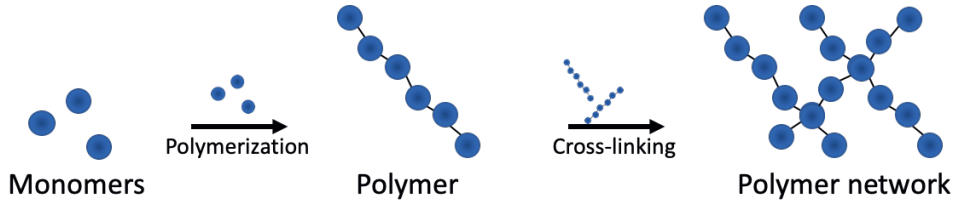

Figure 1.1 Schematic representation of monomers, polymers, and a polymer network. Polymers are made by connecting monomers together and forming long chains. By cross-linking the polymers, a polymer network is formed.

Polymers can be divided into synthetic and biobased categories, based on their source. Synthetic polymers include polyanhydrides, polyamides, polycarbonates, polyesters, and polyurethanes.[4] Synthetic polymers consist of simple fundamental building block units, which have well-known structures and properties.[5] However, their monomers, cross-linking agents, and/or solvents are often derived from non-renewable sources. Accordingly, there is an increased interest to use biobased materials because they are readily available from renewable sources.[6] Examples of biobased polymers are polysaccharides, nucleic acids (polynucleotides), and proteins (polypeptides). Amongst the available biobased materials, this thesis focused on the use of proteins for constructing protein-based materials.

1.2 Protein aggregation and gel network formation

Proteins are versatile biomacromolecules in living organisms and contribute to essential functions (e.g. providing structure to cells, transportation of molecules, catalyzing metabolic reactions and many more) in almost all biological processes.[7] The protein structures are organized in four different levels. The primary structure of proteins is built-up of amino acids, linked through peptide bonds, forming biopolymers. The sequence of amino acids, especially their functional residual groups, is key for the assembly of the specific three-dimensional structure of the protein and determines the protein function.[8] The secondary structures are local folded structures formed within a polypeptide, such as α-helices, β-sheets, turns, loops, and random coils. The tertiary structure is the three-dimensional structure of the polypeptide chain of the protein. A quaternary structure could be formed if a protein consists of multiple polypeptides, which interact with each other. When the stability of the protein

structures decreases, the proteins can unfold and self-assemble into aggregates.[9] At high protein concentrations, the accumulation of aggregates could lead to gel network formation.[10]

In general, protein gel network formation proceeds through several reactions. When proteins are exposed to environmental stresses (e.g. extreme temperatures and pH), their conformational structures could destabilize and convert into partially or totally unfolded states. During the unfolding process, inner reactive amino acids and hydrophobic parts get exposed, which increases attractive forces between neighboring proteins. These intra- and intermolecular interactions induce protein aggregation and eventually form gel networks at sufficient protein concentrations. The protein-protein interactions act as cross-links in the gel network, which could be covalent bonds, hydrogen bond donor-acceptor pairs, or physical entanglements.[11] Typically, studies on protein aggregation and gel network formation focusses on the effects of changes in temperature,[11] protein concentration,[12] pH,[13] ionic strength,[14] pressure,[15] or the addition of chemical[16] or enzymatic[17] cross-linking agents. Depending on the processing conditions, the proteins could form different structural elements with varying dimensions, including strand-like,[18] particulate,[19] and fibrillar aggregates.[20]

Understanding the processes of protein unfolding, aggregation and gel network formation is of major importance in various areas, including biology, medical research and food technology. Controlled protein aggregation in the human body is essential in blood coagulation or inflammatory responses.[21] Uncontrolled protein aggregation, however, is associated with aging processes and a wide variety of neurodegenerative diseases, including Alzheimer's, Amyotrophic Lateral Sclerosis (ALS), Huntington's, Parkinson's, and prion disease.[22, 23] Protein aggregation in food structures is involved in the sensory and textural structures by turning aqueous solutions into soft-solid materials.[24, 25] Yet, the processes of protein unfolding, aggregation and gel network formation are complex and challenging to study by both computational simulations[26, 27] and experimental studies.[28, 29] Properly controlled protein aggregation is not only crucial to prevent and treat aggregation-related diseases, and to structure food products, but also provides opportunities for the development of protein-based materials.

1.3 Protein-based microparticles and microgels

Protein gels can be categorized for their dimensions as macrogels, microgels, and microparticles.[30] Macrogels are defined as bulk network structures with sizes above 100 µm. Microgels and microparticles internally have the same network structure, but have diameters ranging from 10-100 µm, or 0.1-10 µm, respectively. The microgels and microparticles possess properties of both the cross-linked networks (e.g. water-binding, structural integrity) and colloids (e.g. stability, high surface area).[31] Therefore, the micron-sized protein-based materials have attractive functionalities, and their applications range from fat-replacements in food structures,[32] stabilizing oil-in-water emulsions,[33] encapsulants of guest molecules for drug delivery purposes,[34] biosensing,[35] to catalysis.[36] Additionally, proteins consist of different amino acid groups, which contain chemically active sites (e.g. thiol, amine, carboxylic acid groups) for introducing a variety of molecules (e.g. targeting agents).[37-39]

A commonly used method to assemble proteins into microgels or microparticles, is through the use of solid or liquid templates. The proteins can then be cross-linked by interactions of reactive amino acid

side groups of neighboring proteins or the use of chemical/enzymatic cross-linkers, resulting in a protein network inside the templates. In this thesis, hard and droplet reactors templating methods were used to form protein microparticles and microgels, respectively.

1.3.1 Hard templating

Hard templating is based on encapsulating proteins in a sacrificial, solid template, resulting in the formation of an inverse protein MP replica of the template.[40] Different hard templates could be used, including melamine formaldehyde,[41] polystyrene[42] and silica.[43] However, harsh chemicals, e.g. hydrofluoric acid or organic solvents, are required to decompose these templates, which limit their potential use for biological applications. The most popular template is spherical, porous $CaCO_3$, which offers a large inner surface area for encapsulation, is relatively cheap, easy to synthesize, and sacrificial under mild conditions (e.g. chelating agents or under acidic conditions).[44, 45]

Spherical $CaCO_3$ templates, with a size distribution of 4-6 μm and pore sizes of 20-60 nm, can be synthesized through a multistage crystallization pathway.[46] The formation of $CaCO_3$ is initiated through nucleation by mixing supersatured solutions of soluble salts of Ca^{2+} and CO_3^{2-}. The solid nuclei precipitate initially as 100 nm amorphous spherical granules. The crystal formation is terminated when the crystal nuclei aggregate and form single micron-sized polymorph crystal structures, which are in equilibrium with the saturated solution (Figure 1.2).[47]

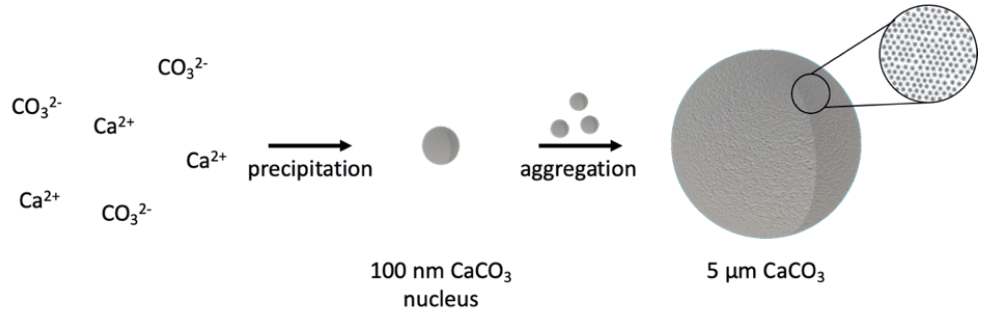

Figure 1.2 Schematic representation of spherical, porous $CaCO_3$. Mixing soluble salts of Ca^{2+} and CO_3^{2-} precipitates as amorphous $CaCO_3$ nuclei. The crystal growth proceeds by aggregation of the $CaCO_3$ nuclei and forms 5 μm spherical $CaCO_3$.

Proteins can be encapsulated into $CaCO_3$ templates via three different routes, including physisorption, infiltration and co-precipitation.[40] For encapsulation through physisorption and infiltration, a protein solution is added to pre-synthesized $CaCO_3$ templates. The proteins adsorb onto the template surface or enter through the pores of the templates by infiltration. Physisorption and infiltration of proteins depend on the $CaCO_3$ pore size, protein size, diffusion, and electrostatic interactions. Co-precipitation is based on capture of the proteins during the $CaCO_3$ synthesis, which allows introducing proteins, independent of their size, into the templates in high amounts in a single step. Additionally, proteins can practically not be released without sacrificing the template.[48] After encapsulation of the proteins into $CaCO_3$ templates, stable protein microparticles could be obtained after cross-linking and selective template removal.

1.3.2 Droplet reactors

Next to the use of solid templates (hard templating), liquid templates could be used as an alternative for the formation of protein microparticles or microgels. A well-known liquid template is liquid biphasic systems, or emulsions, as droplet reactors. Emulsions are transient systems of two immiscible solutions, of which one phase is dispersed (droplet phase) into the other liquid (continuous phase) (Figure 1.3).[49]

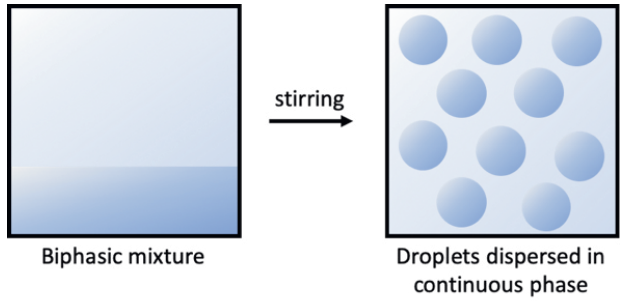

Figure 1.3 Schematic representation of formation of droplets dispersed in a continuous phase by stirring a biphasic mixture.

The liquid biphasic system could act as a template for the fabrication of microgels by compartmentalizing the proteins in the droplet phase. The proteins conserve the shape and size of the droplets by cross-linking. The obtained cross-linked proteins (microgels) can then be separated from the droplet reactors by dialysis and centrifugation.

There are three different systems available for creating liquid biphasic systems, including organic-organic, organic-water, and water-water. Organic-organic biphasic systems can be created by hydrocarbon solvents and polar aprotic solvents due to differences in polarity.[50] Organic-water, or oil-water, biphasic systems phase separate due to differences in hydrophobicity/hydrophilicity.[51] Water-water, or aqueous two-phase systems (ATPSs), are mixtures of immiscible aqueous solutions, containing high concentrations of multiple water-soluble additives, that phase separate above a critical concentration threshold.[52] The use of organic solvents and oil, however, is undesired because they could disrupt the protein structures. For these reasons, the use of ATPS is desired because they do not require organic solvents, and are biocompatible.

1.4 Protein cross-linking through oxidation

To conserve the structures of the proteins assembled in the templates, proteins can be cross-linked. Commonly used methods for protein cross-linking, such as changes in temperature, pH, or using cross-linking agents etc., have been extensively studied and are well-characterized. Protein cross-linking could also occur through oxidation. However, even though it is a common occurring reaction, protein cross-linking through oxidation is much less characterized and the mechanisms are only partly elucidated. The first focus on protein oxidation was in medical research for understanding protein oxidation in aging and the development of diseases.[53] Oxidation of food proteins, however, has only received little attention. This is due to the large and complex structures of proteins, which may lead to

a great number of modifications. Additionally, the impact of protein oxidation on sensory and textural properties of food structures is more subtle compared to lipid oxidation,[54] so its significance has been neglected. Lastly, food is a mixture of proteins, lipids and carbohydrates, of which the oxidation reaction pathways cannot be separated.[55]

Protein cross-linking can be generated through direct and indirect initiated oxidation pathways. Direct oxidation can be initiated by reactive oxygen species, radicals, radiation (X-, γ, UV), or metal ions,[56] and indirect through secondary products of glycan and lipid oxidation.[55] In this thesis, the use of metal ions, specifically Au^{3+} ions, was studied to directly initiate protein oxidation and subsequent cross-linking. In addition, the reduction of Au^{3+} ions by proteins was studied by the formation of gold nanoparticles (AuNPs).

1.4.1 Metal ions for initiating protein oxidation

Metal ions can interact with proteins through binding with metal-coordinating residual amino acid groups, such as thiolates, imidazoles, carboxylic acids, and phosphates. The metal ions are brought into close proximity of potential oxidation targets on proteins, which leads to modifications of diverse residual groups of amino acids. These modified residual groups leads to an increase of attractive forces between residual amino acids groups of neighboring proteins, forming covalent cross-links.[56]

The unique arrangement of amino acids in proteins, in combination with their different susceptibility to oxidation and the large number of formed reaction products, make studying the mechanisms of protein oxidation complex and challenging.[57] Only a few methods are available to detect protein oxidation products, but are limited to detect only a few modifications. The different modifications of amino acids, their reaction products, and detection methods are listed in Table 1.1[56-60]

Table 1.1 Oxidation of residual groups of amino acids and their reaction products and detection methods

Residual group	Amino acid	Reaction product	Detection method
α-carbon	Alanine, isoleucine, leucine, valine, peptide backbones	Carbon-centered radical, hydroperoxides, alcohol groups, carbonyl groups	Electron spin resonance, LC-MS
Amine	Arginine, lysine, proline, threonine	Carbonyl groups (ketones, aldehydes), imines (secondary)	2,4-dinitrophenylhydrazine derivation assay
Aromatic	Phenylalanine, tryptophan	Hydroxy derivatives	LC-MS
Aromatic	Tyrosine	3,4-dihydrophenylalanine, dityrosine	Fluorescence detection
Imidazole	Histidine	2-oxohistidine	LC-MS
Sulfhydryl	Cysteine	Disulfide	5,5'-dithiobis(2-nitrobenzoic acid) assay
Thioether	Methionine	Sulfoxide	LC-MS

Cross-linking of proteins through oxidation is reported in many studies.[57] However, less research is done on directly inducing gel network formation through oxidation. A good understanding of protein

oxidation in this new category of protein cross-linking is therefore needed and could open new paths towards the design of protein gel networks for multiple applications in materials science, such as delivery systems, and coatings.[61]

1.4.2 Au^{3+} reduction and gold nanoparticle synthesis by proteins

Au^{3+} ions were used for cross-linking because of their strong oxidizing properties.[62] Upon protein oxidation, the metal ions are reduced by electron donating residual groups of amino acids (e.g. aspartic acid, phenylalanine, tryptophan, tyrosine).[63, 64] Au^{3+} ions get reduced to Au^{+} and Au^{0}, and can form AuNPs. Neighboring Au^{0} can agglomerate and form small nuclei with Au^{+} ions on their surface. The nuclei grow further due to coalescence, and the Au^{3+} and Au^{+} ions get slowly reduced. Finally, the growth is terminated when the precursor is fully consumed and the nuclei are stabilized by stabilizing agents, resulting in AuNPs (Figure 1.4).[65, 66]

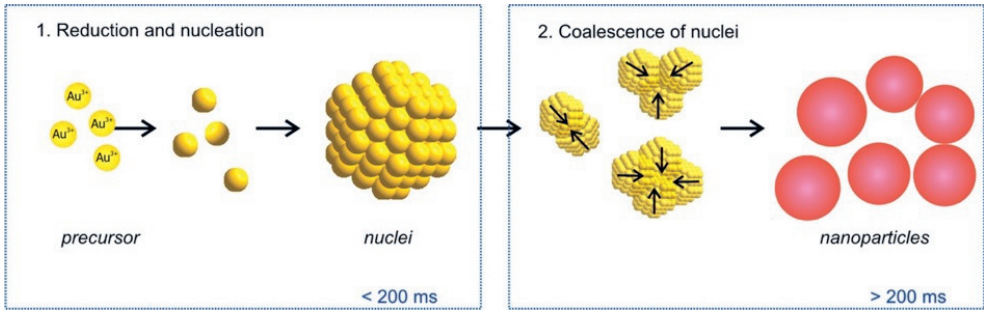

Figure 1.4 Schematic representation of Au^{3+} reduction and AuNPs synthesis. Figure was copied from ref. 66.

AuNPs play a major part in nanotechnology because they exhibit characteristic size-dependent physical and chemical properties compared to their bulk analogs. The electrons on the AuNPs surface interact with a specific light wavelength through localized surface plasmon resonance (LSPR), resulting in strong absorption in the visible and near-infrared regions. The interaction of AuNPs with light is highly dependent on their size, shape, and aggregation state. The optical properties, derived from the LSPR, make AuNPs suitable as optical sensor,[67, 68] and for plasmonic photothermal therapy by selective local heating.[69] AuNPs also provide a high X-ray attenuation coefficient and can be used as an alternative for iodinated agents for X-ray and CT imaging.[70] Other applications include staining in electron microscopy,[71, 72] and catalysis.[73, 74]

For many of the applications, particularly the biological ones, the AuNPs need to be stable against aggregation. Proteins assist in AuNPs synthesis due to the presence of different amino acid groups, which can be involved in reducing and/or stabilizing the AuNPs.[75] Integrating AuNPs in the protein gels prevents further nanoparticle aggregation, while the AuNPs maintain their physical and chemical properties. Therefore, the use of Au^{3+} ions would provide a dual functionality to the design of protein gels, by initiating oxidation and subsequent cross-linking of proteins, and formation of AuNPs, embedded in the gel network.

1.5 Egg yolk high-density lipoprotein

In this thesis, egg yolk high-density lipoprotein (HDL) was mainly used as model protein for the Au^{3+}-initiated gel network formation and AuNPs synthesis. HDL, also known as lipovitellin, is a natural assembly of proteins (75-80%) and lipids (20-25%), and accounts for 36% of the total protein content of egg yolk.[76] HDL has a total molecular size of about 400 kDa and a diameter from 7 to 20 nm. The protein structure is globular-like and contains a funnel-shaped cavity composed by 2 β-sheets with hydrophobic amino acids.[77] The lipids include 65% phospholipids, 30% triglycerides, and 5% cholesterol.[76] The phospholipids interact with the hydrophobic amino acids of the hydrophobic cavity by forming a monolayer. The triglycerides are enclosed in the hydrophobic cavity and phospholipid monolayer. The structure of HDL is shown in Figure 1.5.[78]

Figure 1.5 Cartoon representation of egg yolk HDL monomer structure. Individual α-helices are pink colored, β-strands yellow and turns blue. The structure includes bound lipids, which are depicted as grey spheres. The X-ray crystal structure was imported from the Protein Databank, ref. 78.

Even though HDL is a very abundant protein in the egg yolk, only very few studies have been focused on HDL. HDL has a large, stable structure, which only constitutes of weak inter-protein interactions.[79] Additionally, HDL is poorly soluble in aqueous solutions and requires high ionic strength or extreme alkaline conditions, which limits its potential applications in biological systems. Moreover, HDL is not commercially available and for obtaining HDL, it first needs to be extracted from the hen egg yolk (Figure 1.6).

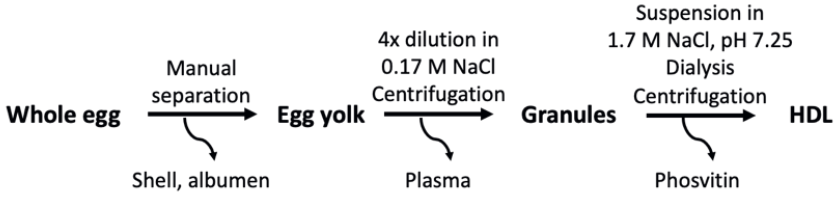

Figure 1.6 General scheme for extraction of HDL from eggs.

Egg yolk is a complex system of non-soluble dense structures (granules) suspended in a clear, yellow, aqueous solution (plasma). Plasma consists of low-density lipoproteins (LDL, 85%), and livetins (15%).[80] The granules are constituted by HDL (70%), phosvitin (16%), and LDL_g (12%). The HDL forms complexes with phosvitin through calcium-phosphate bridges, which make the granules compact and poorly hydrated. The extraction starts with fractionating plasma and granules. The egg yolk is diluted in 0.17 M NaCl and centrifuged to remove the plasma (supernatant).[81] The granules (pellet) are then suspended in 1.71 M NaCl, pH 7.25. The Na^+ disrupts the calcium-phosphate bridges between phosvitin and HDL by replacing the Ca^{2+} ions. HDL can be separated from phosvitin by desalting through dialysis. The HDL precipitates from the granules dispersion and phosvitin remains in the supernatant.[82, 83]

1.6 Motivation and outline of this thesis

The research described in this thesis was focussed on the use of **Au^{3+} ions** for **cross-linking proteins** to construct protein-based materials. Among the protein-based materials, **macrogels, microgels** and **microparticles** were prepared. Therefore, the first part of this thesis is about cross-linking proteins through Au^{3+} initiated oxidation and characterization of the obtained protein gel networks, with embedded **AuNPs**. Subsequently, microparticles and microgels were constructed through the use of solid ($CaCO_3$) and liquid (droplet reactors) templates, and cross-linked through the use of Au^{3+} ions. Additionally, hollow and solid microparticles were obtained through the use of proteins with different structural state (singular, aggregated) in presence of Ca^{2+}. Spherical and urchin-like (branched) microgels were obtained by changing the protein concentration and pH conditions in the ATPS droplet reactor. This thesis consists of 6 chapters, including this introduction (**Chapter 1**), 4 research chapters (**Chapters 2-5**) and a general discussion (**Chapter 6**). By combining the insights of all chapters, we aim to provide a new method of protein cross-linking for the development of protein-based materials.

The general introduction (**Chapter 1**) provides background information on protein gel network formation, constructing protein-based materials, metal initiated protein oxidation and subsequent cross-linking, synthesis of AuNPs by proteins, and the properties and extraction of the model protein egg yolk HDL.

In **Chapter 2**, an alternative method to conventional processing methods (changes in temperature, pH, or using cross-linking agents etc.) for the formation of protein gel networks is presented. Instead, Au^{3+} ions were used. The transition of protein dispersions from a liquid to a soft gel, after the addition of Au^{3+} ions, was investigated, and egg yolk HDL was used as a model protein. The Au^{3+} ions have strong oxidizing properties, which can modify a variety of residual groups of amino acids. The modifications lead to an increase of attractive forces between residual amino acids groups of neighboring proteins, forming covalent cross-links. After the protein gel network formation, the Au^{3+} ions were reduced and formed AuNPs. Different Au^{3+}/HDL ratios and temperature conditions were tested for the protein gel network formation. The obtained protein gel networks, containing AuNPs, were characterized by confocal laser scanning microscopy (CLSM), rheology, and UV-Vis absorbance spectroscopy and compared with a heat-set HDL gel. The Au^{3+} reduction and AuNPs formation was followed by UV-Vis absorbance. The modifications of amino acid were investigated studied by Fourier-Transform Infrared spectroscopy, gel electrophoresis and fluorescence spectroscopy.

In **Chapter 3**, the Au^{3+} initiated redox reaction for protein gel network formation, as described in **Chapter 2**, was applied inside spherical, porous $CaCO_3$ templates for the formation of hollow protein microparticles, with embedded AuNPs. Egg yolk HDL was encapsulated into the $CaCO_3$ templates through co-precipitation with $CaCl_2$ and Na_2CO_3 solutions. However, instead of a uniform distribution, HDL accumulated at the edges of the $CaCO_3$ templates. To keep the hollow microparticles structures intact, Au^{3+} ions were added to initiate protein cross-linking, followed by template removal. As a control, no cross-linking agents were used, while removing the template. The obtained hollow non-cross-linked (HDL-microparticles) and Au^{3+} initiated cross-linked (Au-HDL-microparticles) were characterized with CLSM, Transmission (TEM) and Scanning Electron Microscopy (SEM), Atomic Force Microscopy (AFM), and Dynamic Light Scattering (DLS).

Chapter 4 followed-up on the formation of protein microparticles by the research described in **Chapter 3**. Now, different proteins (β-lactoglobulin (β-lac), Bovine Serum Albumin (BSA), casein, and HDL) were used to obtain solid and hollow core protein microparticles. When proteins (β-lac, BSA) were soluble in presence of $CaCl_2$ and Na_2CO_3, the proteins uniformly distribute inside the $CaCO_3$ templates. However, when proteins (casein, HDL) form aggregates in presence of $CaCl_2$, the proteins accumulate at the template edges. After encapsulation, the proteins were cross-linked through the Au^{3+} initiated redox reaction, which stabilized the spherical solid and hollow structures, and formed AuNPs embedded in their structures.

In **Chapter 5**, the Au^{3+} initiated redox reaction for protein gel network formation, as described in **Chapter 2**, was applied inside an ATPS of polyethylene glycol (PEG) and Na_2SO_4. HDL was compartmentalized in the Na_2SO_4-rich phase of the ATPS. For the formation of protein microgels, the proteins were cross-linked through the Au^{3+} initiated redox reaction. The Au^{3+} ions were added as an aqueous solution, which could create a concentration gradient between the PEG-rich and Na_2SO_4-rich phases. A concentration gradient could result in migration of the components in the ATPS, which allows formation of branches on the droplet phases. Different reaction conditions, such as protein concentration and pH, were studied for the formation of the protein microgels. After cross-linking, random protein aggregates, and urchin-like and spherical microgels were obtained. The different protein-based materials were characterized with brightfield, fluorescence microscopy, CLSM, and SEM.

In **Chapter 6**, a general discussion on the use of Au^{3+} ions for cross-linking proteins to construct protein-based materials is provided. The experimental findings, implications, limitations and opportunities derived from the 4 experimental chapters are discussed. Suggestions for follow-up research projects are given and an overall conclusion is provided.

References

1. C.S. Brazel and S.L. Rosen, *Fundamental principles of polymeric materials*. 2012: John Wiley & Sons.
2. S.T. Knox and N.J. Warren, Enabling technologies in polymer synthesis: accessing a new design space for advanced polymer materials, *Reaction Chemistry & Engineering*, 2020, **5**, 3, 405-423.
3. S. Seiffert and J. Sprakel, Physical chemistry of supramolecular polymer networks, *Chemical Society Reviews*, 2012, **41**, 2, 909-930.
4. R. Song, M. Murphy, C. Li, K. Ting, C. Soo, and Z. Zheng, Current development of biodegradable polymeric materials for biomedical applications, *Drug design, development and therapy*, 2018, **12**, 3117.
5. M.I. Sabir, X. Xu, and L. Li, A review on biodegradable polymeric materials for bone tissue engineering applications, *Journal of materials science*, 2009, **44**, 21, 5713-5724.
6. E. Campos, J. Branquinho, A.S. Carreira, A. Carvalho, P. Coimbra, P. Ferreira, and M. Gil, Designing polymeric microparticles for biomedical and industrial applications, *European Polymer Journal*, 2013, **49**, 8, 2005-2021.
7. J.D. Watson, R.A. Laskowski, and J.M. Thornton, Predicting protein function from sequence and structural data, *Current opinion in structural biology*, 2005, **15**, 3, 275-284.
8. J. Berg, J. Tymoczko, and L. Stryer, *Protein composition and structure. Biochemistry*. 2012, WH Freeman and Company.
9. J.A. Housmans, G. Wu, J. Schymkowitz, and F. Rousseau, A guide to studying protein aggregation, *The FEBS journal*, 2021.
10. T. Nicolai and D. Durand, Protein aggregation and gel formation studied with scattering methods and computer simulations, *Current Opinion in Colloid & Interface Science*, 2007, **12**, 1, 23-28.
11. D. Durand, J.C. Gimel, and T. Nicolai, Aggregation, gelation and phase separation of heat denatured globular proteins, *Physica A: Statistical Mechanics and its Applications*, 2002, **304**, 1-2, 253-265.
12. G.V. Barnett, W. Qi, S. Amin, E.N. Lewis, and C.J. Roberts, Aggregate structure, morphology and the effect of aggregation mechanisms on viscosity at elevated protein concentrations, *Biophysical chemistry*, 2015, **207**, 21-29.
13. A. Kharlamova, C. Chassenieux, and T. Nicolai, Acid-induced gelation of whey protein aggregates: Kinetics, gel structure and rheological properties, *Food Hydrocolloids*, 2018, **81**, 263-272.
14. K. Ako, T. Nicolai, and D. Durand, Salt-induced gelation of globular protein aggregates: structure and kinetics, *Biomacromolecules*, 2010, **11**, 4, 864-871.
15. F. Speroni, V. Beaumal, M. de Lamballerie, M. Anton, M. Añón, and M. Puppo, Gelation of soybean proteins induced by sequential high-pressure and thermal treatments, *Food Hydrocolloids*, 2009, **23**, 5, 1433-1442.
16. A. Sinz, Chemical cross-linking and mass spectrometry to map three-dimensional protein structures and protein–protein interactions, *Mass spectrometry reviews*, 2006, **25**, 4, 663-682.
17. J. Buchert, D. Ercili Cura, H. Ma, C. Gasparetti, E. Monogioudi, G. Faccio, M. Mattinen, H. Boer, R. Partanen, and E. Selinheimo, Crosslinking food proteins for improved functionality, *Annual review of food science and technology*, 2010, **1**, 113-138.
18. L.M. Sagis, C. Veerman, R. Ganzevles, M. Ramaekers, S.G. Bolder, and E. van der Linden, Mesoscopic structure and viscoelastic properties of β-lactoglobulin gels at low pH and low ionic strength, *Food Hydrocolloids*, 2002, **16**, 3, 207-213.
19. T. Farjami and A. Madadlou, An overview on preparation of emulsion-filled gels and emulsion particulate gels, *Trends in Food Science & Technology*, 2019, **86**, 85-94.
20. Y. Cao and R. Mezzenga, Food protein amyloid fibrils: Origin, structure, formation, characterization, applications and health implications, *Advances in colloid and interface science*, 2019, **269**, 334-356.
21. M.F. Gebbink, B. Bouma, C. Maas, and B.N. Bouma, Physiological responses to protein aggregates: fibrinolysis, coagulation and inflammation (new roles for old factors), *FEBS letters*, 2009, **583**, 16, 2691-2699.
22. A. Aguzzi and T. O'connor, Protein aggregation diseases: pathogenicity and therapeutic perspectives, *Nature reviews Drug discovery*, 2010, **9**, 3, 237-248.

23. S. Ahmadi, S. Zhu, R. Sharma, D.J. Wilson, and H.-B. Kraatz, Interaction of metal ions with tau protein. The case for a metal-mediated tau aggregation, *Journal of inorganic biochemistry*, 2019, **194**, 44-51.
24. T. Nicolai and D. Durand, Controlled food protein aggregation for new functionality, *Current Opinion in Colloid & Interface Science*, 2013, **18**, 4, 249-256.
25. T. Nicolai, Gelation of food protein-protein mixtures, *Advances in colloid and interface science*, 2019, **270**, 147-164.
26. A. Morriss-Andrews and J.-E. Shea, Computational studies of protein aggregation: methods and applications, *Annual review of physical chemistry*, 2015, **66**, 643-666.
27. T. Cellmer, D. Bratko, J.M. Prausnitz, and H.W. Blanch, Protein aggregation in silico, *Trends in biotechnology*, 2007, **25**, 6, 254-261.
28. W.S. Gosal and S.B. Ross-Murphy, Globular protein gelation, *Current Opinion in Colloid & Interface Science*, 2000, **5**, 3-4, 188-194.
29. D. Hamann, *Rheology: a tool for understanding thermally induced protein gelation*. 1991, ACS Publications.
30. E. Battista, F. Causa, and P.A. Netti, Bioengineering microgels and hydrogel microparticles for sensing biomolecular targets, *Gels*, 2017, **3**, 2, 20.
31. J.K. Oh, R. Drumright, D.J. Siegwart, and K. Matyjaszewski, The development of microgels/nanogels for drug delivery applications, *Progress in polymer science*, 2008, **33**, 4, 448-477.
32. N. Purwanti, J.P. Peters, and A.J. van der Goot, Protein micro-structuring as a tool to texturize protein foods, *Food & function*, 2013, **4**, 2, 277-282.
33. S. Sridharan, M.B. Meinders, J.H. Bitter, and C.V. Nikiforidis, On the emulsifying properties of self-assembled pea protein particles, *Langmuir*, 2020, **36**, 41, 12221-12229.
34. M. Lengyel, N. Kállai-Szabó, V. Antal, A.J. Laki, and I. Antal, Microparticles, microspheres, and microcapsules for advanced drug delivery, *Scientia Pharmaceutica*, 2019, **87**, 3, 20.
35. R. Zhou, L. Zhao, Y. Wang, S. Hameed, J. Ping, L. Xie, and Y. Ying, Recent advances in food-derived nanomaterials applied to biosensing, *TrAC Trends in Analytical Chemistry*, 2020, **127**, 115884.
36. Y. Yu, E. Jung, H.J. Kim, A. Cho, J. Kim, T. Yu, and J. Lee, Protein particles decorated with Pd nanoparticles for the catalytic reduction of p-nitrophenol to p-aminophenol, *ACS Applied Nano Materials*, 2020, **3**, 10, 10487-10496.
37. L. Schoonen and J.C. van Hest, Functionalization of protein-based nanocages for drug delivery applications, *Nanoscale*, 2014, **6**, 13, 7124-7141.
38. R. Van Vught, R.J. Pieters, and E. Breukink, Site-specific functionalization of proteins and their applications to therapeutic antibodies, *Computational and structural biotechnology journal*, 2014, **9**, 14, e201402001.
39. S.J. Spa, M.M. Welling, M.N. van Oosterom, D.D. Rietbergen, M.C. Burgmans, W. Verboom, J. Huskens, T. Buckle, and F.W. van Leeuwen, A supramolecular approach for liver radioembolization, *Theranostics*, 2018, **8**, 9, 2377.
40. D. Volodkin, CaCO3 templated micro-beads and-capsules for bioapplications, *Advances in colloid and interface science*, 2014, **207**, 306-324.
41. C. Gao, S. Moya, H. Lichtenfeld, A. Casoli, H. Fiedler, E. Donath, and H. Möhwald, The decomposition process of melamine formaldehyde cores: the key step in the fabrication of ultrathin polyelectrolyte multilayer capsules, *Macromolecular Materials and Engineering*, 2001, **286**, 6, 355-361.
42. C. Schüler and F. Caruso, Decomposable hollow biopolymer-based capsules, *Biomacromolecules*, 2001, **2**, 3, 921-926.
43. Y. Wang, A. Yu, and F. Caruso, Nanoporous polyelectrolyte spheres prepared by sequentially coating sacrificial mesoporous silica spheres, *Angewandte Chemie International Edition*, 2005, **44**, 19, 2888-2892.
44. N.S. Singer and J.M. Dunn, Protein microparticulation: the principle and the process, *Journal of the American College of Nutrition*, 1990, **9**, 4, 388-397.
45. D.V. Volodkin, R. von Klitzing, and H. Möhwald, Pure protein microspheres by calcium carbonate templating, *Angewandte Chemie*, 2010, **122**, 48, 9444-9447.

46. D.V. Volodkin, N.I. Larionova, and G.B. Sukhorukov, Protein encapsulation via porous CaCO3 microparticles templating, *Biomacromolecules*, 2004, **5**, 5, 1962-1972.
47. D.V. Volodkin, S. Schmidt, P. Fernandes, N.I. Larionova, G.B. Sukhorukov, C. Duschl, H. Möhwald, and R. von Klitzing, One-Step Formulation of Protein Microparticles with Tailored Properties: Hard Templating at Soft Conditions, *Advanced Functional Materials*, 2012, **22**, 9, 1914-1922.
48. A.I. Petrov, D.V. Volodkin, and G.B. Sukhorukov, Protein—calcium carbonate coprecipitation: a tool for protein encapsulation, *Biotechnology progress*, 2005, **21**, 3, 918-925.
49. B. Aldemir Dikici and F. Claeyssens, Basic principles of emulsion templating and its use as an emerging manufacturing method of tissue engineering scaffolds, *Frontiers in Bioengineering and Biotechnology*, 2020, 875.
50. N.R. Cameron, High internal phase emulsion templating as a route to well-defined porous polymers, *Polymer*, 2005, **46**, 5, 1439-1449.
51. F. Ushikubo and R. Cunha, Stability mechanisms of liquid water-in-oil emulsions, *Food Hydrocolloids*, 2014, **34**, 145-153.
52. J.F. Pereira and J.A. Coutinho, *Aqueous two-phase systems*, in *Liquid-phase extraction*. 2020, Elsevier. p. 157-182.
53. E.R. Stadtman, Protein oxidation in aging and age-related diseases, *Annals of the new York Academy of Sciences*, 2001, **928**, 1, 22-38.
54. T. Waraho, D.J. McClements, and E.A. Decker, Mechanisms of lipid oxidation in food dispersions, *Trends in food science & technology*, 2011, **22**, 1, 3-13.
55. M. Hellwig, Analysis of protein oxidation in food and feed products, *Journal of Agricultural and Food Chemistry*, 2020, **68**, 46, 12870-12885.
56. E.R. Stadtman, Metal ion-catalyzed oxidation of proteins: biochemical mechanism and biological consequences, *Free Radical Biology and Medicine*, 1990, **9**, 4, 315-325.
57. M. Lund and C. Baron, *Protein oxidation in foods and food quality*, in *Chemical deterioration and physical instability of food and beverages*. 2010, Elsevier. p. 33-69.
58. E. Stadtman and R. Levine, Free radical-mediated oxidation of free amino acids and amino acid residues in proteins, *Amino acids*, 2003, **25**, 3, 207-218.
59. L. Su, T. Shu, J. Wang, Z. Zhang, and X. Zhang, Hidden dityrosine residues in protein-protected gold nanoclusters, *The Journal of Physical Chemistry C*, 2015, **119**, 21, 12065-12070.
60. D. Malencik and S. Anderson, Dityrosine as a product of oxidative stress and fluorescent probe, *Amino acids*, 2003, **25**, 3-4, 233-247.
61. L. Chen, G.E. Remondetto, and M. Subirade, Food protein-based materials as nutraceutical delivery systems, *Trends in Food Science & Technology*, 2006, **17**, 5, 272-283.
62. C. Gabbiani, A. Casini, and L. Messori, Gold (III) compounds as anticancer drugs, *Gold Bulletin*, 2007, **40**, 1, 73-81.
63. Y.N. Tan, J.Y. Lee, and D.I. Wang, Uncovering the design rules for peptide synthesis of metal nanoparticles, *Journal of the American Chemical Society*, 2010, **132**, 16, 5677-5686.
64. J.J. Warren, J.R. Winkler, and H.B. Gray, Redox properties of tyrosine and related molecules, *FEBS letters*, 2012, **586**, 5, 596-602.
65. M. Wuithschick, A. Birnbaum, S. Witte, M. Sztucki, U. Vainio, N. Pinna, K. Rademann, F. Emmerling, R. Kraehnert, and J.r. Polte, Turkevich in new robes: key questions answered for the most common gold nanoparticle synthesis, *ACS nano*, 2015, **9**, 7, 7052-7071.
66. J. Polte, R. Erler, A.F. Thunemann, S. Sokolov, T.T. Ahner, K. Rademann, F. Emmerling, and R. Kraehnert, Nucleation and growth of gold nanoparticles studied via in situ small angle X-ray scattering at millisecond time resolution, *ACS nano*, 2010, **4**, 2, 1076-1082.
67. R. De La Rica and A.H. Velders, Supramolecular Au Nanoparticle Assemblies as Optical Probes for Enzyme-Linked Immunoassays, *Small*, 2011, **7**, 1, 66-69.
68. R. de laRica, R.M. Fratila, A. Szarpak, J. Huskens, and A.H. Velders, Multivalent nanoparticle networks as ultrasensitive enzyme sensors, *Angewandte Chemie International Edition*, 2011, **50**, 25, 5704-5707.

69. X. Huang, P.K. Jain, I.H. El-Sayed, and M.A. El-Sayed, Plasmonic photothermal therapy (PPTT) using gold nanoparticles, *Lasers in medical science*, 2008, **23**, 3, 217.
70. J. Hainfeld, D. Slatkin, T. Focella, and H. Smilowitz, Gold nanoparticles: a new X-ray contrast agent, *The British journal of radiology*, 2006, **79**, 939, 248-253.
71. J. Roth, The silver anniversary of gold: 25 years of the colloidal gold marker system for immunocytochemistry and histochemistry, *Histochemistry and cell biology*, 1996, **106**, 1, 1-8.
72. W.P. Faulk and G.M. Taylor, Communication to the editors: an immunocolloid method for the electron microscope, *Immunochemistry*, 1971, **8**, 11, 1081-1083.
73. F. van der Klis, L. Gootjes, N.H. Verstijnen, J. van Haveren, D.S. van Es, and J.H. Bitter, Carbohydrate structure–activity relations of Au-catalysed base-free oxidations: gold displaying a platinum lustre, *RSC advances*, 2022, **12**, 15, 8918-8923.
74. N. Masoud, B. Donoeva, and P.E. de Jongh, Stability of gold nanocatalysts supported on mesoporous silica for the oxidation of 5-hydroxymethyl furfural to furan-2, 5-dicarboxylic acid, *Applied Catalysis A: General*, 2018, **561**, 150-157.
75. C.D. De Souza, B.R. Nogueira, and M.E.C. Rostelato, Review of the methodologies used in the synthesis gold nanoparticles by chemical reduction, *Journal of Alloys and Compounds*, 2019, **798**, 714-740.
76. R.W. Burley and W. Cook, Isolation and composition of avian egg yolk granules and their constituent α-and β-lipovitellins, *Canadian journal of biochemistry and physiology*, 1961, **39**, 8, 1295-1307.
77. T. Anderson, D. Levitt, and L. Banaszak, The structural basis of lipid interactions in lipovitellin, a soluble lipoprotein, *Structure*, 1998, **6**, 7, 895-909.
78. J.R. Thompson and L.J. Banaszak, Lipid− protein interactions in lipovitellin, *Biochemistry*, 2002, **41**, 30, 9398-9409.
79. V. Kiosseoglou and A. Paraskevopoulou, Molecular interactions in gels prepared with egg yolk and its fractions, *Food Hydrocolloids*, 2005, **19**, 3, 527-532.
80. M. Anton, Egg yolk: structures, functionalities and processes, *Journal of the Science of Food and Agriculture*, 2013, **93**, 12, 2871-2880.
81. A. Laca, B. Paredes, M. Rendueles, and M. Díaz, Egg yolk granules: Separation, characteristics and applications in food industry, *LWT-Food Science and Technology*, 2014, **59**, 1, 1-5.
82. J. Ren and J. Wu, Preparation of high purity egg phosvitin using anion exchange chromatography, *Food chemistry*, 2014, **158**, 186-191.
83. M. Chalamaiah, Y. Esparza, H. Hong, F. Temelli, and J. Wu, Physicochemical and functional properties of leftover egg yolk granules after phosvitin extraction, *Food chemistry*, 2018, **268**, 369-377.

Chapter 2

Au^{3+}-induced gel network formation of proteins

This chapter has been published as: L.M.I. Schijven, V. Saggiomo, A.H. Velders, J.H. Bitter, C.V. Nikiforidis (2021). Au $^{3+}$-Induced gel network formation of proteins. *Soft Matter*, *17*(42), 9682-9688. https://doi.org/10.1039/D1SM01031J

Abstract

The formation of protein networks in aqueous systems is a result of intermolecular interactions after an energy input, like heating. In this research, we report that a redox reaction between Au^{3+} ions and proteins can also lead to the formation of a protein gel network. Amino acids, like cysteine and tyrosine, get oxidized and form covalent bonds with neighboring protein molecules, while Au^{3+} ions get reduced to Au^{+} and Au^{0}, and nucleate and form gold nanoparticles (AuNPs). The protein gel network formation occurs within 2 h at room temperature and can be tuned by varying Au^{3+}/protein ratio and accelerated by increasing the incubation temperature. The proposed Au^{3+}-induced gel network formation was applied to different proteins, like egg yolk high-density lipoprotein (HDL), bovine serum albumin (BSA) and whey protein (WPI). This research opens new insights for the investigation of the metal-protein interactions and may aid in the design of novel hybrid-soft nanocomposite materials.

2.1 Introduction

Protein-protein interactions in aqueous systems can lead to the formation of a three-dimensional gel network, leading to soft gel structures. The most common technique to induce protein-protein interactions is by heating the system over the denaturation point of the proteins, resulting in their (partial) unfolding.[1, 2] Unfolded proteins expose residual functional groups of amino acids, such as polar, non-polar and thiol groups, and hydrogen bond donor-acceptor pairs, which leads to an increase of attractive forces between amino acids of neighboring proteins, bond formation and subsequently to a three-dimensional network.[3, 4]

Interactions between amino acids can also be induced with the use of metal ions. Metal ions, such as Cu^{2+} and $Fe^{2+/3+}$ can oxidize thiol- or amino-containing side groups of amino acids (e.g. cysteine, methionine, histidine)[5] leading to di-amino acid covalent bonding.[6, 7]

In this research, we aimed to take advantage of the interactions of metal ions with amino acids, and use it to create covalent bonds between proteins in aqueous solutions. In this way, we can develop a new technique to create protein gel networks. For that, we have used Au^{3+} ions, which have strong oxidizing properties.[8] Additionally, it has been reported that several available amino acid groups (e.g. tryptophan, tyrosine, aspartic acid, or phenylalanine)[9, 10] can act as reduction sites of Au^{3+} and synthesize gold nanoparticles (AuNPs).[11, 12] AuNPs are more stable forms than Au^{3+} ions[13] and their formation limits the protein oxidation rate. On top of that, AuNPs have unique chemical and physical properties, e.g. localized surface plasmon resonance (LSPR), and are attractive contrast agents for medical applications since they can be visualized with different techniques.[14-16] Most of the studies have focused on proteins in solution as reducing and stabilizing agents for AuNPs synthesis.[17-19] The use of Au^{3+} ions for covalently cross-linking protein and protein gel network formation, however, has not been reported before.

The interactions between Au^{3+} ions and proteins for the formation of protein gel networks were studied, using egg yolk high-density lipoprotein (HDL), a rather inactive lipoprotein. First, different Au^{3+}/HDL ratios were tested for the formation of a protein gel network. The formed gel networks were characterized by confocal laser scanning microscopy (CLSM), rheology and UV-Vis. The reduced Au^{3+} formed AuNPs and their formation was followed in time by UV-Vis. Additionally, the temperature influence on the gel network and AuNPs formation were studied. The interactions between the amino acids and Au^{3+} ions, which could be involved in the gel network formation were studied by Fourier-Transform Infrared spectroscopy (FTIR), gel electrophoresis and fluorescence spectroscopy. Finally, the Au^{3+}-induced gel network formation was also successfully applied to two other proteins, namely bovine serum albumin (BSA) and whey protein isolate (WPI).

In this work, we investigated the formation of protein gel networks through the addition of Au^{3+} ions (Scheme 2.1). Our research reveals that Au^{3+} ions rapidly coordinate to the proteins and upon reduction of the Au^{3+} ions, AuNPs are formed and the proteins are covalently cross-linked through oxidation. This research can open new paths towards the design of controlled protein gel networks for multiple applications in materials science. Even inactive proteins, like HDL can be used, while the ability

to incorporate AuNPs in protein gel networks provides dual functionality to the design, since it can be further used for advanced biosensing and catalysis.

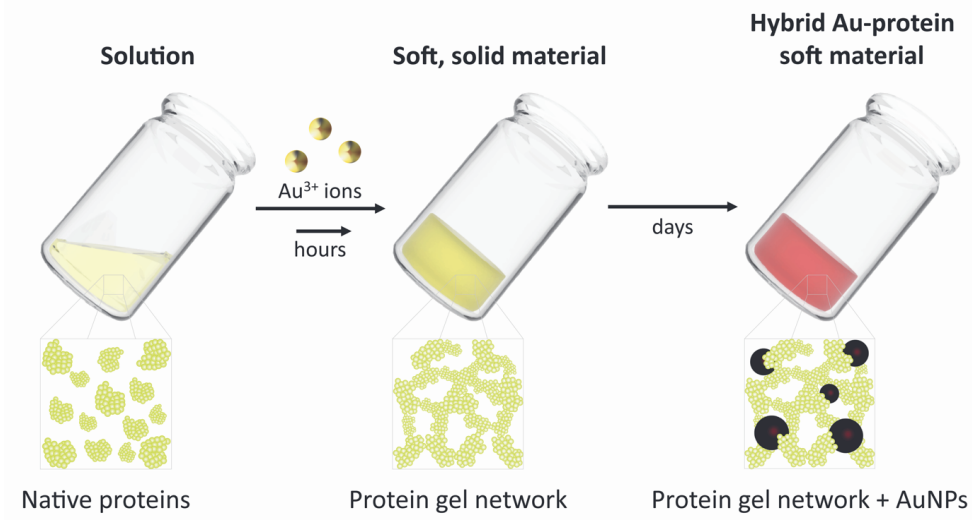

Scheme 2.1 Schematic representation of the process from dispersion of native proteins to gel network formation through addition of Au^{3+} ions. Subsequently, Au^{3+} ions get reduced to Au^{0} after which Au^{0} nucleates and forms AuNPs to result in a hybrid Au-protein soft, solid material.

2.2 Results and Discussion

2.2.1 Au-HDL interactions and gel network formation

HDL is a globular-like protein with a proximate protein composition of 83.3 wt.%.[20]

Au^{3+} ions were added as a solution at pH 7 to a saline, aqueous dispersion of HDL (with a final concentration of 3.0% (w/v) at different molar ratios). Between 10 and 100 molar equivalents of Au^{3+} to HDL, it was observed that HDL aggregated and precipitated. At 150 molar equivalents of Au^{3+}, the viscosity of the HDL solution increased instantly, while after storage of 24 h, a homogeneous, soft-solid material was formed. For 250 molar equivalents of Au^{3+}, a soft-solid gel was formed 2 h after addition into the solution. These findings indicate extensive interactions of Au^{3+} with HDL, even at room temperature, which subsequently lead to the formation of an HDL network. Without the presence of Au^{3+}, HDL was rather inactive and did not form a network.

2.2.2 Properties of Au-HDL gel networks

The transition of the HDL dispersions from a liquid to a soft gel due to the addition of 250 molar equivalents of Au^{3+} was qualitatively assessed by a vial tilting method. The initial HDL dispersion appeared translucent, yellow-colored, and flowed when the vial was tilted. When the Au^{3+} ions were added, the dispersion became cloudy, but the sample was still flowing. After 2 h, the sample appeared yellow, opaque and did not flow anymore (Figure 2.1 A). The cloudiness, that was observed directly

after the addition of Au^{3+}, indicates that the protein-protein interactions and the formation of aggregates started instantly. However, an extensive gel network was only formed after 2 h.

The microstructure of the formed Au-HDL gel network was imaged by CLSM (Figure 2.1 B). In the image, a high contrast difference between the Fast Green FCF stained protein (green colored) and background (black pores) was observed. The addition of Au^{3+} of HDL resulted in the formation of a uniformly packed, dense protein network.

Besides the visual observation, the network formation of the Au-HDL mixture was quantitatively investigated by applying a controlled shear stress test (Figure 2.1 C). To simulate the behavior of the Au-HDL mixture at rest, a very low shear was applied. During the first seconds of the measurement, the graph of the loss modulus (G", viscous-like behavior) was above the storage modulus (G', solid-like behavior) graph, indicating that the mixture had a viscous response. Within seconds, a cross-over was observed, where G' was significantly higher than G". The cross-over indicates stronger interactions in the system, which induced the formation of a soft gel structure. When 2 h passed after the addition of Au^{3+} ions, the formed soft-solid structure was reaching an equilibrium since the G' and G" didn't significantly change after that point. This finding corresponds to the visual observation that during tilting the dispersion was not flowing. At the point of 2 h, the loss factor (tan δ = G"/G') was found at 0.1, which directly shows that the material exhibited more solid-like than liquid-like properties.

The Au^{3+}-induced gelation method was compared to urea- and heat-induced gelation methods. It was found that a rather concentrated HDL solution was required (>10% (w/v)) for urea-induced gelation of HDL. Urea destabilizes hydrophobic interactions and hydrogen bonds in proteins and forms disulfide bonds by cysteine oxidation.[21] For the Au^{3+}-induced gelation, a concentration of 3.0% (w/v) was sufficient to form a gel network, which suggests that stronger protein-protein interactions were involved than in urea-induced gelation.

When the heat-induced gelation was applied to HDL, a white, opaque gel was formed (Figure 2.1 A'). The microstructure of the heat-set gel appeared irregular and contained more pores (Figure 2.1 B'). This suggests that there were fewer inter-protein connections in the heat-set HDL gel. The heat-set HDL gel was also applied to a shear stress test. During heating, the G'>G" cross-over was found at T = 75 °C, where HDL starts to unfold.[3] After 1 h of heating, the gel reached an equilibrium (Figure 2.1 C'). Due to its rigid, globular structure, HDL is less sensitive to heat and the protein unfoldment requires a lot of energy.[3] While cooling down the gel, the G' and G" decreased and the loss factor increased, indicating that the gel became more liquid-like. For the Au^{3+}-induced gelation, this phenomenon was not observed because the protein-protein interactions remained stable after the formation of the protein gel network. This confirms that the heat-set HDL gel is constituted of weak protein-protein interactions compared to the Au-HDL gel.

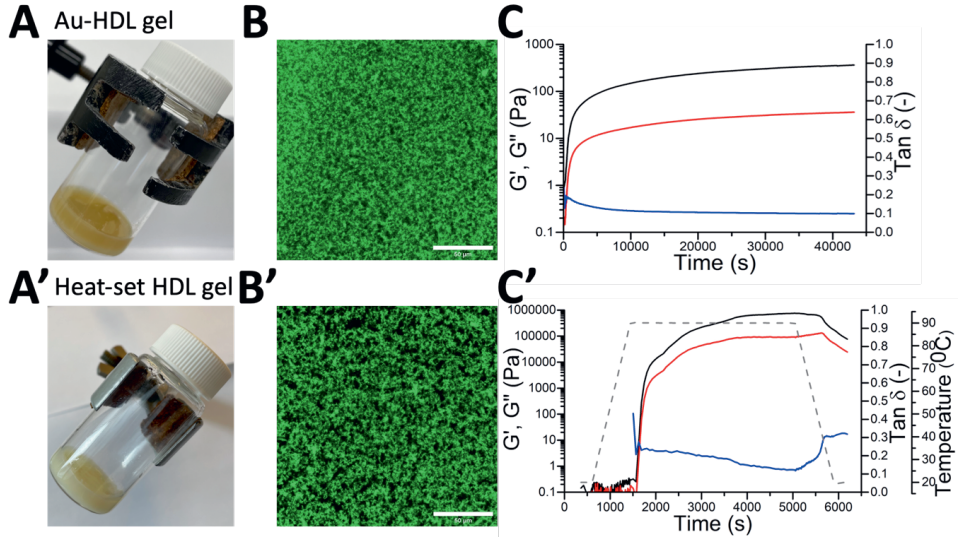

Figure 2.1 Pictures of tilted vials containing (A) Au-HDL gel network (3.0% (w/v), 250 equivalents of Au^{3+}) after 2 h of preparation and (A') heat-set HDL gel (3.0% (w/v) after heating at T = 90 °C for 1 h. CLSM image of (B) Au-HDL gel network after 1 day of preparation and (B') heat-set HDL gel. The gels were stained with Fast Green FCF, scale bars are 50 μm. Time-dependent function of storage modulus (G', black line), loss modulus (G", red line), and loss tangent (tan δ, blue line) of the (C) Au-HDL gel network formation and (C') heat-set HDL gel during heating at T = 90 °C for 1 h (grey dashed line).

2.2.3 AuNPs formation

24 h after the preparation of the Au-HDL network, the soft material gradually changed color from dark yellow to red (Figure 2.2 A). It was hypothesized that the red color of the Au-HDL network originates from the characteristic LSPR absorption of formed AuNPs, which can be found in the absorption region of λ = 500-600 nm.[22] The gradual color change of the Au-HDL soft material was followed by UV-Vis absorbance at λ = 300-800 nm for 7 days (Figure 2.2 B). Two days after preparation of the Au-HDL mixture, a small band was observed in the region of λ = 500-600 nm, confirming the formation of AuNPs. The intensity of this LSPR peak further increased in time, which corresponds to the formation and growth of AuNPs.[23] To confirm the presence of AuNPs, TEM was used by taking images of a mixture of Au-HDL at low concentrations (0.1% (w/v)) to observe the AuNPs. In the image, AuNPs of different sizes were observed (Figure S2.1). These findings indicate that Au^{3+} ions not only induce the formation of a protein network, but the HDL also reduces the Au^{3+} ions and synthesizes AuNPs. Compared to proteins in solution, the synthesis of AuNPs requires a longer reaction time, after HDL gel network formation. This could be due to the rigid protein structure of HDL in the gel network, causing steric hindrance, which slows down the reaction with Au^{3+} ions. Next to the reducing properties, HDL stabilizes the AuNPs through steric stabilization effects, adsorption to the surface and by coordinating Au^{3+} to numerous functional amino acid groups (e.g. amine and carboxylate groups). Therefore, it was suggested that the AuNPs are embedded in the protein gel network and could not be recovered.

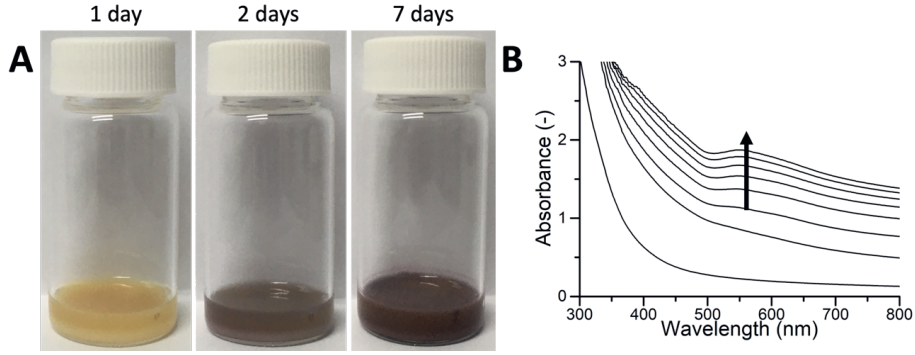

Figure 2.2 Pictures of vials containing Au-HDL gel networks after 1, 2 and 7 days of preparation. The soft material turned from dark yellow (1 day) to dark red (2 and 7 days). (B) Solid UV-Vis absorbance spectra of Au-HDL gel network followed in time from 0-7 days. The characteristic LSPR peak of AuNPs increased in time, as indicated by the arrow.

2.2.4 Influence of temperature on network and AuNPs formation

The Au^{3+}-induced gel network and subsequent AuNPs formation were observed and investigated at room temperature. However, it was expected that heating could accelerate the interactions of HDL with Au^{3+} ions. Accordingly, the Au-HDL mixtures were incubated at different temperatures (T = 4, 20, 40, and 60 °C) and monitored for 5 h using UV-Vis at λ = 300-800 nm (Figure 2.3). For samples incubated at T = 4 and 20 °C, there was no red color visually observed within 5 h and the LSPR peaks were absent (Figure 2.3 A,B,E). Moderately heating the Au-HDL mixture at T = 40 °C resulted in the appearance of a slight red color of the mixture and the LSPR peak after 4 h (Figure 2.3 C,E). Heating at T = 60 °C resulted in the appearance of a red color of the mixture and the LSPR in the spectra after 1 h (Figure 2.3 D,E). Increasing the temperature resulted in notably higher reaction rates, which resulted in a shorter reaction time of AuNPs formation.

Regardless of the incubation temperature, the UV-Vis absorption bands increased in time. This increase is caused by scattering of the light, which is known as optical density (OD). When proteins form aggregates, the light is more scattered compared to dispersed, single proteins ($OD_{aggregates} > OD_{proteins}$). When a dense gel network is formed, the light scatters even more ($OD_{gel} > OD_{aggregates}$).[24] It was hypothesized that the gel network formation can be followed by an increase in OD, which corresponds to the unfolding, formation of aggregates and finally gel networks. Accordingly, the network formation process was characterized by plotting the OD against time. The OD was taken at λ = 400 nm, where there was no inherent absorption of the HDL and AuNPs (Figure 2.3 F). For the Au-HDL mixture incubated at T = 20 °C, which is known to form a soft gel, the OD_{400} gradually increased during the first 2 h and stabilized around 1.0. This result is complementary to the results obtained with the vial tilting method and shear stress test, indicating that the increase in OD_{400} is related to the gel network formation. When the Au-HDL mixture was incubated at T = 4 °C, the OD_{400} also increases gradually up to 1.0. Moderately heating the Au-HDL mixture at T = 40 °C resulted in an increase of the OD_{400} to 1.0 within 15 minutes, which then stabilized. Incubation of the Au-HDL mixture at T = 60 °C resulted in increase of OD_{400} to 1.3, which then further increased. Those results indicate that Au^{3+} ions

induce protein-protein interactions not only at room temperature but also at T = 4 °C and when incubated at higher temperatures. Comparing the OD_{400} values for spectra of the Au-HDL mixtures incubated at T = 4-40 °C, the OD_{400} values were stable for 5 h. Based on that result, we hypothesize that the network formation is completed at OD_{400} = 1.0 and it is expected that OD_{400} values for the Au-HDL mixtures incubated at T = 4 and 20 °C would still increase after 5 h because of the AuNPs formation and growth. When incubating the Au-HDL mixture at T = 60 °C, the OD_{400} further increased to 2.0. This increase was assigned to the contribution of LSPR absorbance due to the AuNPs formation. As a control, HDL solutions (in the absence of Au^{3+}) were incubated at T = 4-60 °C and the OD_{400} values were measured for 5 h (Figure S2.2 A). No observable differences between spectra were found within 5 h, indicating that HDL doesn't unfold while moderately heating and the increase in OD_{400} is only attributed to Au^{3+} induced gel network formation.

When heating the HDL solution at T = 80 °C, the OD_{400} started to increase after 30 min and further increased in time till OD_{400} = 1.8 (Figure S2.2 A). In the rheology experiment of the heat-set HDL gel, it was observed that HDL starts to unfold above T = 75 °C.[3] For this reason, the influence of heat-induced gelation on the Au^{3+}-induced gelation was investigated by incubating the Au-HDL mixture at T = 80 °C. A red color of the sample was already visually observed after 15 min together with the appearance of the LSPR peak (Figure S2.2 B,C). The OD_{400} value for the Au-HDL mixture heated at T = 80 °C was significantly higher than for the Au-HDL mixtures incubated at T = 4-60 °C (Figure S2.2 D). This could be assigned to the combination of the unfolding of HDL by heating, the Au^{3+}-induced network formation and the AuNPs formation.

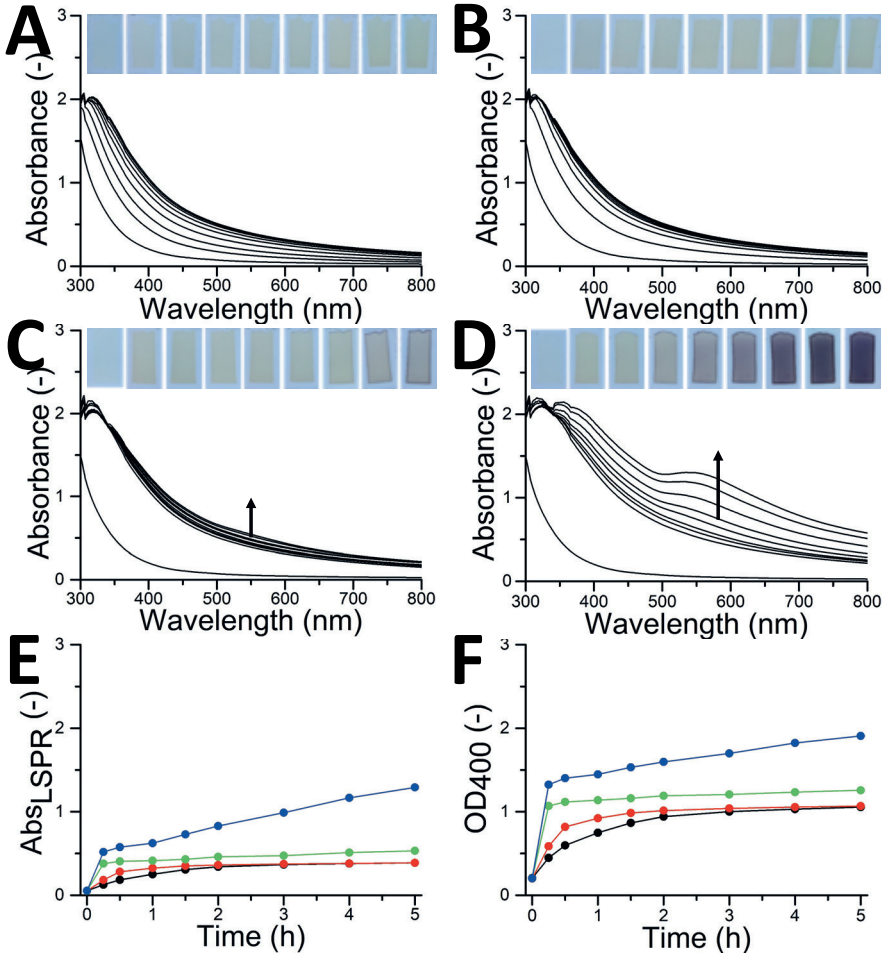

Figure 2.3 (A-D) (A-D) Solid UV-Vis absorbance and (E) derived LSPR absorbance (at λ = 555 nm) and (F) OD400 spectra of Au-HDL gel networks incubated at T = (A) 4 °C (black dotted line), (B) 20 °C (red dotted line), (C) 40 °C (green dotted line) and (D) 60 °C (blue dotted line) followed for 5 h. (insets) optical photographs showing gradual color change of the Au-HDL mixtures at different time intervals.

2.2.5 Nature of Au-HDL interactions

To investigate which amino acids of HDL interact with Au^{3+} ions and contribute to the protein-protein interactions, FTIR spectra of HDL and the Au-HDL gel network were measured (Figure S2.3). The pattern of group vibrations of HDL corresponds to a typical FTIR spectrum of lipoproteins.[25] The FTIR spectra of HDL and the Au-HDL network were very similar, however, the absorbance of the band at region 2260-2010 cm^{-1}, corresponding to SH stretching vibrations, was decreased after the addition of Au^{3+} ions. The decrease of free SH groups could indicate that cysteine is oxidized by Au^{3+} and forms disulfide bonds[26, 27] or forms Au-S bonds.

To further investigate whether other bonds than disulfide bonds are responsible for the protein-protein interactions and subsequent network formation, Au-HDL fractions were qualitatively analyzed using an SDS electropherogram (Figure S2.4). Aliquots of the Au-HDL mixture were taken at different time frames and were dispersed into β-mercaptoethanol solutions. The β-mercaptoethanol reduces the disulfide bonds and allows to investigate their role in the protein-protein network. SDS-PAGE separation of native HDL revealed five major bands, ranging in molecular weight from 28 to 110 kDa (lane 2).[20] After the addition of Au^{3+} ions to the HDL, the pattern in the gel electropherogram remained unchanged (lane 3). Further extending the reaction time to 10 minutes (lane 4), larger protein bands were observed (> 185 kDa), while the smaller bands (28-75 kDa) decreased in intensity. The β-mercaptoethanol breaks down the disulfide bridges, however, there were still large protein fragments present in lane 4-12. This indicates that there are other types of bonds present in the protein network, probably of covalent nature. It was expected that those covalent bonds are derived from other oxidized amino acid groups, such as tyrosine.

Tyrosine exhibits strong reducing properties[9] and in order to evaluate the effect of Au^{3+} on tyrosine of HDL, the physical-chemical properties of HDL and Au-HDL were investigated. Oxidation of tyrosine results in the formation of tyrosine-tyrosine cross-linking (dityrosine) (Figure 2.4 A).[28] Dityrosine has characteristic fluorescent properties with excitation at λ_{ex} = 325 nm and emission at λ_{em} = 410 nm.[28] When the fluorescent spectra of the HDL and Au-HDL mixtures were measured, no dityrosine fluorescence was detected (Figure S2.5). This could be caused by the spectral overlap of the absorbance of Au^{3+} with the excitation band of the dityrosine, known as the inner filter effect (Figure S2.6 A).[28] It has to be noted that the absorption at λ = 280 nm decreased in a period of 0-5 h, due to Au^{3+} complexation and reduction. Extraction of Au^{3+} is required to avoid possible interferences or quenching of the dityrosine fluorescence. Therefore, KCN was added to Au-HDL to form an Au(CN) complex.[29] As a control, KCN was added to HDL. It was observed that the absorbance and excitation spectra of HDL were unaffected by the KCN treatment, indicating that the KCN does not damage the tertiary HDL structure (Figure S2.6). After Au^{3+} extraction of the Au-HDL mixture, the absorbance at λ = 280 nm was decreased because of the formation of the $Au(CN)_2^-$ complex, which exhibits no absorbance (Figure S2.6 A'). When measuring the fluorescent properties of the Au-HDL mixtures after KCN treatment, an excitation peak at λ = 328 nm and emission peak at λ = 400 nm were observed (Figure 2.4 B,C). Those peaks were not observed for native HDL before and after addition of KCN (Figure S2.5, S2.6). The intensity of those peaks further increased in time and stabilized after 1.5 h. Those results confirm that the addition of Au^{3+} to HDL results in the formation of dityrosine, which can lead to the formation of extensive, stable inter- and intra-protein cross-linkages.[6]

However, to further verify the binding of Au^{3+} to other amino acids in the Au-HDL system, more research needs to be done, e.g. combination studies of X-ray crystallography, isotope labeling NMR and mass spectrometry.[30-33]

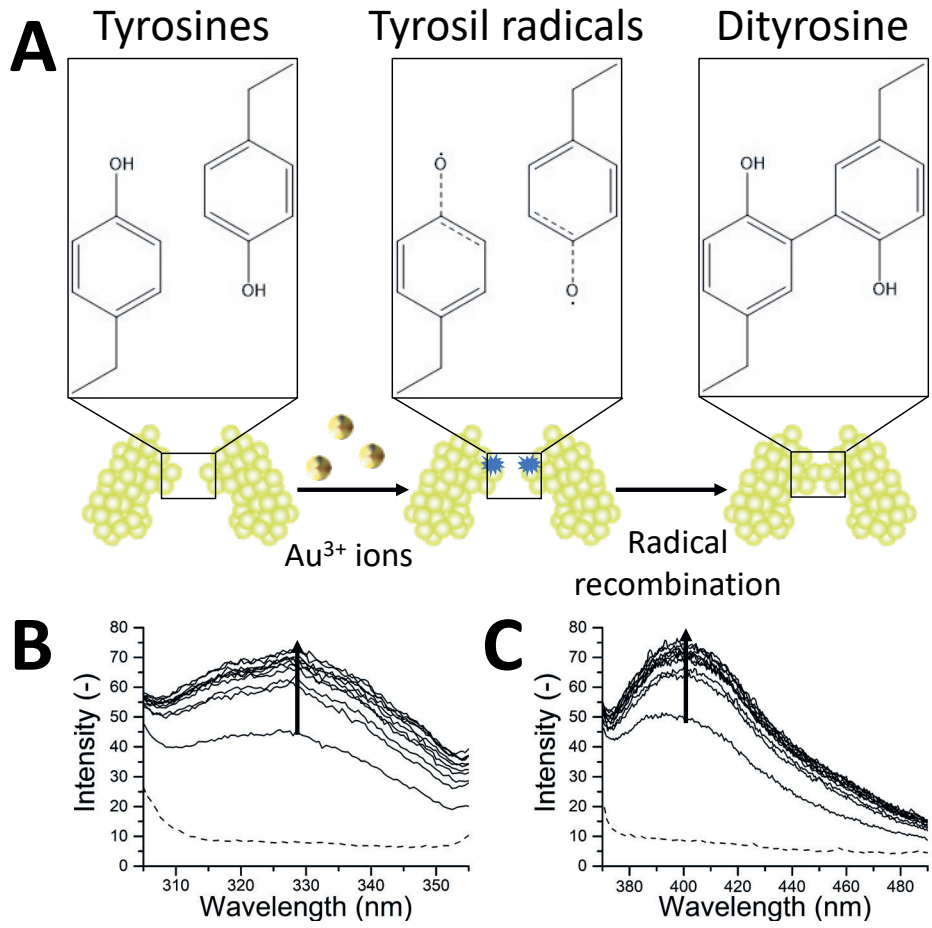

Figure 2.4 (A) Scheme of dityrosine cross-linking between neighboring proteins. Fluorescence (B) excitation (λ_{em} = 410 nm) and (C) emission (λ_{ex} = 325 nm) spectra of 0.01% (w/v) HDL (dashed line) and Au-HDL mixture (solid line) in 1.71 M NaCl after KCN treatment at different time intervals (0-5 h, every 30 minutes). The arrow indicates the increase in intensity in time.

2.2.6 Interactions of Au^{3+} ions with other proteins

To investigate whether Au^{3+} ions could induce network formation of other globular proteins, the same method as for HDL was applied to BSA and WPI, (a mixture of α- and β-lactalbumin, β-lactoglobulin, BSA and immunoglobulin).[34] After the addition of Au^{3+} ions to BSA and WPI, a red color and LSPR peaks were observed after 2 days (Figure S2.7 A,B). This was also observed for HDL, which suggested that the AuNPs formation is not affected by the protein source and potentially the same amino acids are involved in Au^{3+} reduction. However, after the addition of Au^{3+} ions to BSA, the mixture remained liquid-like for 2 days and formed a soft-solid material only after 7 days, which was also observed in the OD_{400} graph (Figure S2.7 C). The Au-WPI mixture started to form a soft material after 1 day. Based on those results, we found that Au^{3+} ions could induce network formation for different protein sources,

but the reaction times and potentially the mechanism differed. More research needs to be done for studying the Au^{3+}-induced gelation for different protein systems.

2.3 Conclusion

In summary, we have demonstrated that a redox reaction can take place between Au^{3+} and proteins, inducing protein-protein interactions and a subsequent gel protein network. The Au^{3+}-induced protein network formation does not require additional heating and even occurs at T = 4 °C. The network formation in time was revealed by vial tilting, rheology and OD measurements. The results show that Au^{3+} induced network was faster as opposed to the heat-induced gelation of proteins. The interactions between Au^{3+} ions and amino acids, responsible for the Au-HDL network formation, were further characterized by FTIR, SDS- PAGE, UV-Vis absorbance, and fluorescence spectroscopy, showing that there were cross-links between cysteine and tyrosine. For 2 days, there was no Au^{3+} reduction, and only then it starts forming AuNPs. The network formation can be further tuned by parameters, such as Au^{3+}/protein ratio, protein source and temperature. The Au^{3+}-induced protein-protein interactions provide new insights into protein network formation and may aid for the design and construction of novel hybrid-soft nanocomposite materials.

2.4 Experimental section

2.4.1 Materials

Fresh hen eggs were purchased from a local organic farm De Hoge Born, Wageningen, the Netherlands. Sodium chloride (NaCl, ≥99.5%), 1 M NaOH solution and potassium cyanide (KCN, ≥97%) were purchased from VWR international B.V. Gold(III) chloride hydrate ($HAuCl_4 \cdot xH_2O$, 99.5%), Fast green FCF fluorescent dye (≥85%) and 76 mm dialysis tubing cellulose membrane (MWCO = 14 kDa) were purchased from Sigma Aldrich. LDS sample buffer, a 10-250 kDa pre-stained PageRuler protein ladder, pre-casted NuPAGE 4-12% Bis-Tris gels, 20x MOPS SDS running buffer and Coomassie R-250 staining solution were purchased from ThermoFisher Scientific. Glacial acetic acid (100%) was purchased from Biosolve B.V. Methanol (99.98%) was purchased from LPS. All chemicals were used without further purification and deionized water was used throughout the experiments.

2.4.2 Methods

Extraction of HDL

HDL was extracted from egg yolk according to the method of Castellani et al. (2006),[35] with slight modifications. Hen eggs were cracked and the egg yolks were separated manually from the albumen. The egg yolks were carefully rolled on a paper tissue to remove the chalazae and adhering albumen. The yolk membranes were then punctured, using a glass pipette, and their contents were collected and pooled in a beaker cooled in iced water. The liquid yolks were diluted with three volumes of 0.17 M NaCl (1% (w/v)) and homogenized by stirring for 1 h. The yolk was fractionated into plasma and granules by centrifugation at 10,000 x g for 45 minutes at 4 °C, using a Thermoscientific Sorvall Legend XFR centrifuge. The pellet (granules) was washed with 0.17 M NaCl and centrifuged once more. The granules were suspended in 1.71 M NaCl (10% (w/v)) and the solution's pH was adjusted to 7.25, using 1 M NaOH. The mixtures were collected in dialysis tubings and were dialyzed against deionized water with 3 changes over 24 h. The HDLs were precipitated. The content of the dialysis tubings were collected and centrifuged. The pellets, rich in HDL, were collected and freeze-dried, using a Salmenkipp alpha 2-4 plus freeze-dryer at a temperature of -76 °C and pressure of 0.0090 mbar for 72 h.

Preparation of Au-HDL gel networks

In a typical experiment, HDL was prepared as a homogeneous 6% (w/v) solution by dissolving 60 mg of HDL (0.14 μmol, mw_{HDL} = 422,480 kDa)[36] in 1 mL of 1.71 M NaCl in a 20 mL glass vial. Au^{3+} solutions, of 10, 100, 150, 200 and 250 molar equivalents to HDL, were prepared by using a 0.1 M $HAuCl_4$ stock solution. For this, 14, 71, 142, 213, 284 and 355 μL of Au stock solution was added to 500 μL of 1.71 M NaCl. The pH of the Au solutions was adjusted to 7, using a 1 M NaOH solution. The total, final volume of the Au^{3+} solutions was kept constant at 1 mL. The Au^{3+} solutions were rapidly injected into the HDL solutions to have a final HDL concentration of 3.0% (w/v).

2.4.3 Characterization

Protein content

The crude protein content was determined by Dumas (Thermo Quest NA 2100 Nitrogen and Protein Analyser) using a protein-to-nitrogen conversion factor of 6.25.

Confocal laser scanning microscopy (CLSM)

The microstructure of the Au-HDL gel was analyzed using a Leica SP8-SMD CLSM. The HDL solution was first incubated 30 minutes with 10 μL of 1.2 mM Fast Green FCF. Then, a 3.0 wt.% Au-HDL mixture was prepared as described above 1 day before imaging. The sample was cut and transferred onto a flat glass slide before imaging. The Fast Green FCF was excited at λ = 633 nm, using a 63x objective. The images were processed using FIJI Is Just ImageJ software.[37]

Rheological properties

Rheological measurements of the Au-HDL and heat-set HDL gel were done on an Anton-Paar® 302 rheometer, using rotational parallel-plate devices, using a shear-stress amplitude of 0.1% and frequency of 1 Hz. For the heat-set gel, the HDL solution was heated to T = 90 °C, kept constant for 1 h and cooled down to T = 20 °C (heat and cool rate = 5 °C/min).

Transmission electron microscopy (TEM)

TEM sample preparation was done by pipetting 5 μL of 0.1 wt.% Au-HDL sample onto a carbon-coated hexagonal 400 mesh copper grid. After one minute, a filter paper was used to remove excess fluid. After air drying, the sample was imaged using a JEOL JEM1400+ microscope and the images were analyzed with FIJI software.

UV-Vis spectrophotometric measurements

A Hitachi U-2010 UV-Visible spectrophotometer was used to measure UV-Visible absorbance spectra. 3.0 wt.% HDL solutions and Au-HDL mixtures were injected rapidly into 1 mm glass cuvettes and incubated at 4 °C (in the fridge), 20 °C (room temperature) or 40-80 °C (using a water bath). The samples were monitored at λ = 300-800 nm for 5 h, 1.71 M NaCl was used as a reference. The Au-HDL mixture incubated at room temperature was also monitored for 7 days.

For the investigation on dityrosine formation, 3 mL solutions of 0.01 wt.% HDL and Au-HDL mixtures were prepared in 10 mm quartz cuvettes and measured from λ = 250-800 nm. The solutions were also treated with KCN for the investigating the effect on HDL and to extract the gold. Therefore, 10 μL of 174 μM KCN solution (11.6 mg/mL, 1.7 nmol, 10 molar equivalents against Au^{3+}) was added to the HDL solution and Au-HDL mixture. After 1 h of exposure to air, the samples were measured again.

Fluorescence spectroscopy measurements

Fluorescence spectroscopy measurements were done on an Agilent Cary Eclipse Fluorescence Spectrophotometer, using 10 mm quartz cuvettes. Excitation spectra were measured from λ = 250-390 nm with λ_{em} = 410 nm, emission spectra were measured from λ = 350-500 nm with λ_{ex} = 325 nm, slits were set at 5 nm. The HDL solution and Au-HDL mixture with and without KCN treatment were prepared as described for the UV-Vis spectrophotometric measurements.

Fourier-transform infrared spectroscopy (FTIR)

The FTIR of HDL and Au-HDL were measured using a Tensor 27 Fourier transform spectrophotometer. Interferograms were accumulated over the spectral range 4000-500 cm^{-1} with a resolution of 4 cm^{-1}.

For each measurement, 11 scans were taken. The samples were freeze-dried prior to the measurement, prepared in KBr pellets and measured at ambient conditions.

Qualitative analysis of Au-HDL gels using electrophoresis

Denaturing SDS-PAGE gel electrophoresis was done to qualitatively analyze the protein content in the Au-HDL gel in time, according to the manufacturer's protocol. A 6.0 wt.% HDL stock solution was prepared in 1.71 M NaCl. The HDL stock solution was divided over 11 microcentrifuge tubes, 33.3 μL each. To 10 microcentrifuge tubes, 33.3 μL of Au^{3+} solution (of 250 molar equivalents) was added. The mixtures were allowed to incubate for a specific time period (0-240 minutes). After each time period, 0.5 mL of LDS sample buffer was added to the reaction mixture and mixed for 15 minutes. Then, 0.5 mL of sample buffer, containing 20% glycerol and 4% β-mercaptoethanol was added to the same reaction mixture. The total concentration of protein in each sample was 1 mg/mL. The samples were heated at 100 °C for 5 minutes and kept in the freezer till loading. 8 μL of a pre-stained PageRuler protein ladder (10-250 kDa) and 20 μL of each sample was loaded into wells of a pre-casted NuPAGE 4-12% Bis-Tris gel. The gel was fixed in a ThermoFisher Scientific mini gel tank. After filling the gel tank with 1x MOPS SDS running buffer, the electrophoresis was run at 200 V for 1 h. After removing the gel from the tank, the gel was washed with deionized water and gently shaken in Coomassie R-250 staining solution for 1 h. The gel was finally de-stained in a solution containing 30% of methanol and 10% of glacial acetic acid in deionized water.

References

1. Nicolai, T., Gelation of food protein-protein mixtures, *Advances in colloid and interface science*, 2019, **270**, 147-164.
2. Durand, D., Gimel, J.C., and Nicolai, T., Aggregation, gelation and phase separation of heat denatured globular proteins, *Physica A: Statistical Mechanics and its Applications*, 2002, **304**, 1-2, 253-265.
3. Kiosseoglou, V. and Paraskevopoulou, A., Molecular interactions in gels prepared with egg yolk and its fractions, *Food Hydrocolloids*, 2005, **19**, 3, 527-532.
4. Cordobés, F., Partal, P., and Guerrero, A., Rheology and microstructure of heat-induced egg yolk gels, *Rheologica Acta*, 2004, **43**, 2, 184-195.
5. Shacter, E., Quantification and significance of protein oxidation in biological samples, *Drug metabolism reviews*, 2000, **32**, 3-4, 307-326.
6. Zhang, W., Xiao, S., and Ahn, D.U., Protein oxidation: basic principles and implications for meat quality, *Critical reviews in food science and nutrition*, 2013, **53**, 11, 1191-1201.
7. Bradshaw, A., Salt, M., Bell, A., Zeitler, M., Litra, N., and Smith, A.M., Cross-linking by protein oxidation in the rapidly setting gel-based glues of slugs, *Journal of Experimental Biology*, 2011, **214**, 10, 1699-1706.
8. Gabbiani, C., Casini, A., and Messori, L., Gold (III) compounds as anticancer drugs, *Gold Bulletin*, 2007, **40**, 1, 73-81.
9. Tan, Y.N., Lee, J.Y., and Wang, D.I., Uncovering the design rules for peptide synthesis of metal nanoparticles, *Journal of the American Chemical Society*, 2010, **132**, 16, 5677-5686.
10. Warren, J.J., Winkler, J.R., and Gray, H.B., Redox properties of tyrosine and related molecules, *FEBS letters*, 2012, **586**, 5, 596-602.
11. Chevrier, D.M., Chatt, A., and Zhang, P., Properties and applications of protein-stabilized fluorescent gold nanoclusters: short review, *Journal of Nanophotonics*, 2012, **6**, 1, 064504.
12. Xie, J., Zheng, Y., and Ying, J.Y., Protein-directed synthesis of highly fluorescent gold nanoclusters, *Journal of the American Chemical Society*, 2009, **131**, 3, 888-889.
13. Zhao, P., Li, N., and Astruc, D., State of the art in gold nanoparticle synthesis, *Coordination Chemistry Reviews*, 2013, **257**, 3-4, 638-665.
14. De La Rica, R. and Velders, A.H., Supramolecular Au Nanoparticle Assemblies as Optical Probes for Enzyme-Linked Immunoassays, *Small*, 2011, **7**, 1, 66-69.
15. de laRica, R., Fratila, R.M., Szarpak, A., Huskens, J., and Velders, A.H., Multivalent nanoparticle networks as ultrasensitive enzyme sensors, *Angewandte Chemie International Edition*, 2011, **50**, 25, 5704-5707.
16. Hainfeld, J., Slatkin, D., Focella, T., and Smilowitz, H., Gold nanoparticles: a new X-ray contrast agent, *The British journal of radiology*, 2006, **79**, 939, 248-253.
17. Annadhasan, M., Muthukumarasamyvel, T., Sankar Babu, V., and Rajendiran, N., Green synthesized silver and gold nanoparticles for colorimetric detection of Hg2+, Pb2+, and Mn2+ in aqueous medium, *ACS Sustainable Chemistry & Engineering*, 2014, **2**, 4, 887-896.
18. Kawasaki, H., Hamaguchi, K., Osaka, I., and Arakawa, R., ph-Dependent synthesis of pepsin-mediated gold nanoclusters with blue green and red fluorescent emission, *Advanced Functional Materials*, 2011, **21**, 18, 3508-3515.
19. Xie, J., Lee, J.Y., and Wang, D.I., Synthesis of single-crystalline gold nanoplates in aqueous solutions through biomineralization by serum albumin protein, *The Journal of Physical Chemistry C*, 2007, **111**, 28, 10226-10232.
20. Anton, M., *High-density lipoproteins (HDL) or lipovitellin fraction*, in *Bioactive egg compounds*. 2007, Springer. p. 13-16.
21. Totosaus, A., Montejano, J.G., Salazar, J.A., and Guerrero, I., A review of physical and chemical protein-gel induction, *International journal of food science & technology*, 2002, **37**, 6, 589-601.
22. Wei, H., Wang, Z., Zhang, J., House, S., Gao, Y.-G., Yang, L., Robinson, H., Tan, L.H., Xing, H., and Hou, C., Time-dependent, protein-directed growth of gold nanoparticles within a single crystal of lysozyme, *Nature nanotechnology*, 2011, **6**, 2, 93.

23. ten Hove, J.B., Schijven, L.M., Wang, J., and Velders, A.H., Size-controlled and water-soluble gold nanoparticles using UV-induced ligand exchange and phase transfer, *Chemical communications*, 2018, **54**, 95, 13355-13358.
24. Mleko, S., Effect of protein concentration on whey protein gels obtained by a two-stage heating process, *European Food Research and Technology*, 1999, **209**, 6, 389-392.
25. Krilov, D., Balarin, M., Kosović, M., Gamulin, O., and Brnjas-Kraljević, J., FT-IR spectroscopy of lipoproteins—a comparative study, *Spectrochimica Acta Part A: Molecular and Biomolecular Spectroscopy*, 2009, **73**, 4, 701-706.
26. Glišić, B.Đ., Rychlewska, U., and Djuran, M.I., Reactions and structural characterization of gold (III) complexes with amino acids, peptides and proteins, *Dalton Transactions*, 2012, **41**, 23, 6887-6901.
27. Le, H., Ting, L., Jun, C., and Weng, W., Gelling properties of myofibrillar protein from abalone (Haliotis Discus Hannai Ino) muscle, *International Journal of Food Properties*, 2018, **21**, 1, 277-288.
28. Malencik, D. and Anderson, S., Dityrosine as a product of oxidative stress and fluorescent probe, *Amino acids*, 2003, **25**, 3-4, 233-247.
29. Wang, X.-B., Wang, Y.-L., Yang, J., Xing, X.-P., Li, J., and Wang, L.-S., Evidence of significant covalent bonding in Au (CN) 2−, *Journal of the American Chemical Society*, 2009, **131**, 45, 16368-16370.
30. Loreto, D., Ferraro, G., and Merlino, A., Protein-metallodrugs interactions: Effects on the overall protein structure and characterization of Au, Ru and Pt binding sites, *International Journal of Biological Macromolecules*, 2020, **163**, 970-976.
31. Marcon, G., Messori, L., Orioli, P., Cinellu, M.A., and Minghetti, G., Reactions of gold (III) complexes with serum albumin, *European journal of biochemistry*, 2003, **270**, 23, 4655-4661.
32. Messori, L. and Merlino, A., Cisplatin binding to proteins: a structural perspective, *Coordination Chemistry Reviews*, 2016, **315**, 67-89.
33. Pratesi, A., Cirri, D., Fregona, D., Ferraro, G., Giorgio, A., Merlino, A., and Messori, L., Structural Characterization of a Gold/Serum Albumin Complex, *Inorganic chemistry*, 2019, **58**, 16, 10616-10619.
34. Butré, C.I., Wierenga, P.A., and Gruppen, H., Influence of water availability on the enzymatic hydrolysis of proteins, *Process Biochemistry*, 2014, **49**, 11, 1903-1912.
35. Castellani, O., Belhomme, C., David-Briand, E., Guérin-Dubiard, C., and Anton, M., Oil-in-water emulsion properties and interfacial characteristics of hen egg yolk phosvitin, *Food Hydrocolloids*, 2006, **20**, 1, 35-43.
36. Ohlendorf, D.H., Wrenn, R.F., and Banaszak, L.J., Three-dimensional structure of the lipovitellin–phosvitin complex from amphibian oocytes, *Nature*, 1978, **272**, 5648, 28-32.
37. Schindelin, J., Arganda-Carreras, I., Frise, E., Kaynig, V., Longair, M., Pietzsch, T., Preibisch, S., Rueden, C., Saalfeld, S., and Schmid, B., Fiji: an open-source platform for biological-image analysis, *Nature methods*, 2012, **9**, 7, 676-682.

2.5 Supporting Information

Au^{3+} reduction by HDL

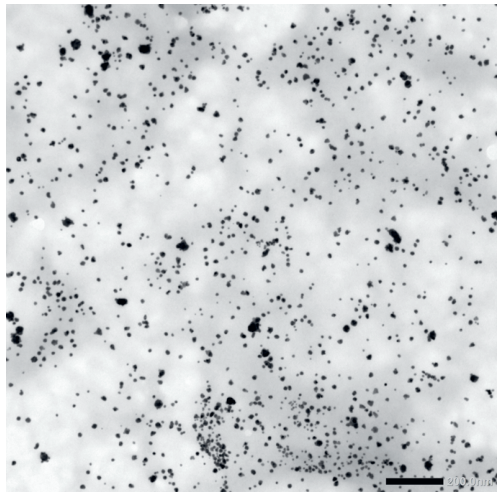

Figure S2.1 TEM image of Au-HDL mixture (0.1% (w/v)) after 3 days of preparation. Scale bar is 200 nm.

Influence of temperature

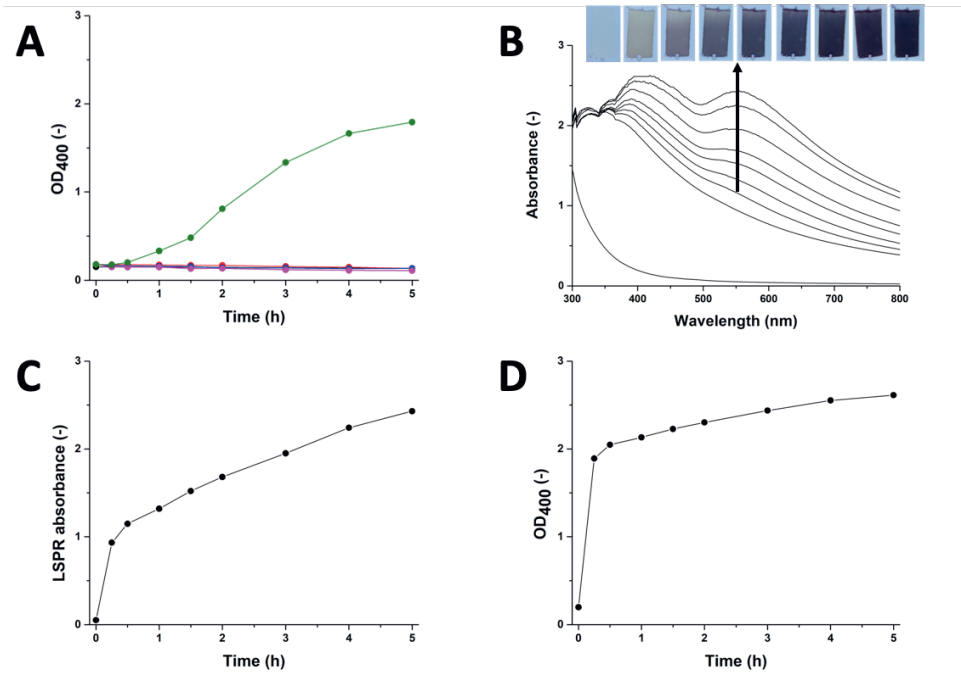

Figure S2.2 (A) Time-dependent OD_{400} plots of 3.0% (w/v) HDL solutions in 1.71 M NaCl incubated at T = 4 °C (black dotted line), 20 °C (red dotted line), 40 °C (blue dotted line), 60 °C (magenta dotted line) and 80 °C (olive dotted line). (B) Solid UV-Vis absorbance and (C) LSPR absorbance (at λ = 555 nm) and (D) OD_{400} spectra of Au-HDL mixture incubated at T = 80 °C followed for 5 h (insets) optical photographs showing gradual color change of the Au-HDL mixture at different time intervals.

FTIR study of Au-HDL interactions

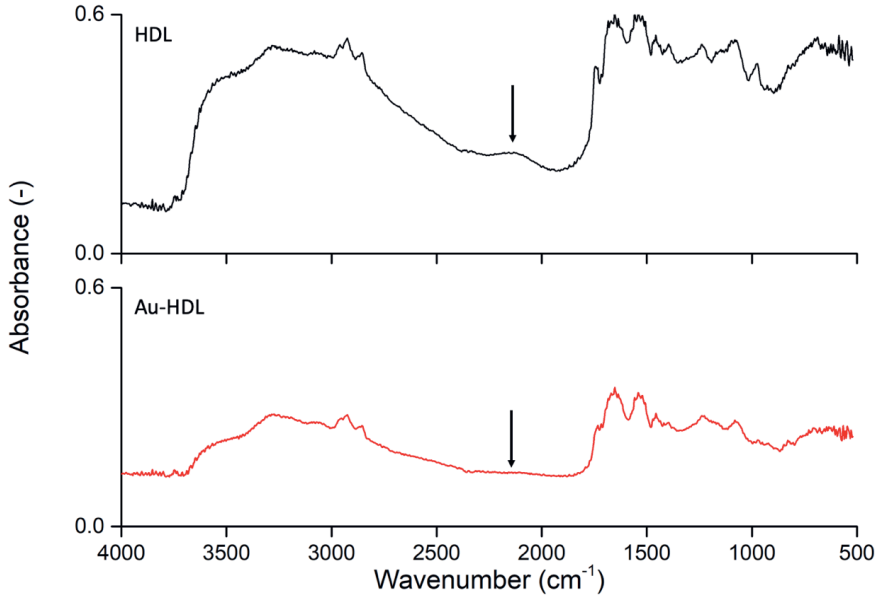

Figure S2.3 FTIR spectra of HDL (top, black graph) and Au-HDL network (bottom, red graph) in the 4000-500 cm^{-1} frequency region at ambient conditions. The arrows are pointing at the SH stretching vibrations.

SDS gel electropherogram of Au-HDL mixtures followed in time

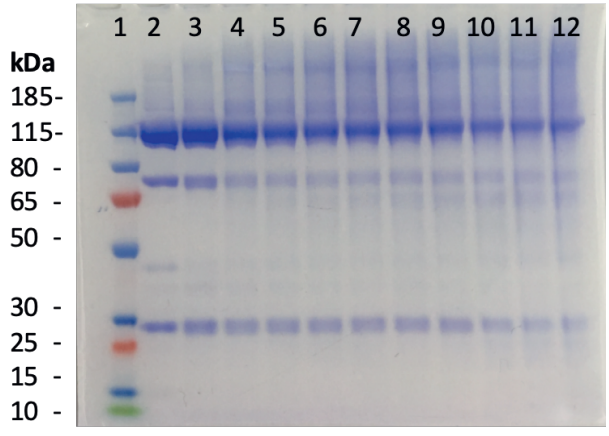

Figure S2.4 SDS gel electropherogram of the protein marker (lane 1), native HDL (lane 2) and Au-HDL gels in time (lane 3-12: 0, 10, 20, 30, 40, 50 60, 120, 180 and 240 mins).

Additional UV-Vis absorbance and fluorescence spectra

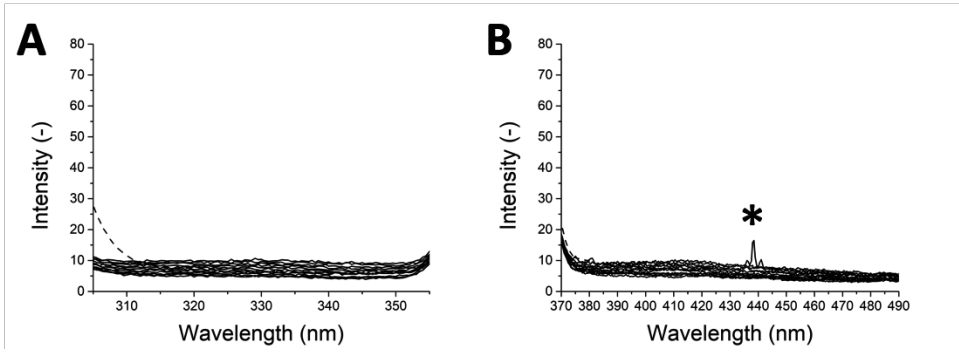

Figure S2.5 Fluorescence (A) excitation (λ_{em} = 410 nm) and (B) emission spectra (λ_{ex} = 325 nm) of 0.01% (w/v) HDL (dashed line) and Au-HDL mixture (solid line) in 1.71 M NaCl at different time intervals (0-5 h, every 30 min). The peak marked * arised from an artefact during measurement.

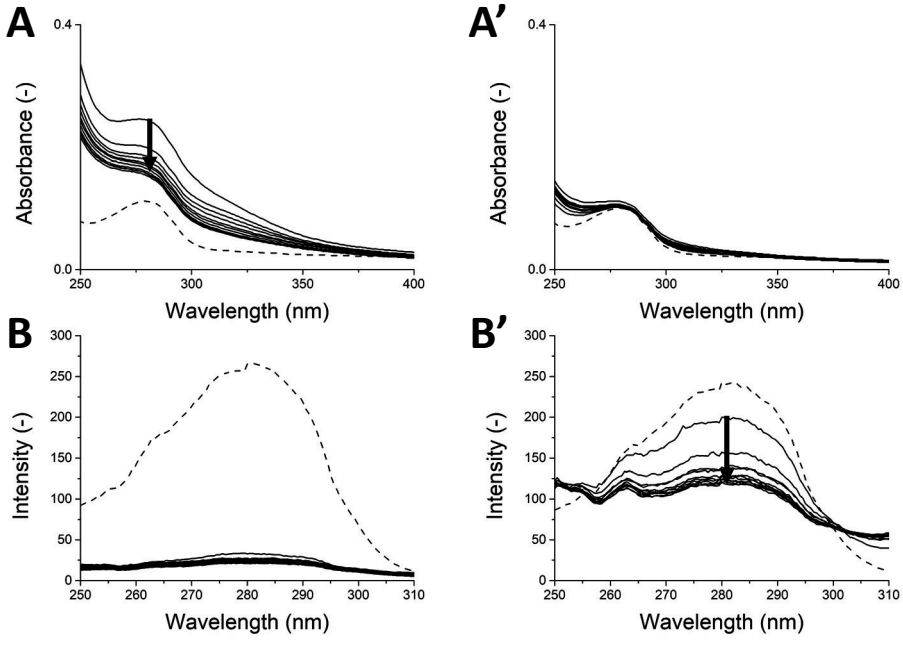

Figure S2.6 (A) UV-Vis absorbance and (B) fluorescence excitation (λ_{em} = 410 nm) spectra of 0.01% (w/v) HDL (dashed line) and Au-HDL mixture (solid line) in 1.71 M NaCl before and (A',B') after KCN treatment at different time intervals (0-5 h, every 30 min, indicated by the black arrow).

Au^{3+}-induced gel network and AuNPs formation of BSA and WPI

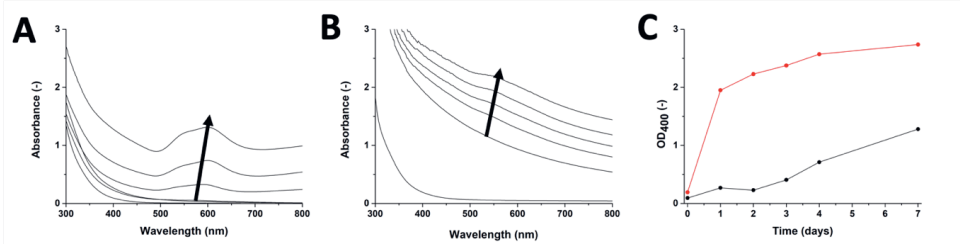

Figure S2.7 Solid UV-Vis absorbance spectra of (A) Au-BSA and (B) Au-WPI mixtures incubated at 20 °C followed in time from 0-7 days. The characteristic LSPR peaks of AuNPs increased in time, indicated by the arrows. (C) Derived OD_{400} spectra of BSA (black dotted-line) and WPI (red dotted-line) against time.

Chapter 3

Hollow protein microparticles through cross-linking by Au^{3+} initiated redox reaction

This chapter has been published as: L.M.I. Schijven, T.D. Vogelaar, S. Sridharan, V. Saggiomo, A.H. Velders, J.H. Bitter, C.V. Nikiforidis (2022). Hollow protein microparticles through cross-linking by Au^{3+} initiated redox reaction. *Journal of Materials Chemistry B,* **10**, 6267-6295. https://doi.org/10.1039/D2TB00823H

Abstract

Hollow microparticles (MPs) are of great relevance in materials industry for a wide range of applications, such as catalysis, coatings, and delivery of theranostics. Here, we report the formation of hollow MPs through the assembly of lipoproteins in $CaCO_3$ templates. Proteins interact in the pores of $CaCO_3$ templates through attractive hydrophobic forces and form dense edges of the hollow MPs. To further cross-link the proteins, Au^{3+} was added to initiate a redox reaction, where proteins were oxidized forming inter- and intramolecular covalent bonds, while Au^{3+} is reduced and formed gold nanoparticles (AuNPs). The obtained protein-based hollow MPs had a diameter of 6 µm and the AuNPs were embedded in their surface. Through this research, we suggest a new route to design biobased Au-protein hollow MPs in simple steps, which can allow new possibilities for carrying functional molecules and bioimaging.

3.1 Introduction

Microparticles (MPs) offer advantageous structural and functional abilities as a carrier system, which are of interest in a wide range of applications, such as,[1] encapsulation,[2] tissue engineering,[3 4] and biosensing.[5 6] Whereas the majority of the MPs are fabricated with synthetic polymers,[7] it is of great importance to use biobased materials, such as proteins, to expand the range of developing biocompatible MPs with functional properties.

For the preparation of protein MPs, proteins are forced to assemble together through the use of liquid or solid templates. The formation of stable MPs includes interactions of reactive amino acid side groups of neighboring protein molecules or the use of cross-linkers, like glutaraldehyde, resulting in a protein gel network.

Besides the formation of MPs with a homogeneous core, hollow MPs are also of high interest because of their ability to encapsulate large quantities of guest molecules in their hollow core.[8] Hollow MPs are mostly obtained with the aid of a hard[9] or soft[10] templates, which have to be removed through thermolysis or extensive acidification, requiring the use of large amounts of chemicals and tedious process steps. Therefore, the use of biobased molecules and environmentally friendly processes to create hollow MPs are highly desired.[11]

Herein, we demonstrate a facile method to fabricate hollow MPs using egg yolk high-density lipoproteins (HDL), inside sacrificial $CaCO_3$ templates (Scheme 3.1). HDL spontaneously forms the hollow MPs, due to intra-protein hydrophobic forces, while to increase the rigidity of the MPs, Au^{3+} ions are used, which has been reported to cross-link HDL through a redox reaction.[12] The cross-linking method is based on the oxidation of HDL amino acids and their subsequent covalent bonding, while residual amino acid groups of proteins act as natural reduction sites of Au^{3+} ions and synthesize gold nanoparticles (AuNPs), which are located on the surface of the MPs. The resulting hollow protein MPs have a well-defined size, morphology and high stability. The ability to produce stabilized hollow protein MPs, using Au^{3+} ions, with embedded AuNPs, opens avenues for manipulating and navigating microcapsules for controlled release and target delivery. The $CaCO_3$ templates can be easily decomposed at acidic pH,[13] releasing stable Au-HDL-MPs. The large inner voids of the Au-HDL MPs could encapsulate and protect molecules of interest. The molecules of interest could be encapsulated through co-precipitation with the proteins and $CaCO_3$,[14] or through passive diffusion into the protein MPs.[15] The embedded AuNPs makes the Au-HDL MPs an attractive platform as multimodal imaging agent due to their optical,[16, 17] photothermal,[18, 19] and high attenuation coefficient properties.[20]

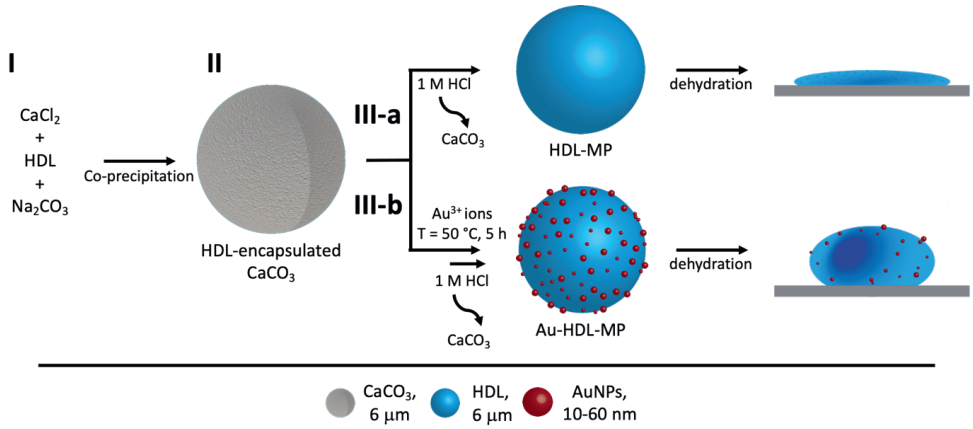

Scheme 3.1 Schematic representation of fabrication of protein hollow MPs. (I) HDL was encapsulated into $CaCO_3$ templates through co-precipitation with $CaCl_2$ and Na_2CO_3. (II) HDL was encapsulated inside the $CaCO_3$ template (gray). For route (III-a), HDL-MPs (blue sphere) were released from the template by lowering the pH. The HDL-MPs collapsed upon dehydration. For route (III-b), Au^{3+} ions were added to HDL-encapsulated $CaCO_3$ templates to induce *in situ* HDL network formation, followed by reduction of Au^{3+} and synthesis of 10-60 nm AuNPs (red spheres) before template removal. The resulting Au-HDL-MPs formed wrinkled, deflated structures after dehydration.

3.2 Results and Discussion

Spherical and porous $CaCO_3$ were synthesized by direct mixing of soluble salts of Ca^{2+} and CO_3^{2-} to initiate precipitation at supersaturation[21] and was used as template for the protein MPs, since it offers a large inner surface area for encapsulation, is biocompatible, economically friendly,[22] easy to prepare and sacrificial under mild conditions (e.g. by chelating reagents or under acidic conditions).[13] The proteins could be encapsulated through diffusion into pre-synthesized $CaCO_3$ templates or by co-precipitation during $CaCO_3$ synthesis.[23]

3.2.1 HDL encapsulated into the $CaCO_3$ templates

HDL is a relatively hydrophobic and insoluble protein, which forms aggregates in aqueous solutions.[24] The aggregates were too large to diffuse into pre-synthesized $CaCO_3$ templates. For this reason, HDL molecules were incorporated in the $CaCO_3$ through co-precipitation, which were expected to form a particle at the core of the $CaCO_3$ template.

When HDL was mixed with $CaCl_2$ before the addition of Na_2CO_3, the ions interacted to form the $CaCO_3$ template, and simultaneously encapsulated HDL aggregates and precipitated (Scheme 3.1 I-II). The $CaCO_3$ templates with the encapsulated HDL were collected and initially analyzed using TEM to get information on macroscopic morphology. The obtained HDL/$CaCO_3$ complexes appeared to be spherical with a diameter around 3.5-5.2 µm and a high electron density, caused by the high mass and crystallinity of the $CaCO_3$ templates (Figure 3.1 A). It has to be noted that also some cubic shapes were observed. However, cubic $CaCO_3$ structures are non-porous,[21, 23] so it was assumed that those did not contain HDL. Next to TEM, SEM was used for analyzing the surface structures of the HDL/ $CaCO_3$ complexes (Figure 3.1 B). In the SEM image, it was observed that the crystal surface was composed of

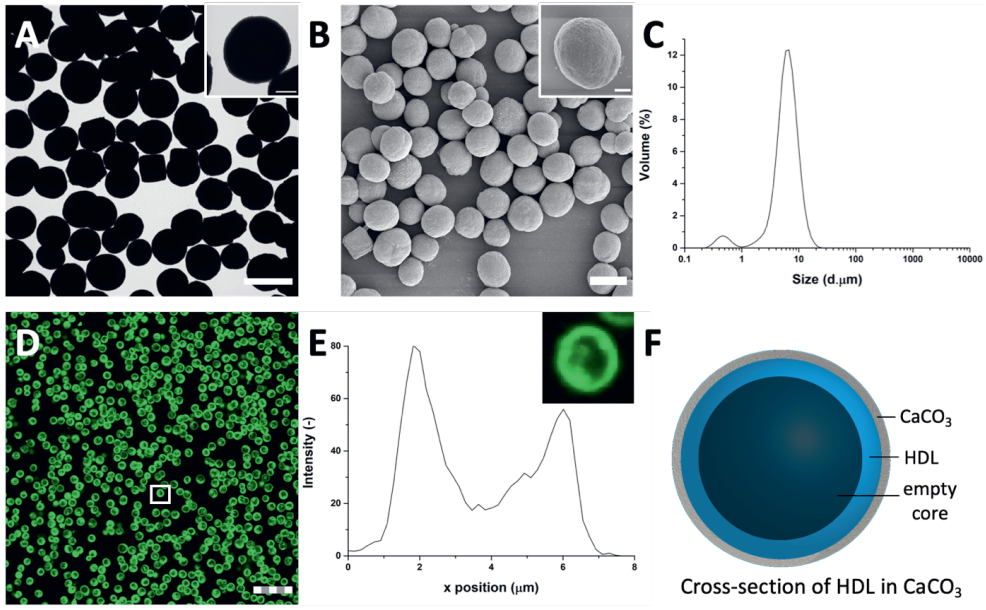

Figure 3.1 The high mass and crystallinity of the $CaCO_3$ templates provides a high contrast for (A) TEM and (B) SEM (scale bars are 5 μm), inset shows single particles (scale bars are 1 μm). (C) Light diffraction reveals a size distribution of HDL-encapsulated $CaCO_3$ templates with a diameter of 6 μm. (D) FITC-labelled HDL in CLSM reveals that HDL is distributed at the edges of the $CaCO_3$ templates, forming dense rings (scale bar is 25 μm, thickness is 0.6 μm). (E) Corresponding fluorescent profile plot of (inset) a FITC-HDL-encapsulated $CaCO_3$ template, indicated by the white box in (D). (F) Schematic illustration of the cross-section of an HDL-encapsulated $CaCO_3$ template.

smaller single particles (Figure 3.1 B, inset). Spherical, micron-sized $CaCO_3$ is synthesized through aggregation of primary $CaCO_3$ nuclei, which instantly formed by mixing Ca^{2+} and CO_3^{2-}.[25] The surface structure is most likely composed of smaller, single $CaCO_3$ nuclei.

To further evaluate the size distribution of the $CaCO_3$/HDL templates, their sizes were measured using light diffraction. As it is shown in Figure 3.1 C, the size distribution was bimodal with peaks at 0.6 μm and 6.7 μm. Previous reports have suggested a size distribution of the $CaCO_3$ templates around 4-6 μm,[21] which agrees with the results we obtained from the TEM analysis. Therefore the smaller peak at 0.6 μm, obtained during the laser diffraction analysis, was attributed to the non-encapsulated HDL aggregates.

To investigate the presence of HDL molecules inside the $CaCO_3$ templates, HDL was covalently labelled with fluorescein isothiocyanate (FITC) before co-precipitation. Using CLSM, the fluorescence of FITC (green color) was detected from the HDL-encapsulated $CaCO_3$ templates, indicating that the excitation wavelength could penetrate the porous templates (Figure 3.1 D, Figure S3.1).[26] As it is shown at the detailed fluorescence profile plot in Figure 3.1 E, a higher fluorescent signal was observed at the edges of the templates, while it gradually decreased from the surface to the internal core, showing the formation of shell-like hollow MPs, as it is given schematically in Figure 3.1 F. The protein border inside

the templates had a thickness of 2.0 ± 0.5 μm. The formation of the hollow protein MPs in the $CaCO_3$ template was surprising because it has been reported earlier when proteins such as bovine serum albumins[25] and β-lactoglobulins[27] were encapsulated in the same template, they formed homogeneous protein MPs. The proposed mechanism of the encapsulation of soluble proteins in the $CaCO_3$ templates was that the proteins adsorb onto the surface of primary $CaCO_3$ nanoparticles and are captured mechanically into the inner pores of $CaCO_3$ during colloidal aggregation of the $CaCO_3$ nanoparticles.[25] However, HDL proteins are poorly soluble and form big aggregates in aqueous solutions, and also in the presence of Ca^{2+} ions. Therefore, it was hypothesized that the HDL aggregates, due to their large size (>100 nm),[24] could not adsorb in the pores (20-60 nm)[21] of the $CaCO_3$ templates during the formation, but were only deposited on the core of the template at a later stage, making a thin spherical film around it.

3.2.2 Properties of hollow HDL microparticles

It is possible that strong attractive hydrophobic forces exist between the HDL molecules in the confined environment of the $CaCO_3$ template, which was expected to be the force that can keep the hollow protein MPs intact when the template will be removed (Scheme 3.1 III-a). During the $CaCO_3$ synthesis, the proteins were under alkaline conditions (pH > 10), which results in exposure of hydrophobic groups and increases hydrophobic interactions.[28] The charge of the HDL molecules was expected to have minor impact, since it was weak and did not exceed the |20| mV at the storage and $CaCO_3$ decomposition conditions (Figure S3.2).

To investigate the stability of the hollow protein MPs, we initially used CLSM to visualize the particle microstructure (Figure 3.2 A, Figure S3.3). The fluorescent signal was again predominantly observed at the edges of the HDL-MPs. The fluorescence profile plot showed the highest fluorescence intensity at the edges, but a significant decrease from the surface to the internal core (Figure 3.2 B). This shows the conservation of the protein distribution within the template after releasing the HDL-MPs from the templates. However, the protein border thickness was decreased to 1.6 ± 0.4 μm, which suggests that some proteins were released from the HDL-MPs during the template removal. This could be due to the weak hydrophobic interactions, which could not keep all the proteins together. Additionally, the HDL-MPs were aggregated, which could be due to the hydrophobic nature of HDL, leading to extensive hydrophobic interactions between neighboring HDL-MPs.

Next, TEM imaging was applied to study the HDL-MPs structure. The HDL-MPs appeared as slightly loose protein matrices with low density (Figure 3.2 C, Figure S3.4) and diameter of 4.7-7.5 μm. The protein-protein interactions in the hollow MPs were constituted by weak hydrophobic forces, resulting in a system with low density. Furthermore, since it was not clear in the TEM image whether the MPs kept their hollow structure, TEM imaging was also done on an ultramicrotome thin section of an HDL-MP (Figure 3.2 D). In the thin section, a dark-colored border was observed, which consisted of proteins. No proteins were observed in the internal core of the HDL-MP, which confirms that the HDL-MPs formed a hollow structure with a low protein density (Figure 3.2 E).

The surface morphology of the HDL-MPs was further examined by SEM (Figure 3.2 F). After the template removal, the HDL-MPs resembled flattened circular discs. During SEM imaging, drying and

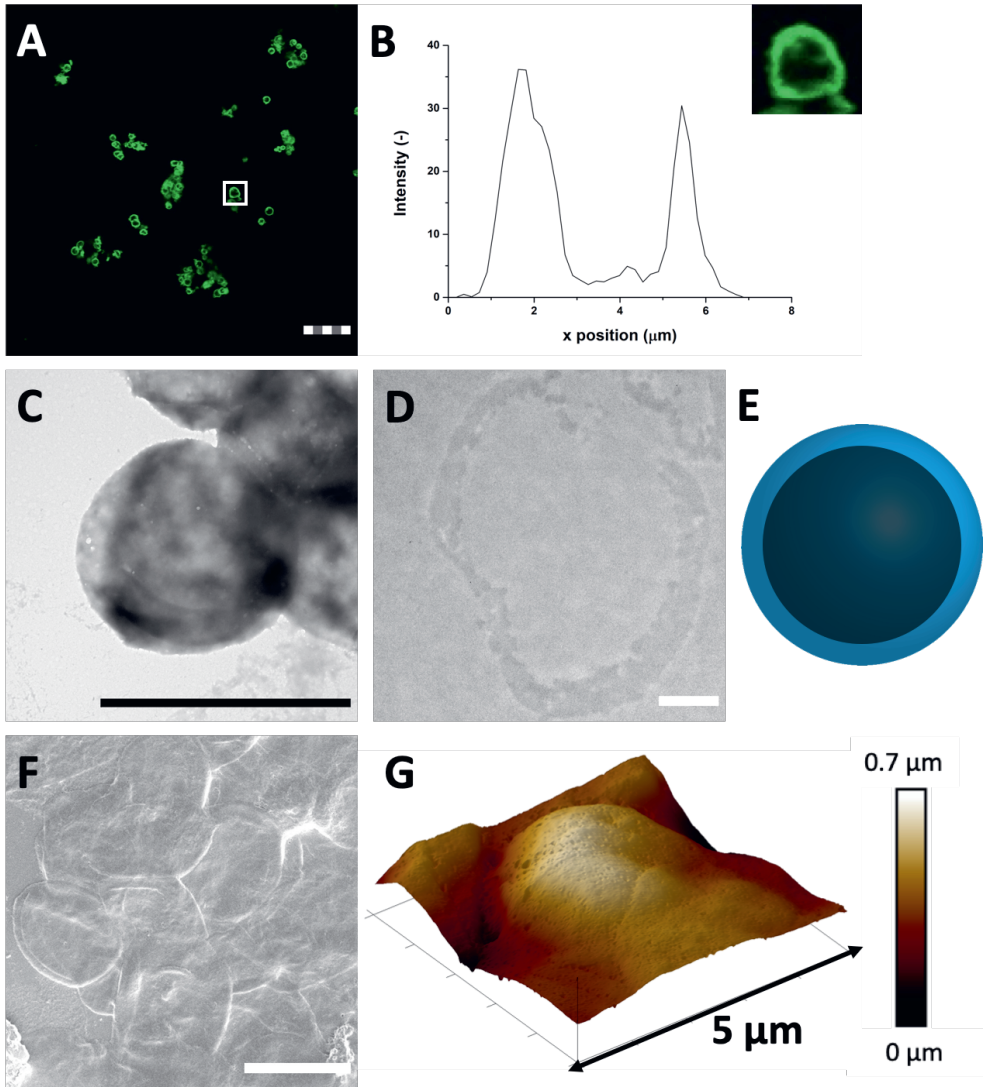

Figure 3.2 (A) FITC-labelled HDL-MPs (scale bar is 25 μm, thickness is 0.9 μm) in CLSM reveals that the HDL distribution in the HDL-MPs is conserved after template removal. (B) The corresponding fluorescent profile plot of (inset) a single HDL-MP, indicated by the white box in (A). The dense protein network provides contrast for (C) TEM (scale bar is 1 μm) and the (D) cross-section (0.05 μm) of the HDL-MP shows that the proteins formed a hollow core-shell morphology (scale bar is 0.5 μm, sample is stained with uranyl acetate and lead citrate). (E) Schematic illustration of the cross-section of an HDL-MP. (F) SEM image of HDL-MPs, coated with tungsten (scale bar is 5 μm). (G) 3-D AFM images of HDL-MPs, with corresponding height scale bar.

high vacuum conditions are applied. These conditions could have caused collapsing of the hollow HDL-MPs, which could be due to the absence of proteins in the internal core and weak protein-protein interactions, resulting in low structural integrity of the HDL-MPs in a dried state.[29] To further investigate the structural stability of the HDL-MPs, in terms of rigidity and self-standing, the particles

were dried on a solid substrate under ambient conditions and imaged with AFM. The AFM images show the topography of the HDL-MPs, where the raised (indicated by white-to-light brown color) and lowered (dark brown color) structures are determined. Upon drying, the HDL-MPs had a flattened, collapsed shape with a porous surface with a thickness varying from 0.01-0.7 μm (Figure 3.2 G). The collapsing of the hollow protein MPs upon drying, indicated that it is necessary to cross-link the proteins, so they will retain their structure.

3.2.3 Using Au^{3+} ions to enhance the rigidity of the hollow protein MPs

Covalent cross-linking of the proteins allows conserving and stabilizing the spherical structure upon template removal. In our previous research, we demonstrated that the addition of (≥150 molar equivalents) Au^{3+} ions to HDL resulted in gel network formation and subsequent AuNPs synthesis.[12] The Au^{3+} ions are known for their strong oxidizing properties on, for instance, thiol- or amine-containing side groups of amino acids, resulting in di-amino acid covalent bonding[30, 31] and, subsequently, gel network formation. Additionally, several available amino acid side groups (e.g. tryptophan, tyrosine, aspartic acid, phenylalanine) can act as reduction sites of Au^{3+} ions and synthesize AuNPs.[32-35] In a previous work, FTIR analysis showed the formation of disulfide bonds and fluorescence spectroscopy the formation of dityrosine in the gel networks.[12] Increasing the amounts of Au^{3+} ions resulted in a faster formation of the gel networks. However, no changes in morphology were observed.

Therefore, 250 molar equivalents of Au^{3+} ions were added to HDL-encapsulated in $CaCO_3$ templates to induce protein-protein interactions and covalent cross-linking of proteins (Scheme 3.1 III-b). During the incubation of the Au^{3+}/HDL/$CaCO_3$ system the suspension gradually changed from white to pink (after 2 h), then to red, indicating the interactions of Au^{3+} with the HDL molecules and the subsequent formation of AuNPs (Figure S3.5 A). Increasing the amounts of Au^{3+} accelerated the color formation of the Au^{3+}/HDL/$CaCO_3$ system. The red color was derived from the characteristic localized surface plasmon resonance (LSPR) absorption of AuNPs, which can be found in the region of λ = 500-600 nm.[36] After precipitation of the HDL/$CaCO_3$ complexes, it was observed that only the solid templates appeared red- colored, while the solution remained transparent (Figure S3.5 B), showing that both HDL and AuNPs were located at the templates. It is important to mention here that the formation of AuNPs and the subsequent red color was not observed in the absence of HDL, clearly proving that the AuNPs formed after their diffusion into the templates and their interaction with the HDL molecules that were entrapped. After removal of the templates, the red color of the Au-HDL-MPs was conserved (Figure S3.5 C). This suggests that HDL not only reduced the Au^{3+} ions for the formation of AuNPs, but also stabilized the AuNPs through steric stabilization effects, adsorption to the AuNP surface and by coordinating Au^{3+} to numerous functional amino acid groups (e.g. amine and carboxylate groups). The steric stabilization could decrease the potential toxicity of the AuNPs, however, since contradictive information on this matter has been published,[37] further investigation is needed.

To confirm whether the red color is derived from AuNPs, the Au-HDL MPs solutions were measured with UV-Vis absorbance at λ = 400-800 nm (Figure S3.5 D). The spectra demonstrated the appearance of an absorption peak centered at λ = 555 nm after 2 h of incubation, which confirmed the presence of the AuNPs.

The Au^{3+} ions and AuNPs formation after template removal may have an impact on the spherical protein structure. For this reason, the microstructure and protein distributions in the protein MPs were studied with CLSM, after labeling HDL using FITC (Figure 3.3 A, Figure S3.6). The CLSM images showed dense rings, which means that the spherical protein structures were still intact after template removal. The fluorescence profile plot also showed a high fluorescence peak, which corresponds to the observed ring, and a gradual decrease from the surface to the internal core (Figure 3.3 B). The protein border had a thickness of 1.9 ± 0.4 μm, which was similar to the thickness before template removal (Figure 3.1 D). Based on these results, the protein distribution and spherical structure seems to be preserved within the hollow MPs after template removal through the addition of Au^{3+} ions.

Next, TEM was used for analyzing the hollow MPs structure after the addition of Au^{3+}. In the TEM image, the MPs appeared as dense protein matrices with a size distribution of 1.6-3.1 μm (Figure 3.3 C, Figure S3.7). Besides the protein MPs, small, dark and spherical spots, with sizes between 10-60 nm, were observed. The AuNPs have a higher electron density than the protein matrix, and this contrast is sufficient to detect the AuNPs in the protein matrix. Based on the contrast difference, the appearance of the red color and the LSPR absorbance, the spherical spots in the TEM image were assigned to AuNPs. However, it could not be clearly observed on the TEM image whether those AuNPs are located on the surface or inside the protein matrix. Therefore, TEM imaging was done on an ultramicrotome thin section (0.05 μm), after agarose embedding (Figure 3.3 D). In the thin section, a dark border was observed, which consisted of stained proteins, and there were some dense electron regions observed in the internal core of the MPs. This confirmed the MPs formed a stable and rigid hollow structure. The AuNPs were predominantly observed on the outside of the dark borders of proteins. This suggests the ability of Au^{3+} ions to infiltrate the $CaCO_3$ templates at the protein surface and there they are reduced to AuNPs (Figure 3.3 E). The darker shades that were observed in the TEM image in Figure 3.3 C could be attributed to folds and creases in the structure, which caused a higher local electron density. These folds are likely formed upon dehydration of the hollow- structure morphology of the hollow MPs under drying and high vacuum conditions during TEM imaging.

Additionally, the surface morphology of the Au-HDL-MPs was further examined by SEM (Figure 3.3 F). After template removal, the Au-HDL-MPs appeared flatten with folds and creases structures. The deflated, wrinkled particle structure likely resulted from the hollow-like and cross-linked shell structure of the Au-HDL-MPs, which collapsed upon drying due to the removal of water, but still the protein molecules remained in the border of the MP. AFM was used to study the effect of dehydration on rigidity and self-standing properties of the hollow Au-HDL-MPs (Figure 3.3 G). The drying of Au-HDL-MPs resulted in the formation of a deflated, wrinkled particle shape with a thickness varying from 0.1-1.7 μm. The thickness of the Au-HDL-MPs was two times higher than the HDL-MPs, indicating that the wall thickness of Au-HDL-MPs was more rigid upon dehydration. This was also observed in the CLSM images, where the wall thickness of the Au-HDL-MPs was higher than of the HDL-MPs (Figure 3.2 A, Figure 3.3 A). Based on that, we hypothesized that the wall thickness is higher due to the covalent cross-linking of the Au-HDL-MPs, which improved the stabilization of the structures upon dehydration.

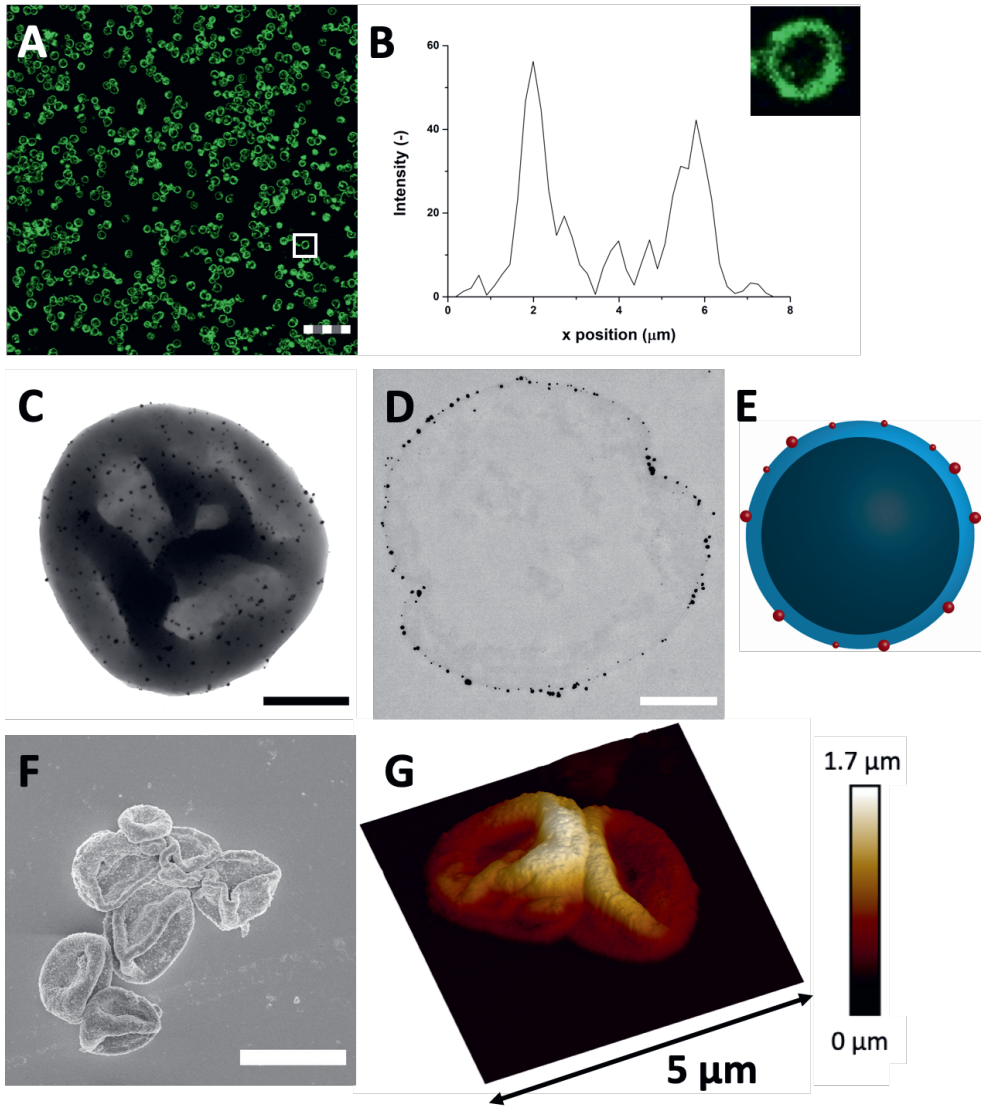

Figure 3.3 (A) FITC-labelled Au-HDL-MPs (scale bar is 25 μm, thickness is 0.9 μm) in CLSM reveals that the HDL distribution in the Au-HDL-MPs is conserved after cross-linking and template removal. (B) The corresponding fluorescent profile plot of (inset) a single Au-HDL-MP, indicated by the white box in (A). The dense protein network and AuNPs provide a high contrast for (C) TEM (scale bar is 1 μm) and the (D) cross-section (0.05 μm) of the Au-HDL-MP shows that the AuNPs are concentrated at the edges of the protein MP surface (scale bar is 0.5 μm, sample is stained with uranyl acetate and lead citrate). (E) Schematic illustration of the cross-section of an Au-HDL-MP with AuNPs on the surface. (F) SEM image of Au-HDL-MPs, coated with tungsten (scale bar is 5 μm). (G) 3-D AFM image of two neighboring Au-HDL-MPs, with corresponding height scale bar.

3.2.4 Stability of the hollow protein MPs at different pH conditions

After preparation of the different particle systems, analytic methods were used to study the stability, in terms of aggregation, of the MPs at different pH values. DLS measurements allowed a comparison of the diameters of the cross-linked (Au-HDL-MPs) and non-cross-linked hollow MPs (HDL-MPs) (Figure 3.4 A). For HDL-MPs, the average size distribution was 0.93 μm at pH 1-3, whereas the sizes increased to 7.7 μm (±19%) at pH 4-10, and decreased to 0.45 μm at pH 11-12. However, it was observed that the sizes of the Au-HDL-MPs were stable around 6.4 μm (±7%) at the pH range 1-12. Before removal of the template, the size distribution of the HDL-encapsulated $CaCO_3$ was 6.7 μm (Figure 3.1 C). The sizes of HDL-MPs were slightly larger at pH 4-10 than before the removal of the template. At the extreme low (pH 1-3) and high (11-12) pH values, the sizes were significantly decreased. These results suggest that the HDL-MPs were not stable in size against pH. In contrast, there were no major changes observed in size of the Au-HDL-MPs after template removal and pH titration. The HDL-MPs and Au-HDL-MPs sizes were originated from the templates (Figure 3.1 C), which indicates that the MPs are inverse replicates of the $CaCO_3$ templates. Additionally, the pH did not affect the size of the Au-HDL-MPs, indicating that the Au-HDL-MPs are predominantly stabilized by covalent protein-protein interactions. These covalent bonds were derived from oxidized amino acids, like cysteine and tyrosine, due to the addition of Au^{3+} ions.[12]

Another important factor in colloidal stability is the surface charge. Zeta-potential measurements allowed a comparison of quantitative values of the overall surface charge and colloidal stability between HDL-MPs and Au-HDL-MPs (Figure 3.4 B). The zeta-potential as a function of pH showed that HDL-MPs have surface charges below |30| mV and a zero surface charge point at pH 7.3. The Au-HDL-MPs have an effective zeta-potential of about -30 mV at pH 4-12, and a zero surface charge point at pH 2.9. When zeta-potential values are ≥|30| mV, the particles are electrostatically stabilized and cause electrostatic repulsion between the particles and prevent aggregation. However, when the zeta-potential values are <|30| mV, attractive forces exceed electrostatic repulsion, causing the particles to aggregate.[27] At pH 4-10, the HDL-MPs sizes were increased and the particles bear surface charges of > |20| mV. Based on that, we concluded that electrostatic repulsion caused swelling of the charged shells. However, a size decrease was observed at pH 7, which is close to the surface zero charge point.

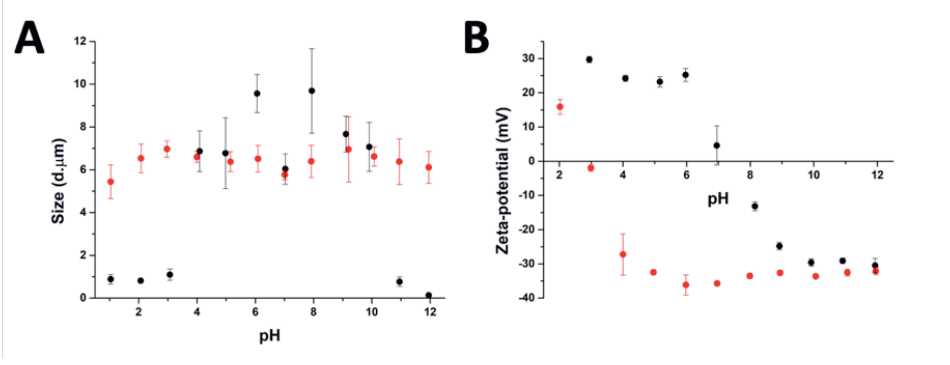

Figure 3.4 The effect of pH on (A) sizes, as derived from DLS measurements, and (B) zeta-potential of HDL-MPs (black dots) and Au-HDL-MPs (red dots). Separate protein-MPs solutions with pH 1-12 were prepared for each individual measurement.

The decrease in size of the HDL-MPs could be due to attractive forces, resulting in shrinkage. Additionally, the high zero surface charge point of the HDL-MPs indicates that strong hydrophobic interactions stabilize the HDL-MPs.[38] At the extreme pH values, the surface charges were |30| mV and the sizes were significantly decreased. This indicates that the high surface charge, and thus high repulsion, at the extreme pH values could lead to more extreme swelling of the HDL-MPs.[39] The swollen HDL-MPs were likely sedimented during the size measurements, resulting in significant size decrease.

The low zero surface charge point of the Au-HDL-MPs suggests that the positively charged groups (e.g. lysine, arginine) of the Au-HDL-MPs are reduced, resulting in a more negative charge. This could be caused by interactions of positively charged groups with the obtained AuNPs,[40] or due the nucleation of the AuNPs,[41] or the oxidation of the positively charged groups.[30] Since we observed that Au-HDL-MPs sizes were stable against pH and have zeta-potential values of -30 mV, we concluded that the covalent cross-linking of the Au-HDL-MPs improved the stabilization of the structures upon template decomposition and could be accelerated by increasing the amounts of Au^{3+} ions.

3.3 Conclusion

In this research, we successfully fabricated stable hollow protein MPs with an average size distribution around 6 μm. For the formation of the hollow MPs, $CaCO_3$ was used as a template. HDL molecules are interacting in the pores of the template through attractive hydrophobic forces and are predominantly concentrated at the edges of the $CaCO_3$ template. However, it appeared that the hydrophobic forces were not enough to sustain the structure of the MPs. Therefore, Au^{3+} ions were added to the HDL molecules encapsulated in $CaCO_3$, as it has been shown that Au^{3+} reacts rapidly with HDL molecules causing protein oxidation and cross-linking. At the same time, Au^{3+} ions are reduced from the amino acids of the proteins and form AuNPs, which are embedded in the surface of the hollow MPs. The hollow MPs with AuNPs were stable in terms of aggregation and self-standing properties. The design we propose here of stable protein hollow MPs opens new avenues for constructing hollow MPs in simple steps using biobased molecules. Besides that, the presence of AuNPs on the surface of the hollow MPs makes the suggested system an attractive platform as carrier of therapeutics and at the same time a multimodal imaging agent due to their optical, high electron density, and high attenuation coefficient properties.

3.4 Experimental section

3.4.1 Materials

Fresh hen eggs were purchased from a local organic farm De Hoge Born, Wageningen, the Netherlands. Sodium chloride (NaCl, ≥99.5%), 1 M NaOH and 1 M HCl solutions were purchased from VWR international B.V. Gold(III) chloride hydrate ($HAuCl_4 \cdot xH_2O$,99.5%), Fluorescein-5-isothiocyanate (FITC, ≥95%), calcium chloride ($CaCl_2$, ≥93%), sodium carbonate (Na_2CO_3, ≥99.5%) and 76 mm dialysis tubing cellulose membrane (MWCO = 14 kDa) were purchased from Sigma Aldrich. All chemicals were used without further purification and deionized water was used throughout the experiments.

3.4.2 Methods

Extraction of HDL

HDL was extracted from egg yolk according to the method developed by Castellani,[42] with slight modifications. Hen eggs were cracked and the egg yolks were separated manually from the albumen. The egg yolks were carefully rolled on a paper tissue to remove the chalazae and adhering albumen. The yolk membranes were then punctured, using a glass pipette, and their contents were collected and pooled in a beaker cooled in iced water. The liquid yolks were diluted with three volumes of 0.17 M NaCl (1% (w/v)) and homogenized by stirring for 1 h. The yolk was fractionated into plasma and granules by centrifugation at 10,000 x g for 45 min at T = 4 °C, using a Thermoscientific Sorvall Legend XFR centrifuge. The pellet (granules) was washed with 0.17 M NaCl and centrifuged once more. The granules were suspended in 1.71 M NaCl (10% (w/v)) and the solution's pH was adjusted to 7.25, using 1 M NaOH. The mixtures were collected in dialysis tubings and were dialyzed against deionized water with 3 changes over 24 h. The HDLs were precipitated. The content of the dialysis tubings were collected and centrifuged. The pellets, rich in HDL, were collected and freeze-dried, using a Salmenkipp alpha 2-4 plus freeze-dryer at a temperature of T = -76 °C and pressure of 0.0090 mbar for 72 h.

Labelling of HDL with FITC

FITC was coupled to HDL through an isothiocyanate/amine reaction. 2 mg of FITC was added to 2 g of HDL (with a molar ratio of ~1:1) dissolved in 50 mL of 1.71 M NaCl. The mixture was allowed to react overnight, while covered against light. The mixture was then dialyzed against deionized water with 5 changes over 48 h. The content of the dialysis bag was collected and centrifuged. The supernatant was discarded and the pellet was washed again with deionized water before freeze-drying. The molar ratio of FITC coupled to HDL was 0.8, based on UV-Vis absorbance measurements.

Preparation of HDL-encapsulated $CaCO_3$ templates

For encapsulation of HDL into porous, spherical $CaCO_3$ templates, a standard procedure reported by Volodkin et al. (2004)[21] was followed with slight modifications. 20 mL of a 0.33 M Na_2CO_3 solution was rapidly poured into 20 mL of 0.33 M $CaCl_2$ containing 5 mg/mL of HDL (100 mg, 0.24 µmol, mw_{HDL} = 422,480 kDa[43]), while stirring at 700 RPM using a magnetic stirrer. A white precipitate formed instantly. The stirring speed was subsequently increased to 2500 RPM for 30 s. The sample was then removed from the stirring plate and was left standing for 15 min to facilitate the formation of $CaCO_3$. The

suspended HDL-encapsulated $CaCO_3$ was collected by centrifugation at 3,000 x g for 5 min (Thermo Scientific ST 8R centrifuge) and washed 3 times with 10 mL of 1.71 M NaCl to remove non-bound HDL.

Preparation of HDL-MPs

HDL-MPs were prepared by dissolution of the $CaCO_3$ templates. The $CaCO_3$ was removed by adjusting the pH of the suspended HDL/$CaCO_3$ templates from 9.6 to 1.5 by addition of a 1 M HCl solution. While lowering the pH, some foam formation due to protein flocculation was observed. The formed HDL-MPs were precipitated by centrifugation (10,000 x g, 10 min, T = 4 °C) and washed 3 times with 10 mL of deionized water, pH 7.

Preparation of Au-HDL-MPs

Au^{3+} ions were added as a solution (59.2 µmol, 250 molar equivalents to initial HDL concentration, at pH 7) to 30 mL of suspended HDL-encapsulated $CaCO_3$ templates, in 1.71 M NaCl. The mixture was allowed to incubate at T = 50 °C, while being stirred at 700 RPM, for 5 h. The templates were removed by adjusting the pH of the solution to 1.5 by addition of a 1 M HCl solution. Finally, the Au-HDL-MPs were collected by centrifugation (10,000 x g, 10 min, T = 4 °C) and washed 3 times with 10 mL of deionized water, pH 7.

3.4.3 Characterization

Transmission Electron Microscopy (TEM)

TEM sample preparation was done by pipetting 6 µL of sample onto a carbon-coated hexagonal 400 mesh copper grid. After 1 min, a filter paper was used to remove excess fluid. After air drying, the samples were imaged using a JEOL JEM1400+ microscope, operating at 120 kV. The images were analyzed using FIJI software.[44]

For the ultramicrotome sample preparation, the HDL-MPs and Au-HDL-MPs were fixed with 2.5% glutaraldehyde in 0.1 M phosphate/citrate buffer and incubated for 1 h, after which they were washed 3 times with 0.1 M phosphate/citrate buffer. The pellets were re-suspended in 100 µL of 2% gelatin in 0.1 M phosphate and were solidified after 20 min at 4 °C. The pellet was removed from the tube by 15 min incubation in 2.5% glutaraldehyde in 0.1 M phosphate/citrate buffer. The specimens were cut into small pieces (approximately 1 mm^3) and were fixated again for 1 h, after which they were washed 6 times with 0.1 M phosphate/citrate buffer. The specimens were fixated again, this time with 1% osmium tetroxide for 1 h, after which they were washed 3 times with MilliQ water. Thereafter dehydration with ethanol was applied, substituting the deionized water for 30%, 50%, 70%, 80%, 90%, 96% (5 min for each step) and 2x 100% ethanol (10 min). Once the specimens were in 100% ethanol, the specimens were infiltrate with Spurr embedding liquid in 3 steps: 2:1, 1:1, 1:2 (ethanol:Spurr, 30 min per step). Then the specimens were left in 100% Spurr for 1 h and was refreshed once more and incubated overnight. The next day the Spurr was refreshed once more for 1 h, after which the samples were polymerized for 8 h at 70 °C. Once the specimens were hardened, they were sectioned into 50 nm thin coupes by using the Leica Ultramicrotome UC7 Rapid. The sections were collected with formvar film 150 mesh copper TEM grids. The sections were stained by incubation for 10 min in 2% uranyl acetate, after which they were washed 5 times with MilliQ. Then the sections were stained by

incubation for 2 min in lead citrate (under a CO_2-free environment), after which they were washed 2 times with CO_2-free water and 3 times with MilliQ.

Scanning Electron Microscopy (SEM)

A 20 μL droplet of sample was put onto a mica sheet surface. After 1 minute, the excess fluid was removed. 100 μL of deionized water was used to remove excess, non-stuck particles from the mica surface. The surface was dried by a filter paper and was then mounted onto a sample holder containing carbon adhesive tab. Before imaging, the sample was coated with tungsten. The samples was then imaged with a FEI Magellan 400 SEM, operating at 2 kV and the images were analyzed using FIJI software.

Size and surface charge

For size determination of the HDL-encapsulated $CaCO_3$ templates, suspensions in a hydro dispenser were measured by light diffraction (Bettersizer Instruments). The sizes of Au-HDL-MPs and HDL-MPs were measured by dynamic light scattering (DLS) measurements at 173°, with a 400 mW argon-helium laser, operating at a wavelength of λ = 632 nm at room temperature (Malvern ZS Nanosizer). For the surface charge and stability of HDL, HDL-MPs and Au-HDL-MPs, a dip cell was inserted into the solution to measure the zeta-potential (Malvern ZS Nanosizer). The HDL, Au-HDL-MPs and HDL-MPs samples were prepared as 1 mL solutions in deionized water at pH of 2-12.

Confocal Laser Scanning Microscopy (CLSM)

For CLSM imaging, FITC-labelled HDL was used instead of HDL. The HDL-encapsulated $CaCO_3$, HDL-MPs and Au-HDL-MPs were imaged using a Leica SP8-SMD microscope. The FITC was excited with $\lambda_{ex,max}$ = 490 nm and emission was collected at $\lambda_{em,max}$ = 525 nm. The laser intensity for HDL-encapsulated $CaCO_3$ and HDL-MPs was set at 50% and for Au-HDL-MPs at 60%. The images were analyzed using FIJI software.

Atomic Force Microscopy (AFM)

Mica surface discs were freshly cleaved by adhesive tape detachment. A 20 μL droplet of sample was put onto a mica sheet surface. After 1 min, a filter paper was used to remove excess fluid. 100 μL of deionized water was used to remove excess, non-stuck particles from the mica surface. The surface was dried by a filter paper, under a stream of nitrogen and dried in air overnight. AFM images were recorded on a Bruker Multimode 5 and processed with Nanoscope Analysis 1.5 software.

UV-Vis spectrophotometric measurements

UV-Vis measurements of the Au-HDL-MPs were done using a Hitachi U-2010 UV-Visible spectrophotometer at λ = 400-800 nm, using deionized water as a reference.

References

1. M. Lengyel, N. Kállai-Szabó, V. Antal, A.J. Laki, and I. Antal, Microparticles, microspheres, and microcapsules for advanced drug delivery, *Scientia Pharmaceutica*, 2019, **87**, 3, 20.
2. D.J. McClements, Encapsulation, protection, and delivery of bioactive proteins and peptides using nanoparticle and microparticle systems: A review, *Advances in colloid and interface science*, 2018, **253**, 1-22.
3. S. Shkarina, R. Shkarin, V. Weinhardt, E. Melnik, G. Vacun, P.J. Kluger, K. Loza, M. Epple, S.I. Ivlev, and T. Baumbach, 3D biodegradable scaffolds of polycaprolactone with silicate-containing hydroxyapatite microparticles for bone tissue engineering: High-resolution tomography and in vitro study, *Scientific reports*, 2018, **8**, 1, 1-13.
4. W. Wijaya, A.R. Patel, A.D. Setiowati, and P. Van der Meeren, Functional colloids from proteins and polysaccharides for food applications, *Trends in Food Science & Technology*, 2017, **68**, 56-69.
5. Y.H. Roh, H.J. Lee, and K.W. Bong, Microfluidic fabrication of encoded hydrogel microparticles for application in multiplex immunoassay, *BioChip Journal*, 2019, **13**, 1, 64-81.
6. F. Bucatariu, C.-A. Ghiorghita, M.-M. Zaharia, S. Schwarz, F. Simon, and M. Mihai, Removal and separation of heavy metal ions from multicomponent simulated waters using silica/polyethyleneimine composite microparticles, *ACS Applied Materials & Interfaces*, 2020, **12**, 33, 37585-37596.
7. S. Roberts, V. Miao, S. Costa, J. Simon, G. Kelly, T. Shah, S. Zauscher, and A. Chilkoti, Complex microparticle architectures from stimuli-responsive intrinsically disordered proteins, *Nature communications*, 2020, **11**, 1, 1-10.
8. J. Han, G. Song, and R. Guo, Synthesis of polymer hollow spheres with holes in their surfaces, *Chemistry of materials*, 2007, **19**, 5, 973-975.
9. Z. Niu, Z. Yang, Z. Hu, Y. Lu, and C.C. Han, Polyaniline–silica composite conductive capsules and hollow spheres, *Advanced Functional Materials*, 2003, **13**, 12, 949-954.
10. Z. Wei and M. Wan, Hollow microspheres of polyaniline synthesized with an aniline emulsion template, *Advanced Materials*, 2002, **14**, 18, 1314-1317.
11. D. Wu, F. Xu, B. Sun, R. Fu, H. He, and K. Matyjaszewski, Design and preparation of porous polymers, *Chemical reviews*, 2012, **112**, 7, 3959-4015.
12. L.M. Schijven, V. Saggiomo, A.H. Velders, J.H. Bitter, and C.V. Nikiforidis, Au 3+-Induced gel network formation of proteins, *Soft Matter*, 2021, **17**, 42, 9682-9688.
13. D.V. Volodkin, R. von Klitzing, and H. Möhwald, Pure protein microspheres by calcium carbonate templating, *Angewandte Chemie*, 2010, **122**, 48, 9444-9447.
14. J. Lademann, H. Richter, F. Knorr, A. Patzelt, M.E. Darvin, E. Rühl, K.Y. Cheung, K. Lai, R. Renneberg, and W.C. Mak, Triggered release of model drug from AuNP-doped BSA nanocarriers in hair follicles using IRA radiation, *Acta Biomaterialia*, 2016, **30**, 388-396.
15. R. Elia, J. Guo, S. Budijono, V. Normand, D. Benczédi, F. Omenetto, and D.L. Kaplan, Encapsulation of volatile compounds in silk microparticles, *Journal of coatings technology and research*, 2015, **12**, 4, 793-799.
16. R. De La Rica and A.H. Velders, Supramolecular Au Nanoparticle Assemblies as Optical Probes for Enzyme-Linked Immunoassays, *Small*, 2011, **7**, 1, 66-69.
17. R. de laRica, R.M. Fratila, A. Szarpak, J. Huskens, and A.H. Velders, Multivalent nanoparticle networks as ultrasensitive enzyme sensors, *Angewandte Chemie International Edition*, 2011, **50**, 25, 5704-5707.
18. X. Huang, P.K. Jain, I.H. El-Sayed, and M.A. El-Sayed, Plasmonic photothermal therapy (PPTT) using gold nanoparticles, *Lasers in medical science*, 2008, **23**, 3, 217-228.
19. X. Huang and M.A. El-Sayed, Gold nanoparticles: Optical properties and implementations in cancer diagnosis and photothermal therapy, *Journal of advanced research*, 2010, **1**, 1, 13-28.
20. J. Hainfeld, D. Slatkin, T. Focella, and H. Smilowitz, Gold nanoparticles: a new X-ray contrast agent, *The British journal of radiology*, 2006, **79**, 939, 248-253.
21. D.V. Volodkin, N.I. Larionova, and G.B. Sukhorukov, Protein encapsulation via porous CaCO3 microparticles templating, *Biomacromolecules*, 2004, **5**, 5, 1962-1972.

22. D.V. Volodkin, A.I. Petrov, M. Prevot, and G.B. Sukhorukov, Matrix polyelectrolyte microcapsules: new system for macromolecule encapsulation, *Langmuir*, 2004, **20**, 8, 3398-3406.
23. D. Volodkin, CaCO3 templated micro-beads and-capsules for bioapplications, *Advances in colloid and interface science*, 2014, **207**, 306-324.
24. M. Anton, Egg yolk: structures, functionalities and processes, *Journal of the Science of Food and Agriculture*, 2013, **93**, 12, 2871-2880.
25. A.I. Petrov, D.V. Volodkin, and G.B. Sukhorukov, Protein—calcium carbonate coprecipitation: a tool for protein encapsulation, *Biotechnology progress*, 2005, **21**, 3, 918-925.
26. N.A. Feoktistova, N.G. Balabushevich, A.G. Skirtach, D. Volodkin, and A.S. Vikulina, Inter-protein interactions govern protein loading into porous vaterite CaCO 3 crystals, *Physical Chemistry Chemical Physics*, 2020, **22**, 17, 9713-9722.
27. A. Madadlou, J. Floury, S. Pezennec, and D. Dupont, Encapsulation of β-lactoglobulin within calcium carbonate microparticles and subsequent in situ fabrication of protein microparticles, *Food Hydrocolloids*, 2018, **84**, 38-46.
28. Y. Yang, Y. Zhao, M. Xu, Y. Yao, N. Wu, H. Du, and Y. Tu, Effects of strong alkali treatment on the physicochemical properties, microstructure, protein structures, and intermolecular forces in egg yolks, plasma, and granules, *Food Chemistry*, 2020, **311**, 125998.
29. S. Schmidt, M. Behra, K. Uhlig, N. Madaboosi, L. Hartmann, C. Duschl, and D. Volodkin, Mesoporous protein particles through colloidal CaCO3 templates, *Advanced Functional Materials*, 2013, **23**, 1, 116-123.
30. W. Zhang, S. Xiao, and D.U. Ahn, Protein oxidation: basic principles and implications for meat quality, *Critical reviews in food science and nutrition*, 2013, **53**, 11, 1191-1201.
31. A. Bradshaw, M. Salt, A. Bell, M. Zeitler, N. Litra, and A.M. Smith, Cross-linking by protein oxidation in the rapidly setting gel-based glues of slugs, *Journal of Experimental Biology*, 2011, **214**, 10, 1699-1706.
32. Y.N. Tan, J.Y. Lee, and D.I. Wang, Uncovering the design rules for peptide synthesis of metal nanoparticles, *Journal of the American Chemical Society*, 2010, **132**, 16, 5677-5686.
33. J.J. Warren, J.R. Winkler, and H.B. Gray, Redox properties of tyrosine and related molecules, *FEBS letters*, 2012, **586**, 5, 596-602.
34. D.M. Chevrier, A. Chatt, and P. Zhang, Properties and applications of protein-stabilized fluorescent gold nanoclusters: short review, *Journal of Nanophotonics*, 2012, **6**, 1, 064504.
35. J. Xie, Y. Zheng, and J.Y. Ying, Protein-directed synthesis of highly fluorescent gold nanoclusters, *Journal of the American Chemical Society*, 2009, **131**, 3, 888-889.
36. H. Wei, Z. Wang, J. Zhang, S. House, Y.-G. Gao, L. Yang, H. Robinson, L.H. Tan, H. Xing, and C. Hou, Time-dependent, protein-directed growth of gold nanoparticles within a single crystal of lysozyme, *Nature nanotechnology*, 2011, **6**, 2, 93.
37. A. Sani, C. Cao, and D. Cui, Toxicity of gold nanoparticles (AuNPs): A review, *Biochemistry and biophysics reports*, 2021, **26**, 100991.
38. S. Schmidt, K. Uhlig, C. Duschl, and D. Volodkin, Stability and cell uptake of calcium carbonate templated insulin microparticles, *Acta biomaterialia*, 2014, **10**, 3, 1423-1430.
39. A.E.I. Coskun, D. Sağlam, P. Venema, E. van der Linden, and E. Scholten, Preparation, structure and stability of sodium caseinate and gelatin micro-particles, *Food hydrocolloids*, 2015, **45**, 291-300.
40. B. Russell, B. Jachimska, I. Kralka, P. Mulheran, and Y. Chen, Human serum albumin encapsulated gold nanoclusters: effects of cluster synthesis on natural protein characteristics, *Journal of Materials Chemistry B*, 2016, **4**, 42, 6876-6882.
41. B.A. Russell, B. Jachimska, P. Komorek, P. Mulheran, and Y. Chen, Lysozyme encapsulated gold nanoclusters: effects of cluster synthesis on natural protein characteristics, *Physical Chemistry Chemical Physics*, 2017, **19**, 10, 7228-7235.
42. O. Castellani, C. Guérin-Dubiard, E. David-Briand, and M. Anton, Influence of physicochemical conditions and technological treatments on the iron binding capacity of egg yolk phosvitin, *Food Chemistry*, 2004, **85**, 4, 569-577.

43. D.H. Ohlendorf, R.F. Wrenn, and L.J. Banaszak, Three-dimensional structure of the lipovitellin–phosvitin complex from amphibian oocytes, *Nature*, 1978, **272**, 5648, 28-32.
44. J. Schindelin, I. Arganda-Carreras, E. Frise, V. Kaynig, M. Longair, T. Pietzsch, S. Preibisch, C. Rueden, S. Saalfeld, and B. Schmid, Fiji: an open-source platform for biological-image analysis, *Nature methods*, 2012, **9**, 7, 676-682.

3.5 Supporting Information

Additional CLSM image of $CaCO_3$ encapsulating HDL

A 3D construct of a series of Z-stack images of the FITC-labelled HDL encapsulated in $CaCO_3$ templates allowed to visualize the localization of HDL throughout the templates. Figure S3.1 shows that the fluorescent signal of the FITC-labelled HDL is present throughout the whole template, but not homogeneously distributed.

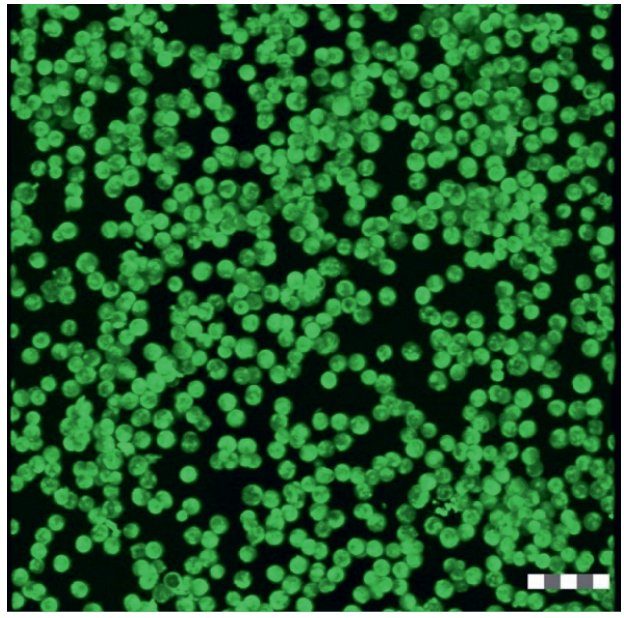

Figure S3.1 CLSM Z-stack (3D reconstruction) of FITC-labelled HDL encapsulated in **$CaCO_3$** templates (scale bar is 25 μm).

Zero surface charge point of HDL

To determine the point of zero surface charge of HDL, zeta-potential measurements were done on HDL solutions at pH 2-12.

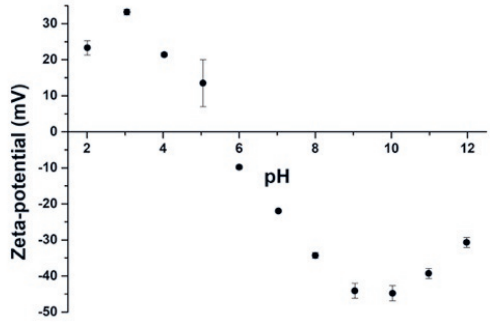

Figure S3.2 The effect of pH on zeta-potential of HDL, the point of zero surface charge was found at pH 5.6.

Additional CLSM and TEM images of HDL-MPs

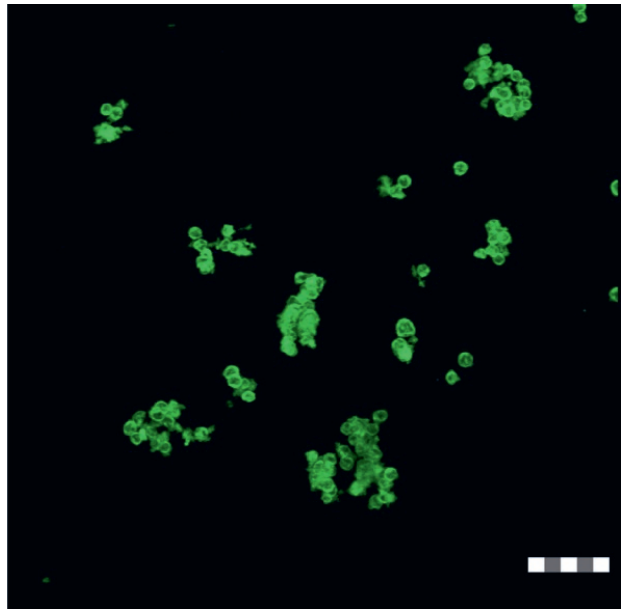

Figure S3.3 CLSM Z-stack (3D reconstruction) of FITC-labelled HDL-MPs (scale bar is 25 μm).

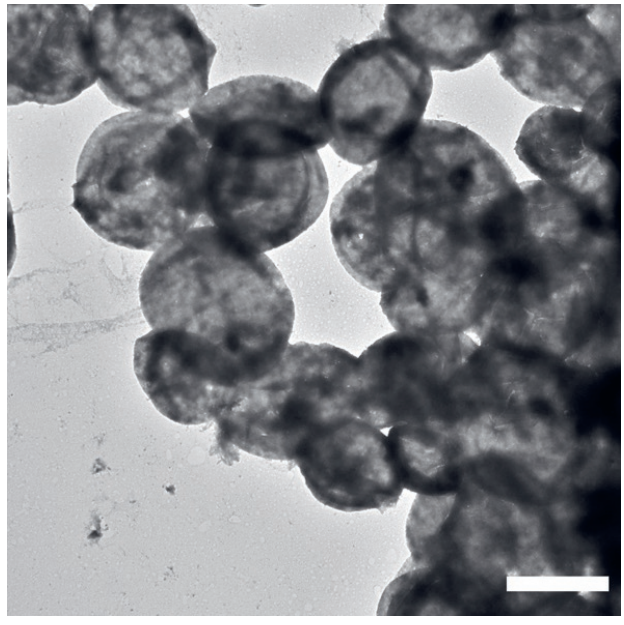

Figure S3.4 Overview TEM image of HDL-MPs, scale bar is 5 μm.

Following the synthesis of AuNPs in time

Au^{3+} ions were added to $CaCO_3$ encapsulating HDL. Initially, the $CaCO_3$ encapsulating HDL were yellow colored (Figure S3.5 A, t = 0 and 0.5 h). The $CaCO_3$ encapsulating HDL gradually changed from yellow to pink, then to red as growth proceeded (t = 2-5 h). When the $CaCO_3$ flocculated, the solutions were transparent and the precipitates were colored (Figure S3.5 B). The color evolution of the $CaCO_3$ encapsulating HDL originates from the characteristic LSPR absorption of AuNPs, indicating the formation and growth of AuNPs inside the $CaCO_3$ templates. When the templates were removed, the Au-HDL-MPs were stable in solution and retained their red color (Figure S3.5 C) The LSPR absorption of the AuNPs was confirmed by UV-Vis absorbance spectra, which demonstrated the appearance and increase of absorption peaks in time in the region of λ = 500-600 nm (Figure S3.5 D).

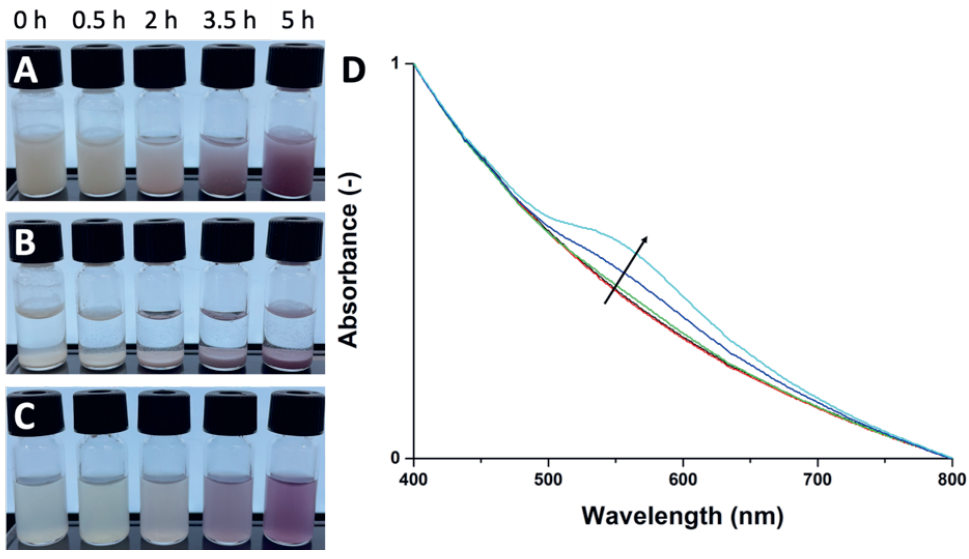

Figure S3.5 Pictures of (A) suspended and (B) flocculated Au-HDL-MPs in **$CaCO_3$** templates and (C) Au-HDL-MPs released from the templates at time points of 0-5 h. (D) Normalized UV-Vis absorbance spectra of Au-HDL-MPs showing a clear red shift of the LSPR peaks in time, as indicated by the arrow. The spectra were normalized at λ = 400 nm. Samples were taken at t = 0, 0.5, 2, 3.5 and 5 h.

Additional CLSM and TEM images of Au-HDL-MPs

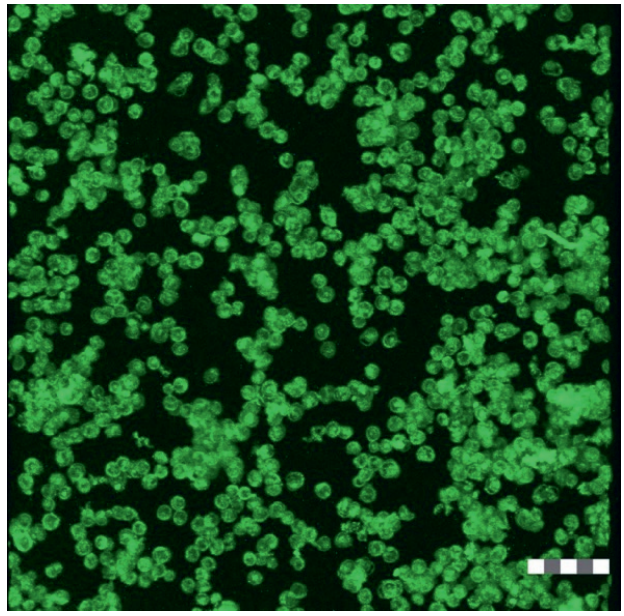

Figure S3.6 CLSM Z-stack (3D reconstruction) of FITC-labelled Au-HDL-MPs (scale bar is 25 μm).

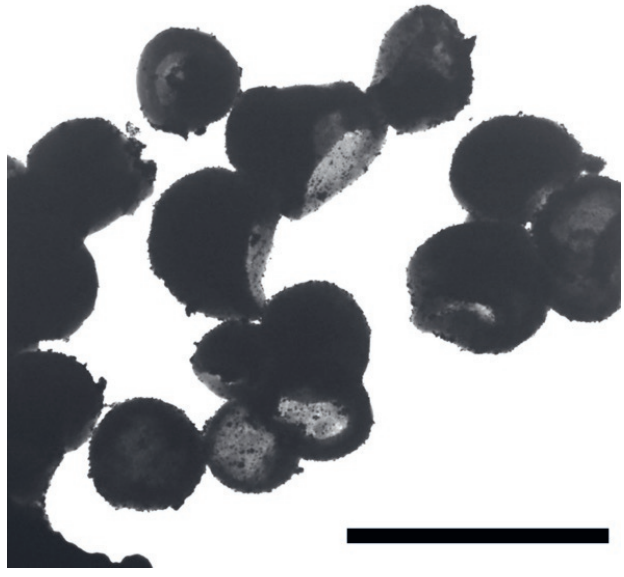

Figure S3.7 Overview TEM image of Au-HDL-MPs, scale bar is 5 μm.

Chapter 4

On the influence of protein aggregate sizes for the formation of solid and hollow protein microparticles

This chapter has been submitted as: L.M.I. Schijven, V. Saggiomo, A.H. Velders, J.H. Bitter, C.V. Nikiforidis (2022). On the influence of protein aggregate sizes for the formation of solid and hollow protein microparticles.

Abstract

Microparticles can function as carriers for different components such as pharmaceuticals and food ingredients. Hollow microparticles can enhance the capacitance as carriers due to their large interior void. Previously, for preparing microparticles, polymers have been assembled into a spherical structure through the use of templates, such as porous $CaCO_3$, followed by cross-linking of the polymers and selective removal of the templates. However, this method often results in the formation of spherical microparticles with a solid core. Here we use proteins with different aggregate size distributions (<10 nm or >100 nm) to either form solid or hollow microparticles. Proteins were mixed with $CaCl_2$ and Na_2CO_3 solutions, which from $CaCO_3$ microcrystals (with 20-60 nm pore size) with encapsulated proteins. Here it will be shown that when the dispersed protein aggregates are smaller than the pore sizes, the proteins were uniformly distributed into the $CaCO_3$ templates. However, when the protein aggregates were larger, the proteins were accumulated at the template edges. Before removal of the templates, the proteins were cross-linked through the use of Au^{3+} ions, which oxidize and cross-link proteins and are reduced to form gold nanoparticles (AuNPs). After removal of the templates, the uniformly distributed proteins formed solid microparticles and the proteins accumulated at the edges formed hollow microparticles. This method of fabrication of solid and hollow protein microparticles, with embedded AuNPs, could be used for generating biomaterials with a broader range of applications, such as hosting molecules and multimodal imaging due to the presence of the AuNPs.

4.1 Introduction

Microparticles are extensively used in biomedical research as carriers of targeted molecules,[1] as biosensors,[2] or for bioimaging.[3] Microparticles can be categorized based on their core density, thus as solid and hollow. The advantage of hollow microparticles is that a large interior void is available for hosting active molecules, such as drugs, genes, or metal nanoparticles.[4] Microparticles are often constructed using synthetic polymers, like polyurethanes,[5] poly(vinyl chloride),[6] silanes,[7] and polymethacrylates.[8] However, there is an increased interest in using biobased polymers, like proteins, because they are readily available from renewable sources.[9] Proteins are excellent candidates for the preparation of microparticles due to the diverse nature of their monomers, which are amino acids. The different amino acid groups in proteins, provide a variety of chemically active sites (e.g. thiol, amine, carboxylic acid groups) for binding guest molecules.[10, 11]

The most commonly used method to assemble proteins into microparticles, is through the use of spherical templates of porous $CaCO_3$ due to its large inner surface area for encapsulation, biocompatibility, easy synthesis and mild sacrificial conditions (e.g. by chelating reagents or under acidic conditions).[12, 13] The $CaCO_3$ templates can act as a cage, holding proteins together,[14] or as a core, on which proteins can form a shell.[15] After cross-linking the proteins and selective removal of the templates, protein microparticles can be obtained.[16] It has been reported that when proteins are encapsulated into $CaCO_3$ templates, solid protein microparticles are obtained.[13] However, in our previous research we show that egg yolk high-density lipoproteins (HDL), assembled into uniquely hollow protein microparticles.[17] We hypothesize that the formation of solid or hollow protein microparticles depends on the size of the protein aggregates. When the protein aggregates are smaller than the $CaCO_3$ template pore sizes (20-60 nm)[18], the proteins uniformly distribute inside the template and form solid protein microparticles. However, when the protein aggregates are larger, they accumulate at the template edges and form hollow protein microparticles.

Here we use proteins with a difference in their tendency to aggregate in an aqueous environment and their subsequent reduced solubility to fabricate solid and hollow protein microparticles (Scheme 4.1). β-lactoglobulin (β-lac) and Bovine Serum Albumin (BSA) were used as representatives of the highly soluble proteins, while caseins and HDL were used as representatives of aggregated proteins. The proteins were mixed with solutions of $CaCl_2$ and Na_2CO_3 and were entrapped into the $CaCO_3$ templates that were formed. Soluble proteins lead to a uniform distribution inside the templates, while the less soluble proteins lead to accumulation at the template edges. Before removal of the templates, proteins were cross-linked through a redox reaction using Au^{3+} ions.[19] This methodology is based on the oxidation of protein amino acids and their subsequent covalent cross-linking. At the same time, the residual amino acid groups of proteins act as reduction sites of Au^{3+} ions and synthesize gold nanoparticles (AuNPs). The embedded AuNPs can have a functional role in bioimaging due to their optical properties.[20, 21]

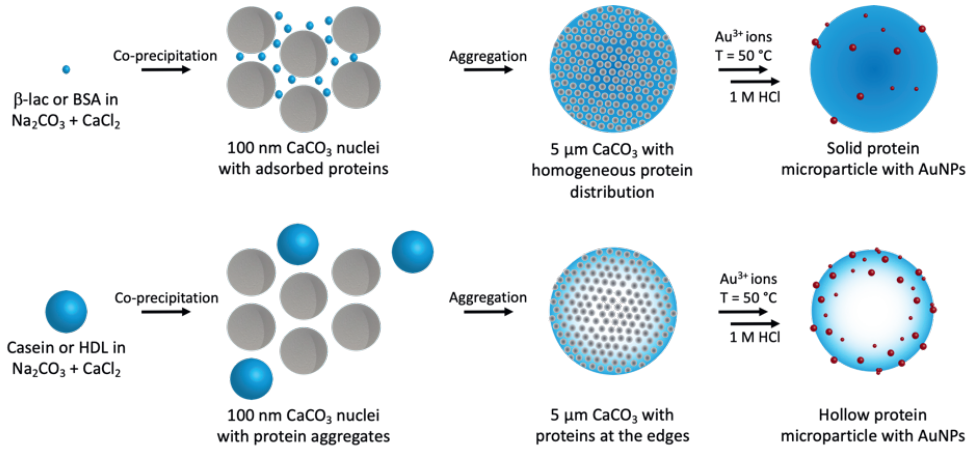

Scheme 4.1 Scheme of the design of solid and hollow protein microparticles, based on different proteins. Top row: soluble proteins (blue spheres), such as β-lac or BSA, are co-precipitated with $CaCl_2$ and Na_2CO_3 and adsorb on the $CaCO_3$ nuclei. After aggregation of the $CaCO_3$ nuclei, micron-sized, spherical $CaCO_3$/protein complexes were formed with homogeneous distribution of proteins. After encapsulation, Au^{3+} ions are added to induce *in situ* covalent cross-linking of the proteins inside the templates. Subsequently, Au^{3+} ions get reduced and form AuNPs (red spheres). Upon decreasing the pH, the $CaCO_3$ dissolves and the solid-like protein microparticles are formed. Bottom row: when using poorly-soluble or aggregated proteins, such as caseins or HDL, the proteins are concentrated at the edges of the templates, resulting in protein microparticles with a hollow-core structure.

This method for the fabrication of hollow and solid microparticles, with embedded AuNPs, will provide possibilities for the formation of highly functional particles for a broad range of applications, such as hosting guest molecules,[22] and multimodal imaging.[23-25]

4.2 Results and Discussion

4.2.1 Protein size distribution in $CaCl_2$ and Na_2CO_3 solutions

$CaCO_3$ templates will be made from $CaCl_2$ and Na_2CO_3 solutions, in which the proteins are present. To investigate the size of the proteins in the presence of the $CaCO_3$ precursor solutions, dynamic light scattering (DLS) was done on the proteins in aqueous (native), $CaCl_2$ or in Na_2CO_3 solutions. In Figure 4.1, the size distributions of the proteins in different aqueous solutions are shown. The graphs of β-lac and BSA showed monomodal size distributions for the proteins of approximately 5.3 nm and 6.7 nm, respectively, under all conditions. The graph of caseins, under native conditions, showed a multimodal size distribution of 33 nm, 350 nm, and 2700 nm. When casein was dispersed in a $CaCl_2$ solution, a bimodal size distribution was observed of 60 nm and 940 nm. However, when casein was dispersed in a Na_2CO_3 solution, the bimodal size distributions were shifted to 10 nm and 1170 nm. The graphs of HDL under native conditions and in Na_2CO_3 solution showed a monomodal size distribution around 13 nm. However, when HDL was dispersed in $CaCl_2$ solution, a multimodal size distribution was observed of 55 nm, 700 nm, and 5070 nm.

β-lac and BSA are relatively soluble proteins in an aqueous environment and did not change in size when mixed with Na_2CO_3 or $CaCl_2$ solutions. Caseins and HDL show larger sizes when dispersed in $CaCl_2$ solution. The larger sizes could be caused by Ca^{2+} induced aggregation. Caseins and HDL contain

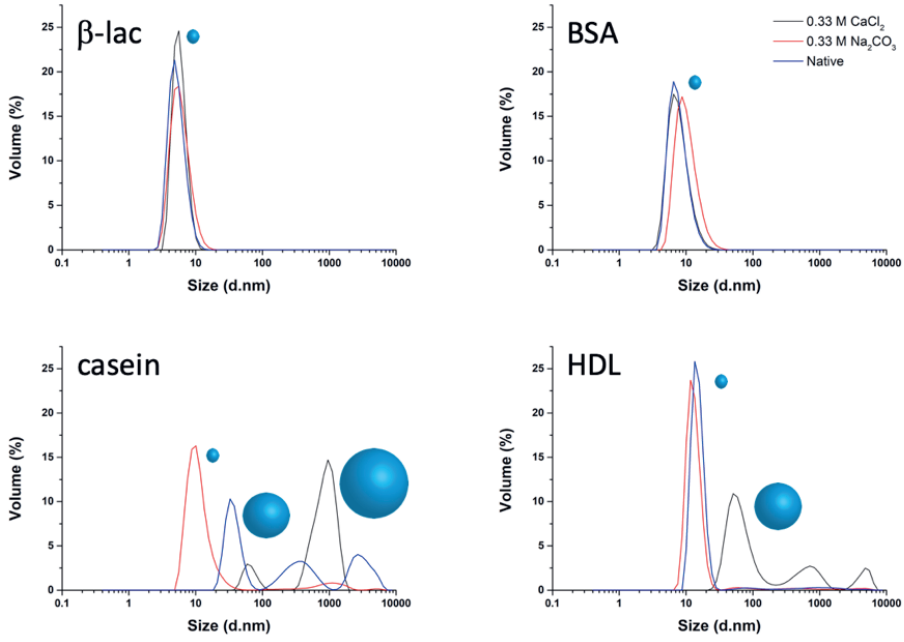

Figure 4.1 Size distributions of β-lac, BSA, caseins, and HDL in native state (blue line), in 0.33 M $CaCl_2$ (black line), and 0.33 M Na_2CO_3 (red line) solutions.

phosphoserine amino acids, of which the phosphate group strongly binds Ca^{2+} ions.[26, 27] And in presence of Ca^{2+} ions, caseins are assembled into micellar structures and HDL forms large aggregates through calcium-phosphate linkages and hydrophobic interactions. Thus to prevent aggregation of the proteins in the starting solution, they were dispersed in Na_2CO_3 solution, before addition of $CaCl_2$ for the encapsulation in $CaCO_3$ templates.

4.2.2 Protein distribution in $CaCO_3$ templates

The $CaCO_3$ templates were then synthesized, in presence of the four different proteins. The Ca^{2+} and CO_3^{2-} ions form $CaCO_3$ microcrystals, while entrapping proteins.[18, 28] The obtained protein/$CaCO_3$ complexes precipitated. To analyze the effect of proteins on the formation of the $CaCO_3$, the size distributions of protein/$CaCO_3$ complexes suspensions were measured using light diffraction. Figure 4.2 A shows the size distributions of the suspensions of the protein/$CaCO_3$ complexes. For β-lac, BSA, and casein, bimodal size distributions were observed of 0.5 μm and 5.0-6.5 μm (Figure 4.2 A-I-III), while for HDL a multimodal size distribution was observed of 0.5 μm, 4.3 μm, and 170 μm (Figure 4.2 A-IV). Previous reports have suggested a size distribution of the $CaCO_3$ templates around 4-6 μm,[29-31] which corroborates with the size ranges (4.3-6.5 μm) obtained in this research. Therefore, the smaller peaks at 0.5 μm were attributed to non-encapsulated protein aggregates. The larger sizes for HDL/$CaCO_3$ complexes (170 μm) was attributed to aggregation due to low repulsive forces[29] between the HDL/$CaCO_3$ complexes.

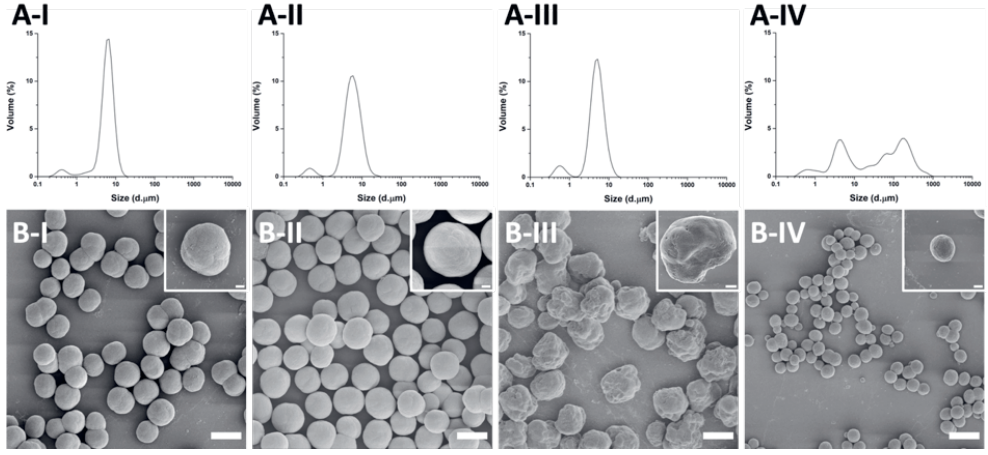

Figure 4.2 (A) Light diffraction measurements and (B) SEM images of $CaCO_3$ templates synthesized through co-precipitation with (I) β-lac, (II) BSA, (III) caseins and (IV) HDL (scale bars are 5 µm). Insets in B show single particles (scale bars are 1 µm), samples were coated with tungsten.

The morphology of the protein/$CaCO_3$ complexes and their surface structure were then analyzed using SEM (Figure 4.2 B I-IV). In the SEM images of the $CaCO_3$ templates, containing β-lac and BSA, spherical structures with a smooth surface were observed (Figure 4.2 B-I,II). However, when the $CaCO_3$ template were synthesized in presence of caseins or HDL, irregular, spherical-like protein/$CaCO_3$ complexes were observed with a rough surface (Figure 4.2 B-III,IV). β-lac and BSA are 7 nm in size, which could not be observed on the particle surface, leading to a smooth surface. However, caseins were assembled and encapsulated as 940 nm aggregates in the spherical $CaCO_3$ template, which lead to a rougher surface. HDL, however, formed smaller (55-700 nm) aggregates, which lead to a smoother surface in comparison to caseins.

The SEM images do not provide information on the protein distribution inside the templates, therefore, to detect and track the proteins, confocal laser scanning microscopy (CLSM) was used. For that, the proteins were covalently labeled with fluorescein isothiocyanate (FITC) before mixing with the precursor salts. The CLSM images of the protein/$CaCO_3$ complexes with all four FITC-labelled proteins are presented in Figure 4.3. In the CLSM images of the $CaCO_3$ templates containing β-lac or BSA, dense spherical shapes are observed (Figure 4.3 A-I,II). The $CaCO_3$ templates containing caseins or HDL showed dense protein rings with a darker internal core (Figure 4.3 A-III,IV). However, since some variations in the shape fill of the templates were observed, a more detailed analysis was done by plotting the fluorescent signals throughout the protein/$CaCO_3$ complexes (Figure 4.3 B). The fluorescent profile plots of β-lac and BSA show a constant fluorescent signal throughout the templates (Figure 4.3 B-I,II). In contrast, the fluorescent signal of caseins was the highest at the edges of the templates and decreased by ~40% towards the inner core (Figure 4.3 B-III). For HDL, a ~60% decrease

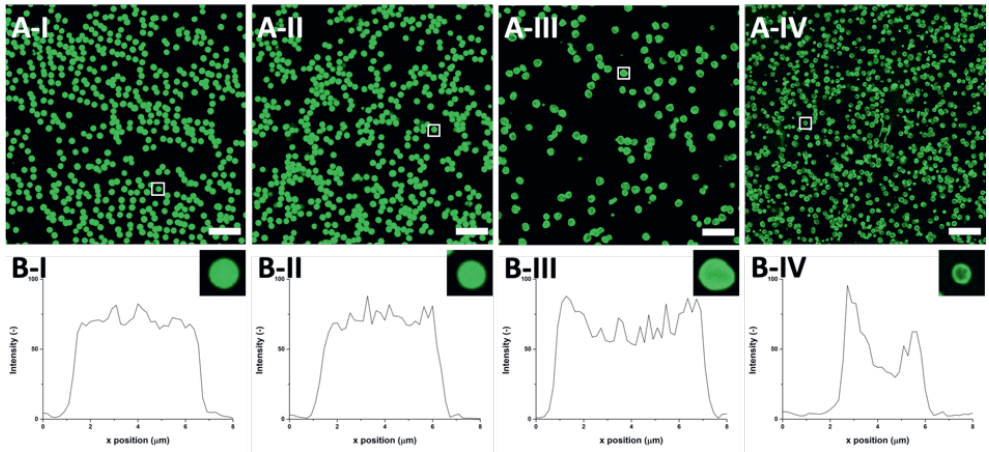

Figure 4.3 (A) CLSM images of $CaCO_3$ templates synthesized through co-precipitation with (I) β-lac, (II) BSA, (III) caseins and (IV) HDL (scale bars are 25 μm, thickness 0.5 μm). (B) The fluorescent profile plots corresponding to single (inset) FITC-protein-encapsulated $CaCO_3$ templates, indicated by the white boxes in A.

of fluorescent signal was observed towards the inner core (Figure 4.3 B-IV). The CLSM images and corresponding fluorescent profile plots show that β-lac and BSA form a uniform distribution inside the templates. However, caseins and HDL accumulate at the edges of the templates.

It was hypothesized that the differences in protein distributions in the templates, uniform or accumulated at the edges, were caused by the differences in sizes of the protein aggregates. When $CaCl_2$ and Na_2CO_3 solutions are mixed in presence of the proteins, porous $CaCO_3$ nuclei crystals are formed, on which the proteins can adsorb.[29, 30] This is followed by mechanical capture of proteins during colloidal aggregation of the $CaCO_3$ nuclei, forming micron-sized spherical protein/$CaCO_3$ particles. β-lac and BSA are present in sizes of approximately 7 nm, so they adsorbed on the initial $CaCO_3$ nuclei and fit in the inner pore size (20-60 nm)[30] of the final $CaCO_3$ microparticle. This resulted in an evenly distributed in the spherical $CaCO_3$.[18] However, caseins and HDL were present as large aggregates, larger than the inner pore sizes of $CaCO_3$. Additionally, the adsorption affinity of protein aggregates to the $CaCO_3$ surface is lower due to their less defined contact area.[32] As a result, they could not be absorbed on the initial nuclei formed, but they were entrapped at a later stage and were accumulated at the edges of the protein/$CaCO_3$ particles.

4.2.3 Obtaining solid and hollow protein microparticles

To obtain the protein microparticles formed in the $CaCO_3$ templates, $CaCO_3$ was removed under acidic conditions. However, before removing the template, it is important to cross-link the proteins and prevent the dissociation of the structures formed.[16] To induce cross-linking with the minimum effect on the spherical structures, Au^{3+} ions were added. It has been reported that Au^{3+} induces protein-protein covalent cross-linking through a redox reaction that takes place at temperatures below the unfolding point of proteins.[19] Au^{3+} can oxidize thiol- or amine-containing side groups of amino acids (e.g. cysteine, lysine) and from covalent bonding.[19] At the same time, Au^{3+} ions are gradually reduced

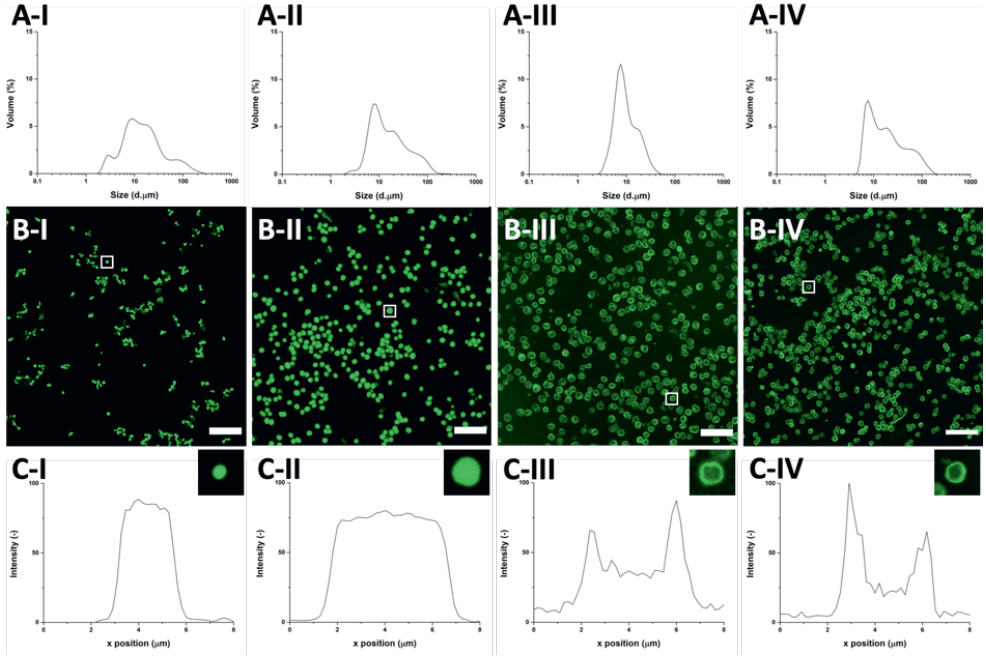

Figure 4.4 (A) Light diffraction measurements and (B) CLSM images of FITC-labelled (I) β-lac, (II) BSA, (III) casein and (IV) HDL microparticles (scale bars are 25 μm, thickness 0.5 μm). (C) The fluorescent profile plots corresponding to single (inset) Au-protein-MPs, indicated by the white boxes in B.

to Au^{+} and Au^{0}, forming AuNPs. A gradual color change was observed after the addition of Au^{3+} ions to the protein/$CaCO_3$ mixture. The reaction mixtures turned from white to pink to red/purple, due to the characteristic surface plasmon resonance absorption of AuNPs.[17]

An indication of the conservation of the spherical structures of the protein microparticles, after cross-linking with Au^{3+} and removal of the template, is by measuring their size distribution. The size distribution data of the obtained protein microparticles, using light diffraction measurements, are presented in Figure 4.4 A. The obtained graphs show that the size distributions of the protein microparticles are in the same size range as before template removal (Figure 4.2 A). However, there are also size distributions observed, which are larger in size than the individual particles. This indicates that the spherical structures are stabilized upon template removal and did not rupture into separate pieces. However, the larger sizes indicate that some microparticles flocculated. The flocculation was reversible and can be attributed to hydrophobic attractive forces.[33]

To confirm whether the protein microparticles kept their structures after cross-linking and template removal, we labelled the proteins with FITC and visualized the obtained protein microparticles using CLSM (Figure 4.4 B). The CLSM images of the β-lac and BSA dispersions demonstrate the presence of spherical particles at a narrow size distribution with a uniform density (Figure 4.4 B-I,II). On the other hand, the CLSM images of the casein and HDL dispersions show again the presence of particles at a narrow size distribution, but with an empty core, as was observed before the template removal (Figure

4.4 B-III,IV). The corresponding fluorescent profile plots of β-lac and BSA microparticles show a constant fluorescent signal throughout the protein microparticles (Figure 4.4 C-I,II). In the case of the casein microparticles, the highest fluorescent signal was observed at the edges of the templates, which decreased by ~60% towards the core (Figure 4.4 C-III). The HDL microparticles had a similar fluorescent signal profile but with a ~75% decrease in the core (Figure 4.4 C-IV).

For analyzing the protein microparticle morphology, SEM was employed as well (Figure 4.5 A). In the SEM images, similar to before the template removal, spherical β-lac and BSA microparticles were observed with a smooth surface (Figure 4.5 A-I,II). The obtained casein microparticles have a rougher surface than before the template removal, however, they appear as a bit flattened with folds and creased structures (Figure 4.5 A-III). During SEM imaging, the protein microparticles are under drying and vacuum conditions. The fact that the β-lac and BSA microparticles retained their spherical structures without flattening upon drying, is additional proof that they have a dense and solid protein core (Figure 4.5 A-I,II). The hollow casein microparticles keep their structure after template removal, but were flattened upon dehydration. In the case of the HDL hollow microparticles, a relatively smooth surface could be observed, which formed discs, similar to blood cells ,upon drying for the SEM analysis (Figure 4.5 A-IV). The formation of the HDL discs indicates the formation of a homogeneous network after the cross-linking, which results in hollow particles with elastic and deformable edges.

In addition to SEM, TEM imaging was done on the protein microparticles to investigate their morphology and density (Figure 4.5 B). In the TEM images, the β-lac and BSA microparticles appeared as dense and spherical protein matrices (Figure 4.5 B-I,II). The casein and HDL microparticles had areas with light grey color and darker shades (Figure 4.5 B-III,IV) that were similar to the folds and creases structures observed in the SEM images. The light areas on the casein and HDL microparticles is an indication that they are less dense areas than the dark black areas observed with the β-lac and BSA particles.

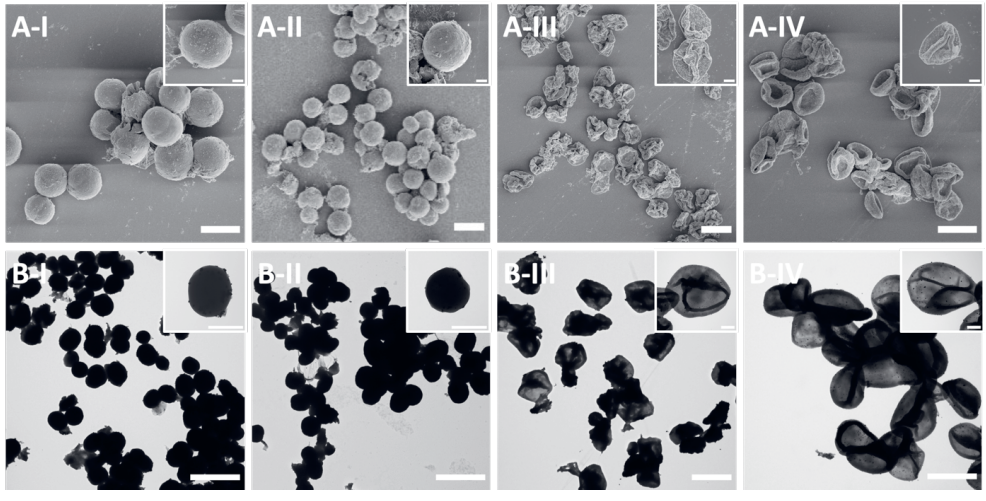

Figure 4.5 (A) SEM and (B) TEM images of ((I) β-lac, (II) BSA, (III) casein and (IV) HDL microparticles (scale bars are 5 μm). Insets show single particles (scale bars are 1 μm). SEM samples were coated with tungsten.

4.2.4 AuNPs on the solid and hollow protein microparticles

In the SEM and TEM images some spherical nano-sized particles are observed on the surface of all the protein particles. The nanoparticles could be originated from proteins, remaining $CaCO_3$, or AuNPs that formed after the addition of Au^{3+} to initiate cross-linking of the proteins. To investigate the nature of the nanoparticles, we performed SEM energy-dispersive X-ray spectroscopy (EDX) as presented in Figure 4.6. Figure 4.6 A shows the SEM image of a single microparticle made with β-lac (I), BSA (II), caseins (III), and HDL (IV), where the nanoparticles are observed on the surface of the microparticles. Figures 4.6 B-D show the EDX analysis for carbon (Figure 4.6 B), gold (Figure 4.6 C) and an overlay of carbon and gold (Figure 4.6 D) for each protein microparticle. When the particles were analyzed for carbon (Figure 4.6 B), a carbon signal could be observed throughout the whole particles. However, there was no signal present at the location of the nanosized spherical particles, showing that the nanoparticles on the surface are not carbon-based materials. When the microparticles were analyzed

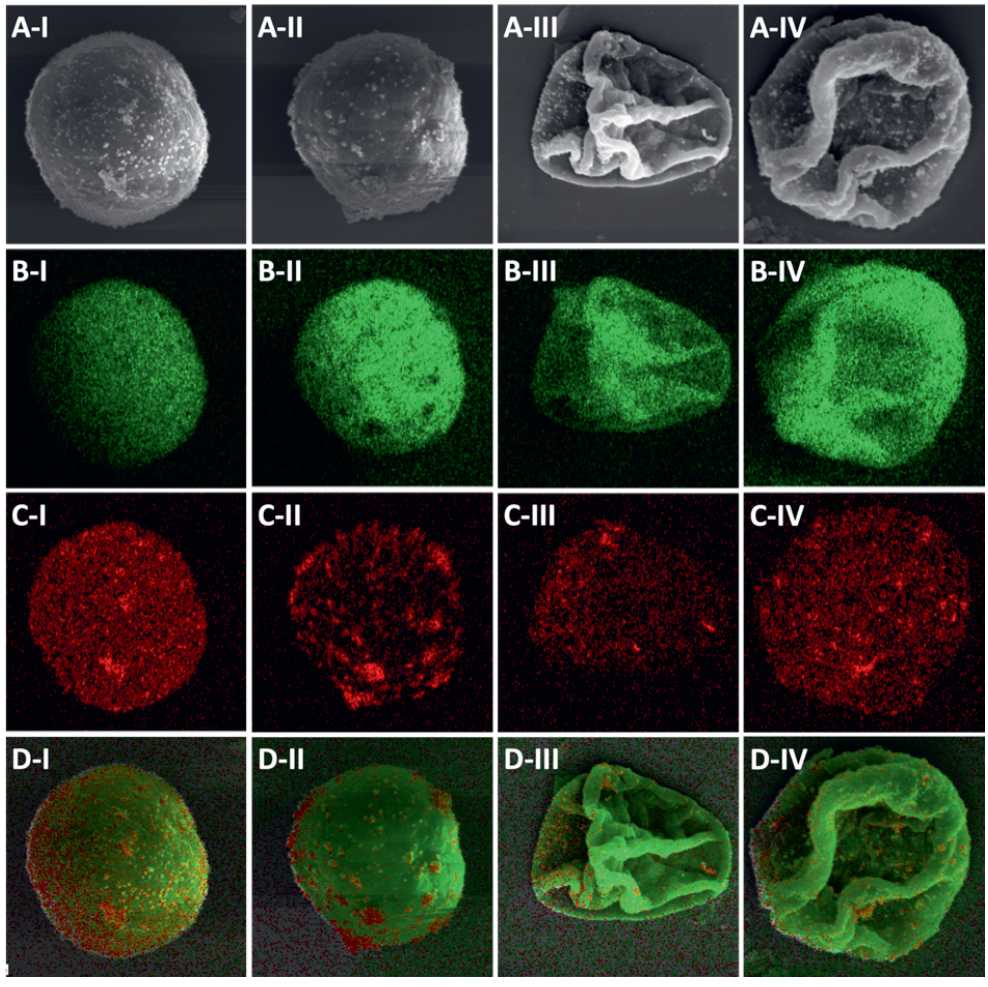

Figure 4.6 (A) SEM images of (I) β-lac, (II) BSA, (III) casein and (IV) HDL microparticles and the corresponding elemental X-ray maps of (B) carbon, (C) gold, (D) overlay of carbon (green) and gold (red). The images are 5x5 μm.

for Au, a clear Au signal could be detected at the spots where the nanoparticles were present (Figure 4.6 C). The elemental mapping of Au and overlay of the mapping of both carbon and Au (Figure 4.6 D), show that the AuNPs, that were formed after the reduction of Au^{3+}, were spread on the surface of the protein microparticles. AuNPs can interact with sulfur and amine groups of the protein amino acids,[34] which bind the AuNPs on the protein particle surface. Besides that, it has been reported that AuNPs are positively charged, due to Au ions (Au^{3+} and/or Au^{+}) that remain on their surface and are not reduced to Au^{0}.[35] All proteins used are negatively charged at pH 7, therefore it is possible that attractive electrostatic forces took place between the positively charged AuNPs and the negatively charged proteins to hold the AuNPs on the protein microparticle surface.

4.3 Conclusion

In this research, we showed that solid and hollow protein microparticles can be formed, based on the difference in the tendency of the proteins to aggregate in an aqueous environment and their subsequent solubility. When the dispersed protein assemblies are below the size of the $CaCO_3$ inner pores (i.e. β-lac, BSA), the proteins are uniformly distributed inside the templates. This uniform distribution is conserved after cross-linking and template removing, resulting in solid protein microparticles. However, when the dispersed protein assemblies have a larger diameter than the $CaCO_3$ inner pores (i.e. caseins, HDL), the proteins accumulate at the edges of the template. This resulted in the formation of hollow protein microparticles. The mechanism suggested for using the size of protein aggregates for the fabrication of solid or hollow protein microparticles opens new paths on the design of biocompatible and functional particles. The use of proteins has the advantage that their chain is comprised of a combination of amino acids, which provide a variety of chemically active sites to interact with hosted molecules. The protein microparticles can find applications as carriers of therapeutics, and besides that, the presence of the AuNPs makes the suggested hybrid structure an attractive platform as a multimodal imaging agent due to the optical, high electron density, and high attenuation coefficient properties of AuNPs.

4.4 Experimental section

4.4.1 Materials

Fresh hen eggs were purchased from a local organic farm De Hoge Born, Wageningen, the Netherlands. Sodium chloride (NaCl, ≥99.5%), 1 M NaOH and 1 M HCl solutions were purchased from VWR International B.V. β-lactoglobulin from bovine milk (β-lac, 85%), Serum albumin from bovine blood (BSA, 98%), caseins from bovine milk (87-94%), gold(III) chloride hydrate ($HAuCl_4 \cdot xH_2O$, 99.5%), Fluorescein-5-isothiocyanate (FITC, ≥95%), calcium chloride ($CaCl_2$, ≥93%), sodium carbonate (Na_2CO_3, ≥99.5%) and 76 mm dialysis tubing cellulose membrane (MWCO = 14 kDa) were purchased from Sigma Aldrich. All chemicals were used without further purification and deionized water was used throughout the experiments.

4.4.2 Methods

Extraction of HDL

HDL was extracted from egg yolk according to the method developed by Castellani *et al.*,[36] with slight modifications. Hen eggs were cracked and the egg yolks were separated manually from the albumen. The egg yolks were carefully rolled on a paper tissue to remove the chalazae and adhering albumen. The yolk membranes were then punctured, using a glass pipette, and their contents were collected and pooled in a beaker cooled in iced water. The liquid yolks were diluted with 3 volumes of 0.17 M NaCl (1% (w/v)) and homogenized by stirring for 1 h. The yolk was fractionated into plasma and granules by centrifugation at 10,000 x g for 45 min at T = 4 °C, using a Thermoscientific Sorvall Legend XFR centrifuge. The pellet (granules) was washed with 0.17 M NaCl and centrifuged once more. The granules were suspended in 1.71 M NaCl (10% (w/v)) and the solution's pH was adjusted to 7.25, using 1 M NaOH. The mixtures were collected in dialysis tubings and were dialyzed against deionized water with 3 changes over 24 h. The HDLs were precipitated. The content of the dialysis tubings was collected and centrifuged. The pellets, rich in HDL, were collected and freeze-dried, using a Salmenkipp alpha 2-4 plus freeze-dryer at a temperature of T = -76 °C and pressure of 0.0090 mbar for 72 h.

Labelling of proteins with FITC

FITC was coupled to the proteins by an isothiocyanate/amine reaction according to the manufacturer's protocol. Briefly, 100 mg of protein was dissolved in 20 mL of 0.1 sodium carbonate buffer, pH 9, by stirring (5 mg/mL protein). For each protein solution, 18.4 µL of 26 nM FITC in DMSO was added, while gently and continuously stirring. The mixture was allowed to react overnight, while covered against light. The mixture was then dialyzed against deionized water with five changes over 24 h. The contents of the dialysis bags were collected and used directly for further experiments by adding solid precursor salt to the FITC-protein solutions.

Preparation of protein-encapsulated $CaCO_3$ templates

For encapsulation of proteins into porous, spherical $CaCO_3$ templates, a procedure reported by Volodkin et al. (2004)[18] was followed with slight modifications. 20 mL of a 0.33 M $CaCl_2$ solution was rapidly poured into 20 mL of 0.33 M Na_2CO_3 containing 5 mg/mL of β-lac, BSA, casein, or HDL while stirring at 700 RPM using a magnetic stirrer. A white precipitate formed instantly upon mixing. The

stirring speed was subsequently increased to 2500 RPM for 30 s. The sample was then removed from the stirring plate and was left standing for 15 min to facilitate the formation of $CaCO_3$. The suspended protein-encapsulated $CaCO_3$ was collected by centrifugation at 7,200 x g for 5 min (Thermo Scientific ST 8R centrifuge) and washed 3 times with 10 mL of deionized water to remove non-bound protein.

Preparation of Au-protein microparticles

Au^{3+} ions were added as a solution (59.2 μmol, at pH 7) to 30 mL of suspended protein-encapsulated $CaCO_3$ templates, in 1.71 M NaCl. The mixture was allowed to incubate at T = 50 °C overnight, while being stirred at 700 RPM. The templates were removed by adjusting the pH of the solution to 1.5 by the addition of a 1 M HCl solution. Finally, the Au-protein microparticles were collected by centrifugation (7,200 x g, 5 min) and washed 3 times with 10 mL of deionized water.

4.4.3 Characterization

Size distributions

For size determination of the protein-encapsulated $CaCO_3$ templates and Au-protein microparticles, suspensions in a hydro dispenser were measured by light diffraction (Bettersizer Instruments). The effect of the presence of salts on the protein size distribution was measured by dynamic light scattering (DLS) measurements at 173°, with a 400 mW argon-helium laser, operating at a wavelength of λ = 632 nm at room temperature (Malvern ZS Nanosizer). For native conditions, β-lac and BSA were dissolved in 5 mM Tris-HCl buffer pH 7, caseins in deionized water pH 10, and HDL in 1.71 M NaCl pH 7. 5 mg/mL protein solutions were prepared in 0.33 M $CaCl_2$ and 0.33 M Na_2CO_3.

Scanning Electron Microscopy (SEM)

A 20 μL droplet of the sample was put onto a mica sheet surface. After 1 minute, the excess fluid was removed. 100 μL of deionized water was used to remove excess, non-stuck particles from the mica surface. The surface was dried by a filter paper and was then mounted onto sample holders containing carbon adhesive tabs. Before imaging, the sample was coated with 10 nm tungsten. The samples were then imaged with a FEI Magellan 400 SEM, operating at 2 kV and the images were analyzed using FIJI software.[37] Elemental maps of carbon and gold were obtained with the use of an Aztec Energy-dispersive X-ray Spectrometer.

Confocal Laser Scanning Microscopy (CLSM)

For CLSM imaging, FITC-labelled proteins were used during the experiments. The protein-encapsulated $CaCO_3$ and Au-protein microparticles were imaged using a Leica SP8-SMD microscope. The FITC was excited with $\lambda_{ex,max}$ = 490 nm and emission was collected at $\lambda_{em,max}$ = 525 nm. The laser intensity for protein-encapsulated $CaCO_3$ was set at 30% and for Au-protein microparticles at 50%. The images were analyzed using FIJI software.

Transmission Electron Microscopy (TEM)

TEM sample preparation was done by pipetting 6 μL of sample onto a carbon-coated hexagonal 400 mesh copper grid. After 1 min, a filter paper was used to remove excess fluid. After air drying, the

samples were imaged using a JEOL JEM1400+ microscope, operating at 120 kV. The images were analyzed using FIJI software.

References

1. M. Lengyel, N. Kállai-Szabó, V. Antal, A.J. Laki, and I. Antal, Microparticles, microspheres, and microcapsules for advanced drug delivery, *Scientia Pharmaceutica*, 2019, **87**, 3, 20.
2. B. Yin, X. Liu, H. Gao, T. Fu, and J. Yao, Bioinspired and bristled microparticles for ultrasensitive pressure and strain sensors, *Nature communications*, 2018, **9**, 1, 1-8.
3. F.M. Galogahi, Y. Zhu, H. An, and N.-T. Nguyen, Core-shell microparticles: Generation approaches and applications, *Journal of Science: Advanced Materials and Devices*, 2020, **5**, 4, 417-435.
4. W. Wichaita, D. Polpanich, and P. Tangboriboonrat, Review on synthesis of colloidal hollow particles and their applications, *Industrial & Engineering Chemistry Research*, 2019, **58**, 46, 20880-20901.
5. E. Campos, R. Cordeiro, P. Alves, M. Rasteiro, and M. Gil, Polyurethane-based microparticles: formulation and influence of processes variables on its characteristics, *Journal of microencapsulation*, 2008, **25**, 3, 154-169.
6. A. Tomas, M. Gil, J. Bordado, P. Goncalves, and P. Rodrigues, Preparation of poly (vinyl chloride) latexes using a dual surfactant system: the effect in the particle size distribution, *Journal of applied polymer science*, 2009, **112**, 3, 1416-1424.
7. H. Jaganathan and B. Godin, Biocompatibility assessment of Si-based nano-and micro-particles, *Advanced drug delivery reviews*, 2012, **64**, 15, 1800-1819.
8. J. Tan, G. Zhao, Y. Lu, Z. Zeng, and M.A. Winnik, Synthesis of PMMA microparticles with a narrow size distribution by photoinitiated raft dispersion polymerization with a macromonomer as the stabilizer, *Macromolecules*, 2014, **47**, 19, 6856-6866.
9. E. Campos, J. Branquinho, A.S. Carreira, A. Carvalho, P. Coimbra, P. Ferreira, and M. Gil, Designing polymeric microparticles for biomedical and industrial applications, *European Polymer Journal*, 2013, **49**, 8, 2005-2021.
10. L. Schoonen and J.C. van Hest, Functionalization of protein-based nanocages for drug delivery applications, *Nanoscale*, 2014, **6**, 13, 7124-7141.
11. R. Van Vught, R.J. Pieters, and E. Breukink, Site-specific functionalization of proteins and their applications to therapeutic antibodies, *Computational and structural biotechnology journal*, 2014, **9**, 14, e201402001.
12. D.V. Volodkin, A.I. Petrov, M. Prevot, and G.B. Sukhorukov, Matrix polyelectrolyte microcapsules: new system for macromolecule encapsulation, *Langmuir*, 2004, **20**, 8, 3398-3406.
13. D.V. Volodkin, R. von Klitzing, and H. Möhwald, Pure protein microspheres by calcium carbonate templating, *Angewandte Chemie*, 2010, **122**, 48, 9444-9447.
14. S. Schmidt, M. Behra, K. Uhlig, N. Madaboosi, L. Hartmann, C. Duschl, and D. Volodkin, Mesoporous protein particles through colloidal CaCO3 templates, *Advanced Functional Materials*, 2013, **23**, 1, 116-123.
15. N.G. Balabushevich, E.A. Sholina, E.V. Mikhalchik, L.Y. Filatova, A.S. Vikulina, and D. Volodkin, Self-assembled mucin-containing microcarriers via hard templating on CaCO3 crystals, *Micromachines*, 2018, **9**, 6, 307.
16. S. Schmidt and D. Volodkin, Microparticulate biomolecules by mild CaCO 3 templating, *Journal of Materials Chemistry B*, 2013, **1**, 9, 1210-1218.
17. L.M. Schijven, T.D. Vogelaar, S. Sridharan, V. Saggiomo, A.H. Velders, J.H. Bitter, and C.V. Nikiforidis, Hollow protein microparticles formed through cross-linking by an Au 3+ initiated redox reaction, *Journal of Materials Chemistry B*, 2022, **10**, 6287-6295.
18. D.V. Volodkin, N.I. Larionova, and G.B. Sukhorukov, Protein encapsulation via porous CaCO3 microparticles templating, *Biomacromolecules*, 2004, **5**, 5, 1962-1972.
19. L.M. Schijven, V. Saggiomo, A.H. Velders, J.H. Bitter, and C.V. Nikiforidis, Au 3+-Induced gel network formation of proteins, *Soft Matter*, 2021, **17**, 42, 9682-9688.
20. R. De La Rica and A.H. Velders, Supramolecular Au Nanoparticle Assemblies as Optical Probes for Enzyme-Linked Immunoassays, *Small*, 2011, **7**, 1, 66-69.

21. R. de laRica, R.M. Fratila, A. Szarpak, J. Huskens, and A.H. Velders, Multivalent nanoparticle networks as ultrasensitive enzyme sensors, *Angewandte Chemie International Edition*, 2011, **50**, 25, 5704-5707.
22. L. Chen, G.E. Remondetto, and M. Subirade, Food protein-based materials as nutraceutical delivery systems, *Trends in Food Science & Technology*, 2006, **17**, 5, 272-283.
23. J. Hainfeld, D. Slatkin, T. Focella, and H. Smilowitz, Gold nanoparticles: a new X-ray contrast agent, *The British journal of radiology*, 2006, **79**, 939, 248-253.
24. X. Huang and M.A. El-Sayed, Gold nanoparticles: Optical properties and implementations in cancer diagnosis and photothermal therapy, *Journal of advanced research*, 2010, **1**, 1, 13-28.
25. X. Huang, P.K. Jain, I.H. El-Sayed, and M.A. El-Sayed, Plasmonic photothermal therapy (PPTT) using gold nanoparticles, *Lasers in medical science*, 2008, **23**, 3, 217-228.
26. Y.D. Livney, Milk proteins as vehicles for bioactives, *Current opinion in colloid & interface science*, 2010, **15**, 1-2, 73-83.
27. M. Anton, Egg yolk: structures, functionalities and processes, *Journal of the Science of Food and Agriculture*, 2013, **93**, 12, 2871-2880.
28. G.B. Sukhorukov, D.V. Volodkin, A.M. Günther, A.I. Petrov, D.B. Shenoy, and H. Möhwald, Porous calcium carbonate microparticles as templates for encapsulation of bioactive compounds, *Journal of Materials Chemistry*, 2004, **14**, 14, 2073-2081.
29. A. Madadlou, J. Floury, S. Pezennec, and D. Dupont, Encapsulation of β-lactoglobulin within calcium carbonate microparticles and subsequent in situ fabrication of protein microparticles, *Food Hydrocolloids*, 2018, **84**, 38-46.
30. A.I. Petrov, D.V. Volodkin, and G.B. Sukhorukov, Protein—calcium carbonate coprecipitation: a tool for protein encapsulation, *Biotechnology progress*, 2005, **21**, 3, 918-925.
31. Y. Liu, Y. Cui, H. Mao, and R. Guo, Calcium carbonate crystallization in the presence of casein, *Crystal growth & design*, 2012, **12**, 10, 4720-4726.
32. A. Vikulina, N. Feoktistova, N. Balabushevich, A. Skirtach, and D. Volodkin, The mechanism of catalase loading into porous vaterite CaCO 3 crystals by co-synthesis, *Physical Chemistry Chemical Physics*, 2018, **20**, 13, 8822-8831.
33. M. Tirado-Miranda, A. Schmitt, J. Callejas-Fernandez, and A. Fernandez-Barbero, The aggregation behaviour of protein-coated particles: a light scattering study, *European Biophysics Journal*, 2003, **32**, 2, 128-136.
34. H.E. Toma, V.M. Zamarion, S.H. Toma, and K. Araki, The coordination chemistry at gold nanoparticles, *Journal of the Brazilian Chemical Society*, 2010, **21**, 7, 1158-1176.
35. M. Wuithschick, A. Birnbaum, S. Witte, M. Sztucki, U. Vainio, N. Pinna, K. Rademann, F. Emmerling, R. Kraehnert, and J.r. Polte, Turkevich in new robes: key questions answered for the most common gold nanoparticle synthesis, *ACS nano*, 2015, **9**, 7, 7052-7071.
36. O. Castellani, C. Guérin-Dubiard, E. David-Briand, and M. Anton, Influence of physicochemical conditions and technological treatments on the iron binding capacity of egg yolk phosvitin, *Food Chemistry*, 2004, **85**, 4, 569-577.
37. J. Schindelin, I. Arganda-Carreras, E. Frise, V. Kaynig, M. Longair, T. Pietzsch, S. Preibisch, C. Rueden, S. Saalfeld, and B. Schmid, Fiji: an open-source platform for biological-image analysis, *Nature methods*, 2012, **9**, 7, 676-682.

Chapter 5

Formation of protein microgels with spherical and urchin-like shapes within a fully aqueous droplet reactor

A manuscript of this chapter is in preparation as: L.M.I. Schijven,[*] K. Hu,[*] A. Madadlou, V. Fogliano, J.H. Bitter, C.V. Nikiforidis, A.H. Velders, V. Saggiomo. Formation of protein microgels with spherical and urchin-like shapes within a fully aqueous droplet reactor

[*]The authors have contributed equally to this work and share first authorship

Abstract

Protein-based microgels are used in various fields, such as in sensors, catalysis, separation technology, and encapsulation of host molecules. Compared to common spherically shaped microgels, branched (urchin-like) microgels have attracted considerable attention due to their much higher surface area to volume ratio. However, common templating methods for preparing microgels often result in spherical microgels due to the fixed shape of the templates. Here we report the fabrication of urchin-like and spherical microgels through the use of egg yolk high-density lipoproteins (HDL) within a fully aqueous droplet reactor (FADR), followed by cross-linking. The FADR is composed of an aqueous two-phase system (ATPS), in which HDLs are compartmentalized in the droplet phase. HDL is then cross-linked through the use of Au^{3+} ions, which oxidize and cross-link proteins and are reduced to form gold nanoparticles (AuNPs). We show that random aggregates, urchin-like, and spherical microgels can be formed by changing the HDL concentration and pH values in the FADRs. We propose that this method for generating urchin-like and spherical microgels may be used for generating other biomaterials for applications in drug delivery and photocatalytic reactions.

5.1 Introduction

Microgels are an intriguing class of polymeric materials, partly because they are soft, while having a stable structure of the cross-linked network.[1] These properties offer possibilities for multivalent bioconjugation for specific targets[2-4] and the incorporation of bioactive molecules,[5, 6] which make microgels attractive vehicles for sensing, catalysis, and encapsulation and releasing applications.

Microgels are predominantly fabricated with synthetic polymers, like poly-acrylates,[7] polylactide, and polyurethane.[1] Synthetic polymers are synthesized by polymerization of monomers, which allows control over their properties, such as mechanical, thermal stability, length, functional groups.[8] However, synthetic materials are often produced from monomers derived from non-renewable resources. Accordingly, there is an increasing interest to use biobased materials, which are readily available from renewable resources.[9] Amongst the available biobased materials, proteins are excellent candidates for the preparation of microgels due to the presence of different amino acid residues, which contain chemically active sites (e.g. thiol, amine, carboxylic acid groups) for cross-linking.[10]

In our previous research, it was found that proteins can be cross-linked through the use of Au^{3+} ions.[11] The Au^{3+} ions oxidize protein amino acids and subsequently covalently cross-link proteins, specifically egg yolk high-density lipoprotein (HDL), and form a gel network. Upon protein oxidation, residual amino acid groups of proteins act as natural reduction sites of Au^{3+} ions and synthesize gold nanoparticles (AuNPs). It was also found that the Au^{3+} ions could be used to initiate cross-linking of proteins inside a solid template, such as porous $CaCO_3$, to form protein microparticles with embedded AuNPs.[12] By using proteins with different aggregate size distributions, such as β-lactoglobulins, bovine serum albumins, caseins, and HDL, we could form protein microparticles with solid or hollow-core densities. However, the protein microparticles have a fixed size and spherical shape due to the solid $CaCO_3$ templates.

The majority of the microgels have a spherical shape because it has a uniform and predictable surface area.[13] However, non-spherical microgels, e.g. urchin-like (containing multiple branches), provide a much higher surface area to volume ratio, depending on the height and thickness of the branches. The urchin-like microgels expose more active sites for functionalization with targeting molecules[14] or absorption of light to improve photocatalytic reactions.[15] Microgels can be formed by using liquid biphasic systems, or emulsions, as droplet reactors. An emulsion is a transient system of two immiscible solutions, of which one liquid is dispersed (droplet phase) into the other liquid (continuous phase). The droplets serve as compartmentalized microreactors for preparing microgels. Moreover, the droplets can deform by changing the volume of the droplet phase in presence of the continuous phase.[16] The change in volume creates an osmotic pressure, which could aid in forming branches on the droplets. The most well-known pair for making emulsions is organic solvent (oil) and water, which do not mix due to differences in hydrophobicity/hydrophilicity. The use of organic solvents and (edible) oils is undesired because it can cause denaturation of biological compounds at the interfaces. As an alternative, fully aqueous droplet reactors (FADRs), which are prepared by emulsification of aqueous two-phase systems (ATPSs), are considered of great potential. ATPSs are mixtures of immiscible aqueous solutions, containing high concentrations of multiple water-soluble additives, that phase

separate at above a critical concentration threshold.[17] Formation of FADRs from ATPSs does not require oil or organic phases and can be easily removed through dialysis or centrifugation.

In this research, we will show that we can form microgels within a FADR, by using Au^{3+} ions to cross-link the proteins (Scheme 5.1). HDL was compartmentalized in an ATPS of a Na_2SO_4 solution as droplet phase, dispersed in a polyethylene glycol (PEG) solution as continuous phase. The Au^{3+} ions were added as an aqueous solution, which oxidizes protein amino acids and subsequently forms covalent cross-linking between the proteins. By preparing the FADRs at low, medium, high HDL concentrations (5-40 mg/mL) and pH values (5-9), followed by the addition of Au^{3+} ions, different shapes of microgels could be obtained, such as cross-linked random aggregates, urchin-like microgels, and spherical microgels.

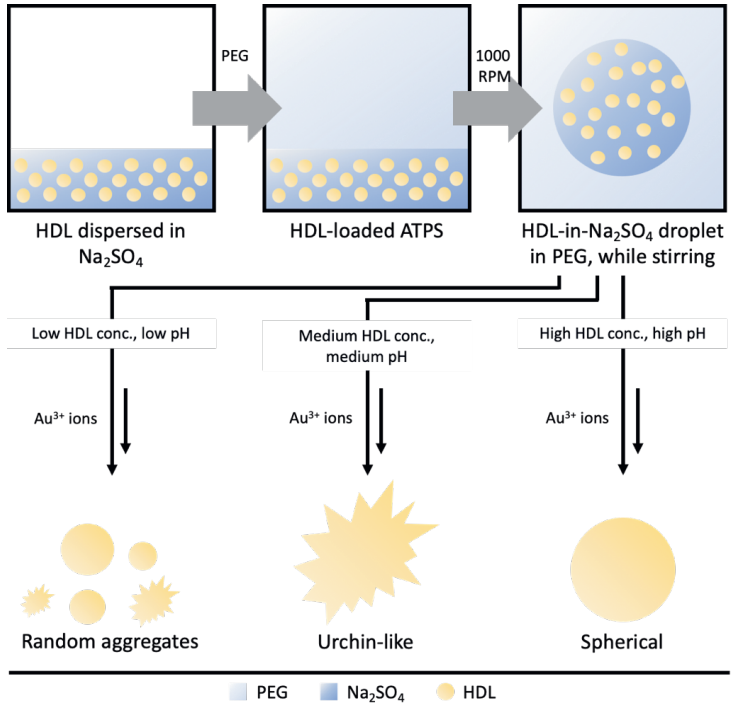

Scheme 5.1 Schematic overview of protein microgel formation within a FADR. HDL was loaded in Na_2SO_4, before mixing with PEG. A Na_2SO_4-in-PEG ATPS type was formed, while stirring, compartmentalizing HDL. The FADRs were prepared at low HDL conc. (5 mg/mL), low pH (pH 5), medium HDL conc. (10-20 mg/mL), medium pH (pH 7), and high HDL conc. (40 mg/mL), high pH (pH 9). Au^{3+} ions were added as an aqueous solution (at 500 molar equivalents to HDL) to cross-link the proteins. After 30 minutes of stirring, the FADRs were diluted 10x with deionized water. FADRs prepared at low HDL conc., low pH, resulted in the formation of random aggregates. Urchin-like microgels were obtained at medium HDL conc., medium pH. Spherical microgels were obtained at high HDL conc., high pH.

5.2 Results and Discussion

The microgels were prepared using a FADR, where the droplets serve as compartmentalized microreactors. The FADRs were made from an ATPS of solutions of PEG and Na_2SO_4, which do not mix. The FADRs were loaded with HDL at low, medium, and high HDL concentrations and pH values to study the behavior of HDL in the droplet phase in the ATPSs. This was followed by the addition of Au^{3+} ions as an aqueous solution to initiate protein oxidation and cross-linking. Different shapes of microgels, such as random aggregates, urchin-like, and spherical, were obtained at low, medium, and high HDL conc. and pH conditions, respectively. The structures of the obtained microgels were imaged with brightfield and fluorescence microscopy, and confocal laser scanning microscopy (CLSM).

5.2.1 Loading HDL in fully aqueous droplet reactors at pH 5-9

FADRs can be prepared from pairs of non-charged polymers (e.g. PEG and dextran (Dex)), non-charged polymer with a salt (e.g. PEG and Na_2SO_4), non-charged and charged polymer (e.g. PEG and chitosan), and two co-charged polymers.[18] The most commonly used ATPS pair is made of PEG and Dex. However, Dex can directly reduce Au^{3+} ions,[19] which would affect the reactivity between the Au^{3+} ions and the proteins. Additionally, HDL is poorly soluble in PEG and Dex because HDL has a high molecular weight and solubilizes under high ionic strength conditions.[20] Accordingly, the FADRs were prepared from solutions of PEG and Na_2SO_4, which are known to separate into two immisicible liquid phases, either rich in PEG or Na_2SO_4.[21] Additionally, a 7:3 volume ratio of PEG/Na_2SO_4 was chosen to create a FADR with Na_2SO_4 as the droplet phase, and PEG as the continuous phase (Supporting Information, Figure S5.1).

To investigate the behavior of HDL in the FADRs, the ATPSs were loaded with HDL under acidic (pH 5), medium (pH 7), and alkaline (pH 9) conditions. The pH determines the net electrical charge on proteins and can play an important role in the interactions between the ions of the salt and the protein.[22] When proteins are at pH conditions close to their point of zero charge (pH 5.6),[12] there is not enough electrostatic repulsion between the proteins and they tend to aggregate and precipitate.[23] However, when the pH conditions are further below or above their point of zero charge, the proteins have a higher surface charge and repel each other. To visualize the location of HDL loaded in the ATPS, 12.5% of the HDL was replaced with covalently labeled fluorescein isothiocyanate (FITC) HDL, stirred for 30 minutes, and imaged with brightfield and fluorescence microscopy. Figure 5.1 shows the brightfield, fluorescent and overlay (merged) of brightfield and fluorescent images of FADRs loaded with HDL, at pH 5-9. In the brightfield images, the droplets could be observed, while in the fluorescent images, the HDL was visualized by the green color derived from the fluorescent signal of the FITC-HDL and was observed inside the droplets. In the brightfield microscopy images, the droplets of the FADRs at pH 5-9 appeared in sizes ranging from sub-micron to 200 μm. The interfacial tension between the two immiscible aqueous phases is reported to be extremely low (~1 μN/m),[24] and phase separates, after stop stirring, within seconds. After loading the FADRs with HDL, the differences in droplet sizes indicate that the proteins did not stabilize the droplet interface, which resulted in droplet merging and different droplet sizes. It has been reported earlier that the adsorption energy of proteins, such as β-lac[25] and whey protein,[26] are too low to stabilize the FADR. In summary, these results show that loading the

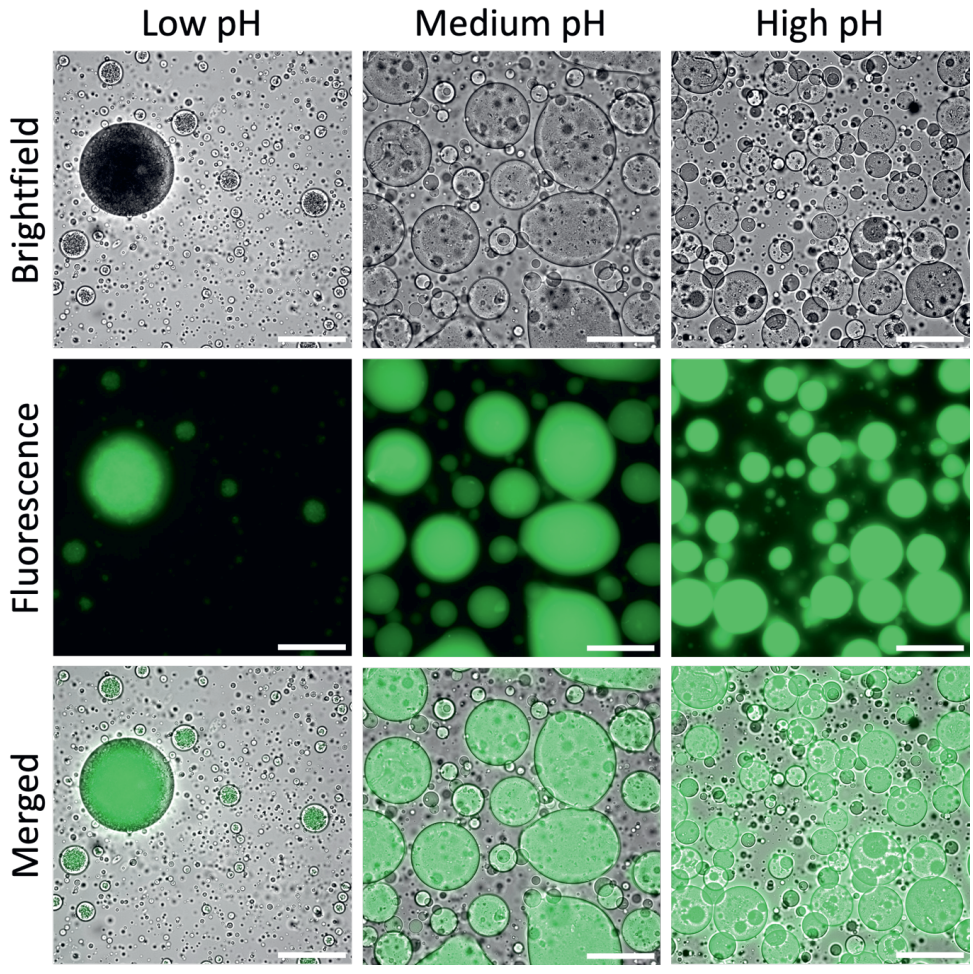

Figure 5.1 Brightfield, fluorescent and merged microscopy images of 40 mg/mL FITC-labelled HDL-loaded FADRs at pH 5, pH 7, and pH 9, after 30 minutes of stirring at 1000 RPM. Scale bars are 150 µm.

FADR with HDL, prepared at a PEG/Na_2SO_4 volume ratio of 7:3, allows compartmentalizing HDL in the Na_2SO_4 droplet phase. Additionally, the pH did not affect the partition of the HDL since the HDL was only observed inside the droplets. However, the HDL does not stabilize the interface because the ATPSs phase separate within seconds after stop stirring.

In addition, the fluorescent and merged microscopy images in Figure 5.1 clearly demonstrated that HDL was compartmentalized within the Na_2SO_4-rich droplet phase at pH 5-9. However, when the FADR was prepared at pH 5, the HDL was densely confined as aggregates in the droplets, while at pH 7 and 9, HDL was more evenly confined and homogeneously distributed. The differences in behavior of HDL at pH 5-9 could be explained by the differences in surface charge at pH 5-9. The FADR at pH 5 formed HDL aggregates because it is close to the point of zero charge of HDL. However, in the FADRs at pH 7-

9, HDL has a higher surface charge (> -20 mV),[12] and the repulsion between the proteins resulted in a homogeneous confinement within the droplet phase.

5.2.2 Affinity partitioning of HDL and Au^{3+} ions in the FADRs

The formation of microgels in FADRs relies on the prefential partitioning of the reactants (polymers, cross-linkers, etc.) between the two different phases.[27] The differences in affinity partitioning should lead to the retention of one reactant (the proteins) in the droplet phase, while the other reactant (cross-linkers) can freely migrate from the continuous phase into the droplet phase to react with each other.[27] We have already observed that HDL is compartmentalized within the Na_2SO_4-rich droplet phase (Figure 5.1). The other reactant is Au^{3+}, which will be used for oxidation and cross-linking of HDL.[11] To determine the preferential partitioning of the HDL and Au^{3+} ions reactants towards the two different aqueous phases, the amounts of reactants in the separate aqueous phases were measured. For this purpose, the FADRs were either loaded with HDL and/or supplemented with Au^{3+} ions and stirred for 30 mins. Subsequently, the ATPSs were allowed to macroscopically phase separate by stopping stirring. Then, the recovery extents and partition coefficients (K) were calculated (Experimental Section). The recovery extent provides the percentage of a reactant (HDL or Au^{3+}) partitioned in either of the phases in respect to its initial concentration added into the ATPS. The partition coefficient (K) estimates the distribution of the reactant in the ATPS.[28] When the K<1, the compound has a higher affinity towards the bottom (Na_2SO_4-rich) phase, and when K>1 to the top (PEG-rich) phase.

Table 5.1 shows the recovery extent and K values for the ATPSs samples either loaded with HDL and/or supplemented with Au^{3+} ions. When the ATPS was loaded with HDL, the recovery extent was ~25 folds higher in the Na_2SO_4-rich phase than in the PEG-rich phase (Figure 5.2, left column). In contrast, when the ATPS was supplemented with Au^{3+} ions, in the absence of HDL, the recovery extent of the Au^{3+} ions was ~9 folds higher in the PEG-rich phase than in the Na_2SO_4-rich phase (Figure 5.2, middle column). It is noteworthy that the sum of HDL and Au^{3+} recovery was not 100% because a portion of HDL and Au^{3+} ions did not dissolve in either of the ATPS phases and precipitated. When HDL and Au^{3+} ions were concurrently present in the ATPS, the sum of the recovery extents of HDL and Au^{3+} ions decreased ~25 and ~3 times, respectively (Figure 5.2, right column). Additionally, the K_{HDL} and K_{Au} increased ~158 and ~5 times, respectively.

Table 5.1 Amounts, recovery and K of reactants (HDL and Au^{3+} ions determined by ATPSs loaded with HDL and/or supplemented with Au^{3+} ions

Reactant in ATPS	Phase	Recovery (%)		K_{HDL}	K_{Au}
		HDL	Au^{3+}		
HDL	PEG-rich	3.2 ± 1.2		0.04	
	Na_2SO_4-rich	81.1 ± 4.9			
Au^{3+} ions	PEG-rich		68.4 ± 0.8		9.1
	Na_2SO_4-rich		7.5 ± 0.5		
HDL and Au^{3+} ions	PEG-rich	2.9 ± 0.3	24.8 ± 0.7	6.3	45.2
	Na_2SO_4-rich	0.5 ± 0.0	0.5 ± 0.1		

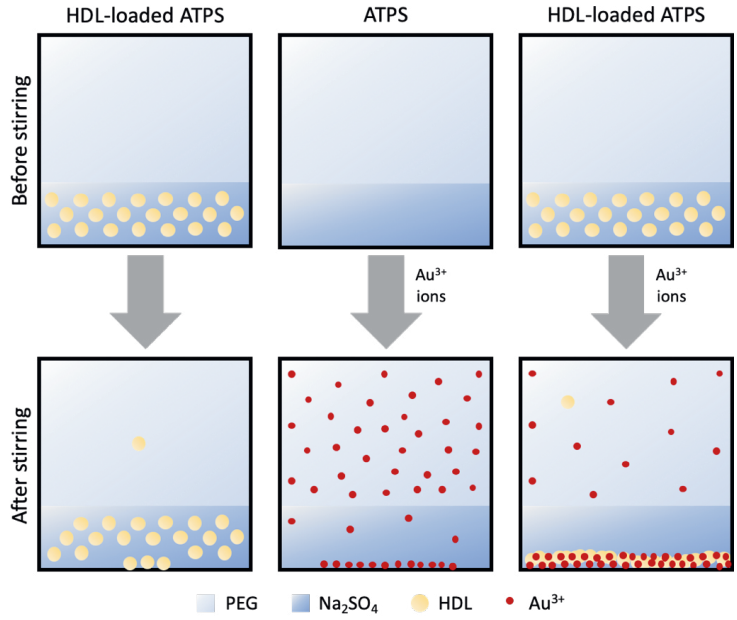

Figure 5.2 Schematic representation of the partition of HDL and Au^{3+} ions in ATPSs, after stirring and phase separation. The yellow spheres represent HDL, which are loaded in the ATPS. The red spheres represent Au^{3+} ions, which are added during stirring the ATPS.

These results show that HDL has a high partitioning preference towards the Na_2SO_4-rich phase, which corroborates with the observations of the compartmentalized HDL in the microscopy images in Figure 5.1. However, Au^{3+} has a partitioning preference towards the PEG-rich phase, and a weak partitioning preference towards the Na_2SO_4-rich phase. The combination of HDL-in-Na_2SO_4 and Au^{3+}-in-PEG could lead to compartmentalization of HDL in the droplet phase, while Au^{3+} ions could still migrate between the two immiscible phases. This could then result in a reaction between the Au^{3+} ions and HDL inside the droplets and form microgels. After supplementing Au^{3+} ions to the HDL-loaded ATPS, a decrease in recovery extents of both reactants was observed. This is due to the formation of solid materials, which sedimented, and were not part of the ATPS anymore. Based on the decrease of recovery extents, it was assumed that the Au^{3+} ions induced cross-linking of the proteins, resulting in the formation of solid microgels.

5.2.3 Formation of microgels under different reaction conditions

After calculations of the recovery extents and partition coefficients of HDL and Au^{3+} ions, the effect of HDL concentrations (5-40 mg/mL) and pH values (pH 5-9) on the structures of the microgels was investigated. After the addition of Au^{3+} ions, solid structures (microgels) were formed within 30 minutes, which sedimented after stopping stirring. The structures of the microgels in the FADRs were then studied by brightfield and fluorescence microscopy before and after 10x dilution with deionized water. In Figure S5.2, the FADRs at different conditions are shown before (uneven columns) and after 10x dilution with deionized water (even columns). The FADRs were diluted with water because the

microgels were clustered together inside the droplets and dilution decreases the interfacial tension between the two immiscible phases, and allows mixing of the phases. Solid microgels were already formed within 30 minutes after the addition of the Au^{3+} ions, indicating that HDL rapidly interacts with the Au^{3+} ions and gets cross-linked. Moreover, multiple microgels were observed in a single droplet, which were separed after dilution. This indicates that the cross-linking did not occur between neighboring microgels. Therefore, it was hypothesized that the HDL-in-Na_2SO_4 droplets have a fixed size during stirring of the FADRs and a droplet would only from a single microgel. When the FADRs were stopped stirring, the droplets merged, and as a result, contained multiple microgels.

Different microgels structures were observed, such as random aggregates, urchin-like, and spherical microgels, which will each be discussed separately. Representative images of these structures are shown in Figure 5.3.

Random aggregates

In Figure 5.3 (left column) and Figure S5.2 (5-40 mg/mL HDL, pH 5, and 5 mg/mL HDL, pH 7-9), structures with sizes between 10-50 µm with different shapes (elongated, spherical-like) were observed. Since the structures vary a lot in size and shape, we defined those structures as random aggregates. The random structures were formed at pH 5, independently of the HDL concentration. Before addition of Au^{3+} ions, we observed that HDL was present as aggregates at pH 5, due to low repulsive forces (Figure 5.1). Therefore, it was hypothesized that the formation of homogeneous

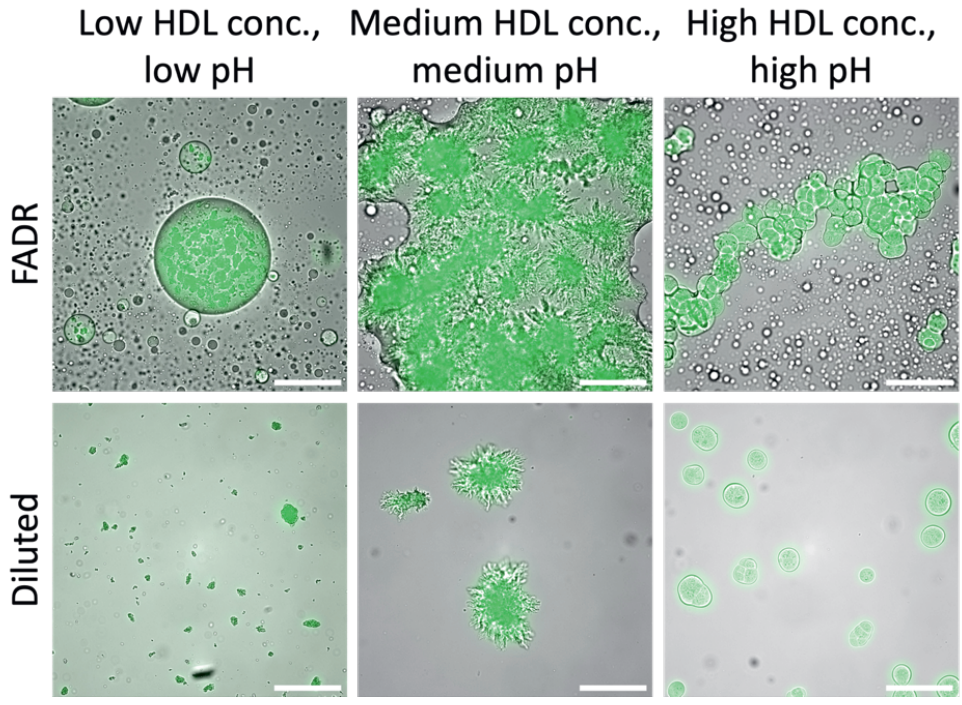

Figure 5.3 Merged brightfield and fluorescence microscopy images of random aggregates (5 mg/mL HDL, pH 5), urchin-like (20 mg/mL, pH 7), and spherical microgels (40 mg/mL HDL, pH 9) before (top row) and after 10x dilution (bottom row). The FADRs were supplemented with 500 molar equivalents of Au^{3+} ions to HDL, at corresponding pH. Scale bars are 150 µm.

microgels was hindered by the presence of the aggregates. Additionally, random structures were formed at 5 mg/mL HDL, independently of the pH. It has been reported earlier that when HDL concentration or amount of Au^{3+} ions are too low, no protein gel network could be obtained.[11] The molar equivalents of Au^{3+} ions was fixed, which suggests that the HDL concentration was too low to form a stable gel network. As a result, the loose gel network broke during droplet merging and formed random protein aggregate structures.

Urchin-like microgels

In Figure 5.3 (middle column) and Figure S5.2 (10-20 mg/mL HDL, pH 7-9), elongated structures containing multiple branches (urchin-like) were observed. Similar urchin-like microgels were also reported for Ca^{2+}-polymerized alginate in a PEG-Dex ATPS through osmotic pressure.[29] We hypothesize that a similar phenonemon occurs within our system. The Au^{3+} ions were added as an aqueous solution, which could create a concentration gradient in the HDL-loaded FADR. Due to the change in concentration gradient, water, PEG, and Au^{3+} ions migrate in the PEG-rich phase. Next, the HDL-in-Na_2SO_4 droplets go out-of-equilibrium with the surrounding PEG-rich phase. A new equilibrium would be reached by diffusion of water, HDL, and Na_2SO_4, out of the droplets to the PEG-rich phase, as branches. The Au^{3+} ions surrounding the HDL-in-Na_2SO_4 droplets then rapidly induced cross-linking of the HDL in the branches, resulting in the formation of urchin-like microgels.

Spherical microgels

In Figure 5.3 (right column), spherical microgels were observed for microgels prepared in a FADR of 40 mg/mL HDL, pH 9. There were no branches observed on the surface, which indicates that the HDL-in-Na_2SO_4 droplets were stable against the concentration gradient, caused by the aqoeus Au^{3+} solution, at these conditions. This could be due to the high surface charge of HDL at pH 9, which lead to stronger adsorption of HDL at the PEG/Na_2SO_4 interface.[30] The droplets were more stable, which prevented migration of water and HDL, resulting in cross-linking of HDL in a spherical shape.

5.2.4 Protein distribution in urchin-like and spherical microgels

After studying different conditions for obtaining urchin-like and spherical microgels, we analyzed the protein distribution within the microgels by confocal laser scanning microscopy (CLSM). In Figure 5.4, images of 1 µm slices and z-stack projections (45x and 66x 1 µm slices, respectively) of the urchin-like and spherical microgels are shown. The 1 µm slices allow visualization of the protein distributions at the center of the microgels, while the z-stack projections shows the protein distribution on the microgel surface. In the CLSM image slice of the urchin-like microgel, the fluorescence was observed in the border of the structures, and was further spread into branch-like structures. However, there was no fluorescence observed inside the border. The projection of the urchin-like demonstrated the presence of an elongated structure with branches. In the CLSM image slice of the spherical microgel, circular structures were observed with a uniform fluorescence distribution. The projection showed spherical structures with smooth surfaces. When the FADR was prepared at 40 mg/mL HDL, pH 7-9, the HDL was homogeneously distributed within the droplets (Figure 5.1). After addition of Au^{3+} ions in the FADR at pH 9, this homogeneous distribution of HDL was conserved, resulting in the formation of a spherical microgel. However, at pH 7, the proteins were distributed on the edges, in branch-like

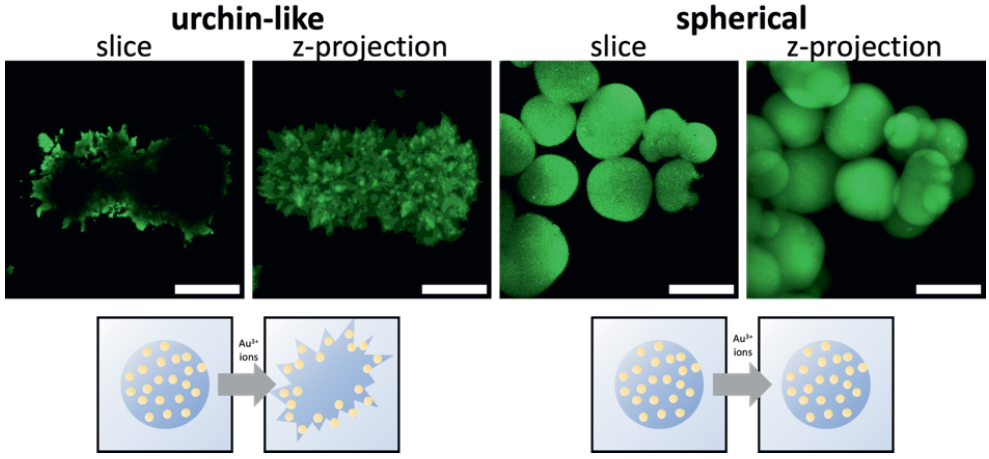

Figure 5.4 CLSM images of 1 µm slices and Z-stack projection (3D reconstruction) of microgels prepared at 40 mg/mL HDL and 500 molar equivalents of Au^{3+} in PEG/Na_2SO_4 at pH 7 (urchin-like), and pH 9 (spherical) after 10x dilution with deionized water. Scale bars are 50 µm. The schemes below the CLSM images represent the movement of HDL after addition of Au^{3+} ions from the droplet phase to the continuous phase, forming urchin-like microgels. At 40 mg/mL HDL, pH 9, the droplets were stable and the HDL remained uniformly distributed inside the droplets, forming spherical microgels.

structures, and absent in the core. This suggests that the addition of Au^{3+} ions to FADRs prepared at 10-20 mg/mL HDL, pH 7-9 destabilizes the droplet phase. The HDL migrated from the Na_2SO_4-rich droplet phase to the PEG-rich phase, forming branches on the droplets. During the migration of HDL, the Au^{3+} ions rapidly interacted with HDL and initiated cross-linking. The branches remained on the droplet, forming a solid, cross-linked urchin-like microgels.

5.3 Conclusion

In this research, we showed that microgels can be formed through compartmentalizing the proteins in a FADR, followed by cross-linking through the addition of Au^{3+} ions. Different shapes of the microgels, including random aggregates, urchin-like, and spherical, were obtained by changing the HDL concentrations (5-40 mg/mL) and pH values (5-9). Random aggregates were obtained when the proteins were at pH conditions close to their point of zero charge, and when the HDL concentrations were too low to form a stable gel network. Urchin-like microgels were formed when the HDL-in-Na_2SO_4 droplet phase got out-of-equilibrium, through addition of an aqueous solution of Au^{3+} ions, and formed cross-linked branches. However, at 40 mg/mL HDL, pH 9, the HDL-in-Na_2SO_4 droplet phase remained stable and their spherical structures were conserved after cross-linking. The use of FADRs for microgel preparation method can be used and implemented for generating biocompatible spherical and urchin-like structures, which may find applications different fields, such as catalysis, optical switches, or sensors.

5.4 Experimental section

5.4.1 Materials

Fresh hen eggs were purchased from a local organic farm De Hoge Born, Wageningen, the Netherlands. Sodium chloride (NaCl, ≥99.5%), 1 M NaOH and 1 M HCl solutions were purchased from VWR international B.V. Gold(III) chloride hydrate ($HAuCl_4 \cdot xH_2O$,99.5%), Fluorescein-5-isothiocyanate (FITC, ≥95%), Fluorescein Isothiocyanate-Dextran (FITC-Dex), polyethylene glycol (Mw = 3.350 kDa), sodium sulfate (Na_2SO_4), and 76 mm dialysis tubing cellulose membrane (MWCO = 14 kDa) were purchased from Sigma Aldrich. All chemicals were used without further purification and deionized water was used throughout the experiments.

5.4.2 Methods

Extraction of HDL

HDL was extracted from egg yolk according to the method developed by Castellani,[31] with slight modifications. Hen eggs were cracked and the egg yolks were separated manually from the albumen. The egg yolks were carefully rolled on a paper tissue to remove the chalazae and adhering albumen. The yolk membranes were then punctured, using a glass pipette, and their contents were collected and pooled in a beaker cooled in iced water. The liquid yolks were diluted with 3 volumes of 0.17 M NaCl (1% (w/v)) and homogenized by stirring for 1 h. The yolk was fractionated into plasma and granules by centrifugation at 10,000 x g for 45 min at T = 4 °C, using a Thermoscientific Sorvall Legend XFR centrifuge. The pellet (granules) was washed with 0.17 M NaCl and centrifuged once more. The granules were suspended in 1.71 M NaCl (10% (w/v)) and the solution's pH was adjusted to 7.25, using 1 M NaOH. The mixtures were collected in dialysis tubings and were dialyzed against deionized water with 3 changes over 24 h. The HDLs were precipitated. The content of the dialysis tubings were collected and centrifuged. The pellets, rich in HDL, were collected and freeze-dried, using a Salmenkipp alpha 2-4 plus freeze-dryer at a temperature of T = -76 °C and pressure of 0.0090 mbar for 72 h.

Labelling of HDL with FITC

FITC was coupled to the proteins by an isothiocyanate/amine reaction according to the manufacturer's protocol. 100 mg of protein was dissolved in 20 mL of 0.1 sodium carbonate buffer, pH 9, by stirring (5 mg/mL protein). For each protein solution, 18.4 µL of 26 nM FITC in DMSO was added, while gently and continuously stirring. The mixture was allowed to react overnight, while covered against light. The mixture was then dialyzed against deionized water with 5 changes over 24 h. The contents of the dialysis bags were collected and centrifuged. The supernatant was discarded and the pellet was washed again with deionized water before freeze-drying.

Formation of HDL-loaded FADRs and protein microgels

Initially, HDL was dissolved in a 15% (w/w) Na_2SO_4 solution at different concentrations (5, 10, 20, and 40 mg/mL) and the pH was adjusted to 5, 7, and 9. A 40% (w/w) PEG solution, at the same pH, was added to the HDL-in-Na_2SO_4 solution, in a 3:7 volume ratio with a total volume of 3 mL. The ATPSs were stirred at 1000 RPM, using a magnetic stirring bar and stirring plate. In the meantime, a 0.1 M Au^{3+} stock solution, in deionized water was prepared at pH 5, 7, or 9. The aqueous Au^{3+} solutions were

rapidly injected into the FADRs to have 500 molar equivalents of Au^{3+} to HDL (0, 53.5, 107, 213, and 426 μL). The FADRs were stirred for 30 minutes at 1000 RPM. When left sitting, the resultant mixture separated into a PEG-rich phase, a salt-rich phase and solidified microgels.

Determination of the amounts, recovery, and partition coefficients of Au^{3+} ions and HDL in the PEG-rich and Na_2SO_4-rich phases

The amounts of HDL in the PEG-rich and Na_2SO_4-rich phases, and ATPS, were measured both in absence and presence of Au^{3+}. Known weights of the different phases were dried in the oven at 70 °C. Subsequently, the protein contents were determined by DUMAS (Thermo Quest NA 2100 Nitrogen and Protein Analyser) using a protein-to-nitrogen conversion factor of 6.25. The measurements were averaged over 3 samples.

The amounts of Au^{3+} in the PEG-rich and Na_2SO_4-rich phases, and ATPS, were measured both in absence and presence of HDL. Known weights of the different phases were diluted and treated with a microwave acid (10% aqua Regia and H_2O_2) digestion. The Au^{3+} concentrations were then analyzed with a Perkin Elmer AVIO 500 inductively coupled plasma (ICP-OES) analyzer. The measurements were averaged over 3 samples.

The recovery of the reactant (r) was defined as the amount of the compound in 1 of the phases, after mixing and reaching the equilibrium, relative to the total amount of the compound added to the ATPS.

$$Recovery\ extent\ (\%) = \frac{m_{r,1\ phase\ (mg)}}{m_{r,ATPS}} * 100$$

The partition coefficient (K) was defined as the ratio between the equilibrium amounts of the partitioned reactant in the PEG-rich and Na_2SO_4-rich phases.

$$K_r = \frac{m_{r\ in\ PEG\ (mg)}}{m_{r\ in\ Na_2SO_4\ (mg)}}$$

5.4.3 Characterization

Brightfield and fluorescence Microscopy

To visualize the HDL, 5 mg of HDL was replaced with FITC-labelled HDL. 50 μL droplet of sample was placed on a microscopy slide and covered with a coverslip before imaging. The samples were imaged using a Leica DMi8 epifluorescence microscope with a non-immersion 20x magnification objective lens, 100% laser intensity and an exposure time of 278 ms. The FITC was excited at a wavelength λ_{ex} = 460-500 nm and the emission was collected at λ_{em} = 512-542 nm, using a FITC filter cube. The images were analyzed using FIJI software.[32]

Confocal Laser Scanning Microscopy (CLSM)

For CLSM imaging, the Au-HDL microgels were imaged using a Leica SP8-SMD microscope. The FITC was excited with $\lambda_{ex,max}$ = 490 nm and emission was collected at $\lambda_{em,max}$ = 525 nm. A z-stack was taken with a z-step of 1 μm. The images were analyzed using FIJI software.

References

1. J.K. Oh, R. Drumright, D.J. Siegwart, and K. Matyjaszewski, The development of microgels/nanogels for drug delivery applications, *Progress in polymer science*, 2008, **33**, 4, 448-477.
2. N.M. Smeets and T. Hoare, Designing responsive microgels for drug delivery applications, *Journal of Polymer Science Part A: Polymer Chemistry*, 2013, **51**, 14, 3027-3043.
3. Y. Guan and Y. Zhang, PNIPAM microgels for biomedical applications: from dispersed particles to 3D assemblies, *Soft Matter*, 2011, **7**, 14, 6375-6384.
4. S. Seiffert, Small but smart: sensitive microgel capsules, *Angewandte Chemie International Edition*, 2013, **52**, 44, 11462-11468.
5. M. Wang, T. Doi, and D.J. McClements, Encapsulation and controlled release of hydrophobic flavors using biopolymer-based microgel delivery systems: Sustained release of garlic flavor during simulated cooking, *Food Research International*, 2019, **119**, 6-14.
6. W.-F. Lai, A.S. Susha, and A.L. Rogach, Multicompartment microgel beads for co-delivery of multiple drugs at individual release rates, *ACS applied materials & interfaces*, 2016, **8**, 1, 871-880.
7. F.A. Plamper and W. Richtering, Functional microgels and microgel systems, *Accounts of chemical research*, 2017, **50**, 2, 131-140.
8. A. Sionkowska, Current research on the blends of natural and synthetic polymers as new biomaterials, *Progress in polymer science*, 2011, **36**, 9, 1254-1276.
9. E. Campos, J. Branquinho, A.S. Carreira, A. Carvalho, P. Coimbra, P. Ferreira, and M. Gil, Designing polymeric microparticles for biomedical and industrial applications, *European Polymer Journal*, 2013, **49**, 8, 2005-2021.
10. A. Totosaus, J.G. Montejano, J.A. Salazar, and I. Guerrero, A review of physical and chemical protein-gel induction, *International journal of food science & technology*, 2002, **37**, 6, 589-601.
11. L.M. Schijven, V. Saggiomo, A.H. Velders, J.H. Bitter, and C.V. Nikiforidis, Au 3+-Induced gel network formation of proteins, *Soft Matter*, 2021, **17**, 42, 9682-9688.
12. L.M. Schijven, T.D. Vogelaar, S. Sridharan, V. Saggiomo, A.H. Velders, J.H. Bitter, and C.V. Nikiforidis, Hollow protein microparticles formed through cross-linking by an Au 3+ initiated redox reaction, *Journal of Materials Chemistry B*, 2022, **10**, 6287-6295.
13. K. Midha, M. Nagpal, and S. Arora, Microspheres: a recent update, *Int. J. Recent. Sci. Res., l (8)*, 2015, 5859-67.
14. R.C. Mundargi, M.G. Potroz, S. Park, H. Shirahama, J.H. Lee, J. Seo, and N.J. Cho, Natural sunflower pollen as a drug delivery vehicle, *Small*, 2016, **12**, 9, 1167-1173.
15. R. Ma, L. Xiang, X. Zhao, and J. Yin, Progress in Preparation of Sea Urchin-like Micro-/Nanoparticles, *Materials*, 2022, **15**, 8, 2846.
16. N. Nakajima, K. Yamakoshi, Y. Yajima, M. Yamada, and M. Seki. *Shape control of cell-embedding hydrogel microstructures utilizing non-equilibrium aqueous two-phase systems*. in *2014 International Symposium on Micro-NanoMechatronics and Human Science (MHS)*. 2014. IEEE.
17. J.F. Pereira and J.A. Coutinho, *Aqueous two-phase systems*, in *Liquid-phase extraction*. 2020, Elsevier. p. 157-182.
18. A. Madadlou, V. Saggiomo, K. Schroën, and V. Fogliano, All-aqueous emulsions as miniaturized chemical reactors in the food and bioprocess technology, *Current Opinion in Food Science*, 2020, **33**, 165-172.
19. W.-J. Chiu, W.-Y. Chen, H.-Z. Lai, C.-Y. Wu, H.-L. Chiang, and Y.-C. Chen, Dextran-encapsulated photoluminescent gold nanoclusters: synthesis and application, *Journal of nanoparticle research*, 2014, **16**, 7, 1-11.
20. M. Anton, Egg yolk: structures, functionalities and processes, *Journal of the Science of Food and Agriculture*, 2013, **93**, 12, 2871-2880.
21. I.V. Ho-Gutierrez, E.L. Cheluget, J.H. Vera, and M.E. Weber, Liquid-liquid equilibrium of aqueous mixtures of poly (ethylene glycol) with Na2SO4 or NaCl, *Journal of Chemical and Engineering Data*, 1994, **39**, 2, 245-248.

22. U. Gündüz and K. Korkmaz, Bovine serum albumin partitioning in an aqueous two-phase system: Effect of pH and sodium chloride concentration, *Journal of Chromatography B: Biomedical Sciences and Applications*, 2000, **743**, 1-2, 255-258.
23. A. Salis, M. Boström, L. Medda, F. Cugia, B. Barse, D.F. Parsons, B.W. Ninham, and M. Monduzzi, Measurements and theoretical interpretation of points of zero charge/potential of BSA protein, *Langmuir*, 2011, **27**, 18, 11597-11604.
24. Y. Zou, J. Song, X. You, J. Yao, S. Xie, M. Jin, X. Wang, Z. Yan, G. Zhou, and L. Shui, Interfacial complexation induced controllable fabrication of stable polyelectrolyte microcapsules using all-aqueous droplet microfluidics for enzyme release, *ACS applied materials & interfaces*, 2019, **11**, 23, 21227-21238.
25. B.T. Nguyen, T. Nicolai, and L. Benyahia, Stabilization of water-in-water emulsions by addition of protein particles, *Langmuir*, 2013, **29**, 34, 10658-10664.
26. A. Madadlou, A. Saint-Jalmes, F. Guyomarc'h, J. Floury, and D. Dupont, Development of an aqueous two-phase emulsion using hydrophobized whey proteins and erythritol, *Food Hydrocolloids*, 2019, **93**, 351-360.
27. Q. Ma, Y. Song, J.W. Kim, H.S. Choi, and H.C. Shum, Affinity partitioning-induced self-assembly in aqueous two-phase systems: Templating for polyelectrolyte microcapsules, *ACS Macro Letters*, 2016, **5**, 6, 666-670.
28. J.A. Asenjo and B.A. Andrews, Aqueous two-phase systems for protein separation: a perspective, *Journal of Chromatography A*, 2011, **1218**, 49, 8826-8835.
29. N. Abbasi, M. Navi, J.K. Nunes, and S.S. Tsai, Controlled generation of spiky microparticles by ionic cross-linking within an aqueous two-phase system, *Soft Matter*, 2019, **15**, 16, 3301-3306.
30. O. Gmach, A. Bertsch, C. Bilke-Krause, and U. Kulozik, Impact of oil type and pH value on oil-in-water emulsions stabilized by egg yolk granules, *Colloids and Surfaces A: Physicochemical and Engineering Aspects*, 2019, **581**, 123788.
31. O. Castellani, C. Guérin-Dubiard, E. David-Briand, and M. Anton, Influence of physicochemical conditions and technological treatments on the iron binding capacity of egg yolk phosvitin, *Food Chemistry*, 2004, **85**, 4, 569-577.
32. J. Schindelin, I. Arganda-Carreras, E. Frise, V. Kaynig, M. Longair, T. Pietzsch, S. Preibisch, C. Rueden, S. Saalfeld, and B. Schmid, Fiji: an open-source platform for biological-image analysis, *Nature methods*, 2012, **9**, 7, 676-682.
33. M. Iqbal, Y. Tao, S. Xie, Y. Zhu, D. Chen, X. Wang, L. Huang, D. Peng, A. Sattar, and M.A.B. Shabbir, Aqueous two-phase system (ATPS): an overview and advances in its applications, *Biological procedures online*, 2016, **18**, 1, 1-18.
34. J.A. Asenjo and B.A. Andrews, Aqueous two-phase systems for protein separation: phase separation and applications, *Journal of Chromatography A*, 2012, **1238**, 1-10.

5.5 Supplementary Information

Type of FADRs at different volume ratios

In the formulation and utilization of FADRs it is of importance to know which phase makes the continuous and which one is the dispersed (droplet) phase. The density of a 15% (w/w) Na_2SO_4 solution (1.3 M, 1.14 g/cm^3) is higher than that of a 40% (w/w) PEG solution (0.01 M, 1.02 g/cm^3), so, in a vial, the top phase is PEG, while the bottom phase is Na_2SO_4. To study the different FADRs type (PEG-in-Na_2SO_4 or Na_2SO_4-in-PEG), ATPSs of PEG and Na_2SO_4 solutions were prepared at different volume ratios. To visualize the Na_2SO_4 phase, fluorescein isothiocyanate (FITC)-labelled dextran (Dex) was used, which partitions only in the ATPS phase.[33] The FADRs prepared at different volume ratios were stirred for 30 mins at 1000 RPM. After stirring, the samples were put between two microscopy slides and imaged with fluorescence microscopy.

Figure S5.1 shows images of droplets, in which the fluorescent signal of the FITC-Dex was green colored. It has to be noted that the FADRs phase separate within seconds because the ATPSs are not stabilized. In the images of the FADRs prepared with PEG-to-Na_2SO_4 volume ratios of 1:9-4:6, black droplets were observed in a green colored continuous phase, while at volume ratios of 6:4-9:1, green droplets were observed in a black continuous phase. In the image of the FADR with a volume ratio of 5:5, both green and black droplets were observed. We found that at volume ratios of PEG-to-Na_2SO_4 < 1, the FADR type was PEG-in-Na_2SO_4, and at PEG-to-Na_2SO_4 > 1 Na_2SO_4-in-PEG. However, at PEG-to-Na_2SO_4 = 1, a bi-continuous phase was observed. The type of FADR is determined by the system properties, such as viscosity, density, interfacial tension, and rate of phase separation.[34] We found that PEG-in-Na_2SO_4, Na_2SO_4-in-PEG, and bi-continuous types of FADRs could be formed based on the volume ratios.

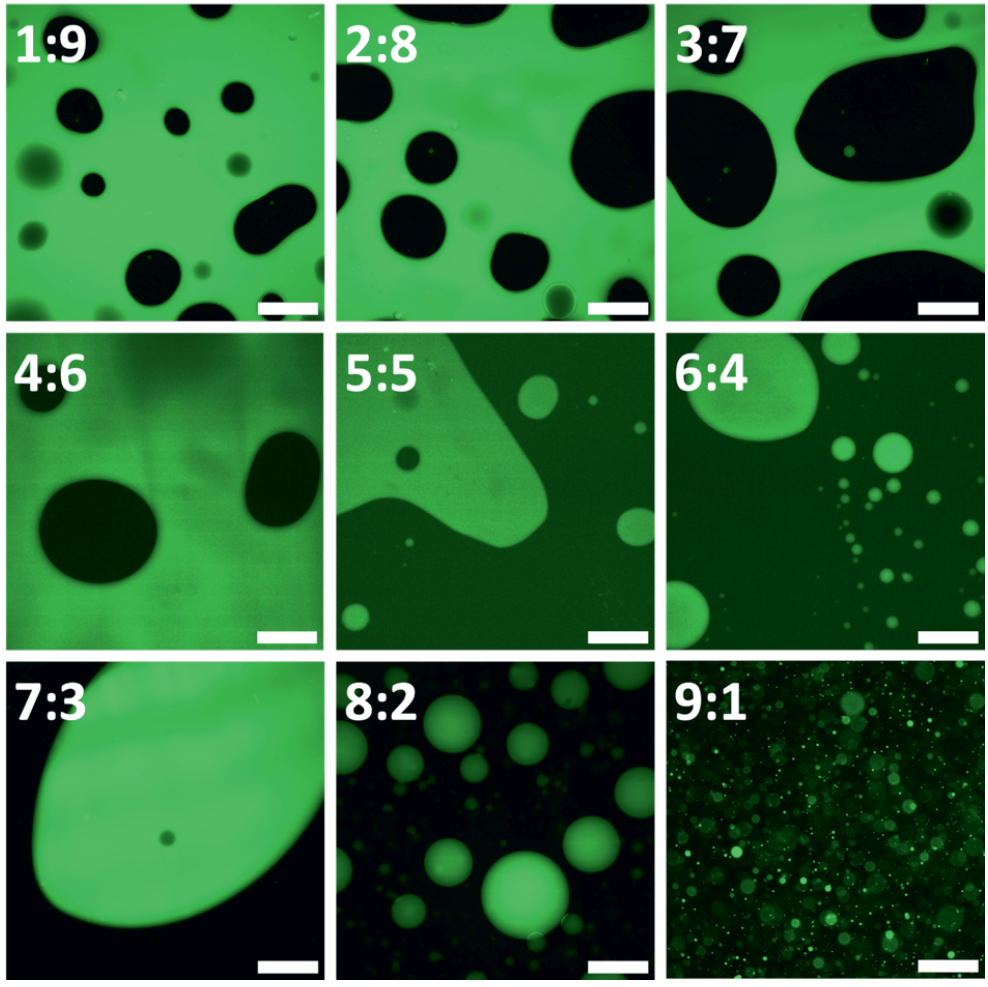

Figure S5.1 Fluorescent microscopy images of FITC-Dex loaded PEG/Na_2SO_4 FADRs at volume ratios of 1:9, 2:8, 3:7, 4:6, 5:5, 6:4, 7:3, 8:2, and 9:1. After 30 minutes of stirring at 1000 RPM, the samples were imaged. Scale bars are 500 µm. The FITC-Dex partitioned in the Na_2SO_4-rich phase. PEG-in-Na_2SO_4 FADRs were observed at volume ratios >1, and Na_2SO_4-in-PEG FADRs at volume ratios >1. A bi-continuous FADR was observed at volume ratio = 1.

Microgels prepared in FADRs at different HDL conc. and pH values

FADRs were prepared at different HDL concentrations (5-40 mg/mL) and pH values (5-9). After the addition of 500 molar equivalents of Au^{3+} ions to HDL, at corresponding pH, and stirring for 30 mins, solid structures were obtained. The microgels were imaged before (uneven columns) and after 10x dilution with deionized water (even columns). Random aggregates were observed when FADRs were prepared at 5-40 mg/mL HDL, pH 5, and 5 mg/mL HDL, pH 7-9. Urchin-like microgels were observed when FADRs were prepared at 10-20 mg/mL, pH 7-9. Spherical microgels were observed when FADRs were prepared at 40 mg/mL HDL, pH 9. A mixture of urchin-like and spherical microgels was obtained at 40 mg/mL HDL, pH 7.

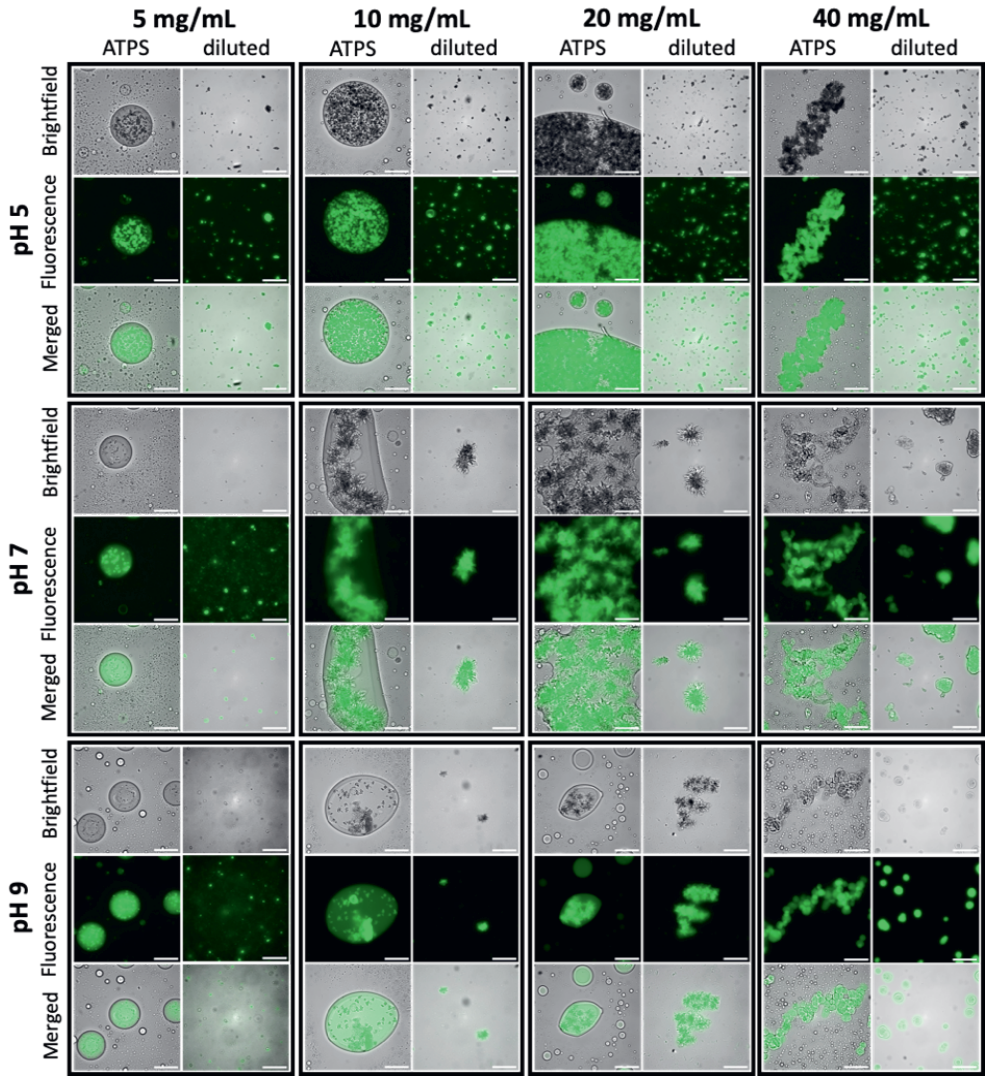

Figure S5.2 Brightfield, fluorescent and merged microscopy images of 5-40 mg/mL HDL-loaded ATPS, supplemented with 500 molar equivalents of Au^{3+} ions, at pH 5-9, and after 10x diluted with deionized water. Scale bars are 150 µm.

Chapter 6

General Discussion

6.1 Introduction

The research described in this thesis was focused on the formation of protein gel networks for constructing protein-based materials. Among the protein-based materials, macrogels, microparticles with solid and hollow core densities, and microgels with spherical, and branched (urchin-like) were constructed. To this end, Au^{3+} ions were used to initiate covalent cross-linking of the proteins. The Au^{3+}-initiated oxidation and cross-linking method allowed for constructing protein-based materials by assembling proteins into spherical structures through the use of templates. As emerging and concomitant benefit, the Au^{3+} ions got reduced and formed gold nanoparticles (AuNPs), which provided a wider range of applications, due to their physical and chemical properties, such as optics (fluorescence, absorbance, and scattering)[1] and electronics.[2]

Chapter 2 is dedicated to obtain insights in the interactions between Au^{3+} ions and proteins, and the obtained soft-solid gel materials were characterized. In **Chapters 3 and 4**, we used spherical, porous $CaCO_3$ as solid templates to construct protein microparticles. Furthermore, we used an aqueous two-phase system (ATPS) to compartmentalize proteins in droplets to construct protein microgels in **Chapter 5**.

6.2 Main findings

Protein cross-linking can be achieved through oxidation pathways. However, the mechanisms of protein oxidation have been less elucidated.[3] In **Chapter 2**, we used Au^{3+} ions, which have strong oxidizing properties,[4] for cross-linking proteins. Egg yolk high-density lipoprotein (HDL) was used as a model protein, which has poor gel network forming abilities during heating. When the amount of Au^{3+} ions was too low (10-100 molar equivalents of Au^{3+} to HDL), the proteins formed aggregates, but no stable gel networks. When 150 molar equivalents of Au^{3+} were added, a soft-solid material was formed after 1 day, as a result of a stable gel network. With further increasing the amounts of Au^{3+} ions, the time for the gel network formation decreased to 1 h. We noticed that after 1 day of preparation, the soft-solid material obtained a red color. The red color was derived from the AuNPs, which formed due to Au^{3+} reduction by electron donating residual amino acid groups (e.g. tryptophan, tyrosine). We then investigated the modification of residual groups of amino acids caused by the addition of Au^{3+} ions. We found that thiols formed disulfide bonds and tyrosine formed dityrosine.

In **Chapter 3**, we investigated the use of Au^{3+} ions for cross-linking HDL inside $CaCO_3$ templates to construct protein microparticles. First the encapsulation of HDL inside $CaCO_3$ was studied and then obtained protein microparticles, after cross-linking through Au^{3+} ions and template removal, were characterized. HDL was encapsulated inside $CaCO_3$ templates by synthesis of $CaCO_3$ in presence of the proteins. We found that 5 µm spherical HDL/$CaCO_3$ complexes were obtained, in which HDL was accumulated at the edges of the template, leaving an empty core inside the template. When the templates were removed, without cross-linking, spherical microparticles with a hollow core were obtained. The particles were not stable against pH, in terms of aggregation, because the HDLs were connected with each other through weak hydrophobic forces. To improve the stability of the hollow protein microparticles, we added Au^{3+} ions to the HDL/$CaCO_3$ complexes before template removal. The

Au^{3+} ions initiate covalent protein cross-linking, which improved the stability of the obtained protein microparticles.

In **Chapter 4**, we used proteins with a different tendency to aggregate in an aqueous environment and their subsequent reduced solubility to fabricate solid and hollow protein microparticles, through the use of $CaCO_3$ templates. The different proteins were β-lactoglobulin (β-lac), Bovine Serum Albumin (BSA), casein, and HDL. We found that using β-lac and BSA resulted in the formation of spherical protein/$CaCO_3$ complexes with a smooth surface and uniform protein distribution inside the templates. However, using caseins and HDL resulted in the formation of irregular shaped protein/$CaCO_3$ complexes with a rough surface and the proteins were accumulated at the template edges. The differences in the protein distributions (uniform, or accumulated at the edges) were attributed to the sizes of the proteins. β-lac and BSA were present in sizes of 7 nm and fit inside the pore sizes of $CaCO_3$ (20-60 nm),[5] while caseins and HDL were present as large aggregates (ranging from 30-5000 nm in size) and did not fit inside the $CaCO_3$ inner pores. To obtain protein microparticles, the proteins were cross-linked, using Au^{3+} ions, and the templates were removed. The protein distributions of the formed protein microparticles were conserved after cross-linking and template removal. Additionally, the formation of solid and hollow protein microparticles was confirmed by imaging the particles under dry and vacuum conditions. Solid microparticles had a rigid structure, while hollow microparticles flattened and formed creased structures. Finally, the presence of the AuNPs, embedded in the gel network structure, was confirmed by SEM(-EDX) and TEM.

Next to the use of solid templates, liquid templates could be used for the formation of protein microgels. In **Chapter 5**, we investigated the use of Au^{3+} ions for cross-linking HDL in a fully-aqueous droplet reactor (FADR) to construct protein microgels with urchin-like (branched) and spherical shapes. The FADR was prepared of an aqueous two-phase system (ATPS) of a Na_2SO_4 as droplet phase, dispersed into polyethylene glycol (PEG) as continuous phase. HDL was compartmentalized in the Na_2SO_4 droplet phase, while stirring. For cross-linking the proteins inside the droplets, Au^{3+} ions were added as an aqueous solution, which participate in the PEG-rich phase. When the Au^{3+} ions were added to the HDL-loaded ATPS, solid microgels were formed, which sedimented. The shapes of the microgels were affected by reaction conditions of the FADRs, such as protein concentrations (5-40 mg/mL) and pH values (5-9). When the HDL concentrations (5 mg/mL) and/or pH (5) were too low, no stable protein gel network could be obtained, which resulted in the formation of random aggregates. The FADRs prepared at 10-20 mg/mL HDL, pH 7-9, resulted in the formation of multiple branches on the microgels (urchin-like), after addition of the Au^{3+} ions. However, the FADR prepared at 40 mg/mL HDL, pH 9, resulted in the formation of spherical microgels. The different FADRs reaction conditions could be destabilized after the addition of the aqueous Au^{3+} ions, which resulted in formation of branches on the microgels. However, when the FADRs were stable, spherical microgels were obtained.

On the basis of the main findings described in the experimental chapters in this thesis, we can conclude that the use of Au^{3+} ions for cross-linking proteins is promising for constructing protein-based materials. Adding Au^{3+} ions to a protein dispersion resulted in the formation of macrogels. Microparticles were obtained through cross-linking the proteins inside spherical, porous $CaCO_3$

templates. By using soluble or aggregated proteins, solid and hollow microparticles were formed. Furthermore, the addition of Au^{3+} ions to HDL in FADRs resulted in urchin-like and spherical microgels.

An overview of all the experimental chapters found in this thesis and their main findings is given in Figure 6.1.

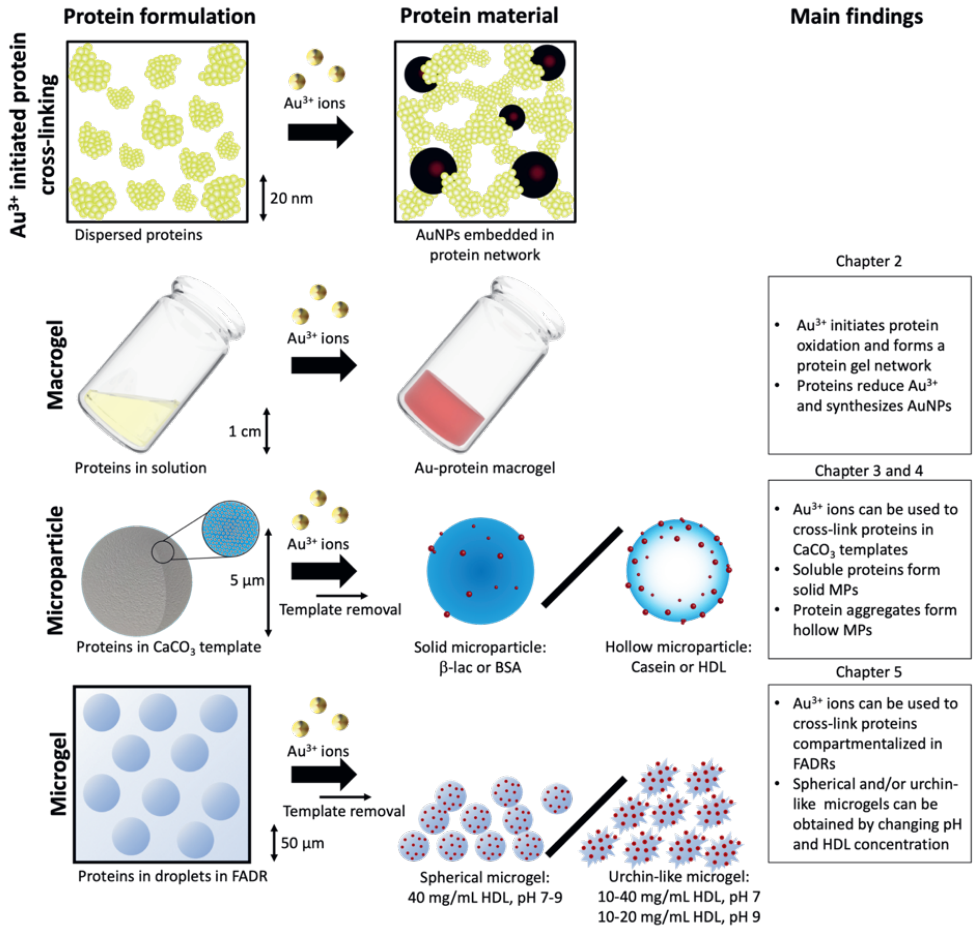

Figure 6.1 Overview of thesis outline and main findings.

6.3 Main findings put into a wider perspective

The main findings of this thesis are split into the use of Au^{3+} ions for cross-linking proteins, AuNPs synthesis by proteins, constructing hollow particles, and alternative cross-linking methods.

6.3.1 Protein cross-linking and gel network formation through Au^{3+} ions

Cross-linking of proteins, and subsequently gel network formation, is mostly done by changing reaction conditions, such as temperature, protein concentration, pH, ionic strength, pressure, or through the

addition of chemical or enzymatic cross-linking agents.[6] Protein cross-linking could also be done through oxidation. However, protein cross-linking through oxidation is much less studied and the mechanisms are only partly elucidated. Additionally, the oxidative modifications of proteins could affect their physical properties, such as solubility, hydrophobicity, water-holding capacity, and the ability to form gel networks.[3] It has been reported that, in addition to changing reaction conditions, mild oxidative modifications of proteins increases protein-protein interactions and improves the gel network formation abilities, while strong oxidative conditions weakens the gel network formation abilities.[3] However, the use of oxidative agents, like metal ions, for direct gel network formation (without changing additional reaction conditions) was not explored yet.

In this thesis, we showed that Au^{3+} ions can be used to induce protein cross-linking and gel network formation of egg yolk HDL (**Chapter 2**). The use of Au^{3+} ions for the formation of protein gel networks has some advantages over the use of heat:

- A lower minimum protein concentration was required (3% (w/v) vs. 5% (w/v)[7]), so less protein material is required for constructing protein-based materials
- Au^{3+} ions react with multiple types of residual group of amino acids (e.g. amines, thiols) and is therefore applicable to other proteins (e.g. BSA and WPI).
- No additional heating was required, the protein cross-linking even occurred at 4 °C.
- The Au^{3+} ions provided a dual functionality to the design, next to protein cross-linking, AuNPs were formed. No separate AuNPs synthesis is required for incorporating AuNPs in a gel network.
- The AuNPs conserved their optical properties, when embedded in the gel network, and provided a novel hybrid-soft nanocomposite material.

However, safety issues of the obtained materials were not discussed, which we will address below.

Safety issues regarding protein-based materials constructed through the use of Au^{3+} ions

Next to the advantages of the use of Au^{3+} ions for initiating the formation of protein gel networks, the potential safety and biocompatibility issues of the materials should be addressed. The oxidized protein products in the material and the presence of unreacted Au^{3+} ions will be considered as the main potential harmful components.

The addition of Au^{3+} ions to proteins leads to modifications of diverse residual groups of amino acids of the proteins, through oxidation, which have potential toxic effects. The oxidation of the proteins could modify the cleavage sites of proteases (e.g. serine, cysteine, aspartic acid)[8] or decrease their accessibility.[9] Consequently, the protein-based materials are not easily broken down in the body. Additionally, toxic compounds, such as methionine sulfoximine and α-aminoadipic acid, could be formed directly in the material or during metabolism in the body.[10] Moreover, amino acid oxidation products are similar to their native amino acids and could replace them. For example, m- and o-tyrosine could be mis-incorporated into proteins during synthesis, which could affect the protein functionality and lead to cytotoxicity.[11] Finally, the reactivity of the oxidized residual groups of amino

acid does not stop upon formation of the protein-based material. When the material is inside the organism, the oxidative modifications could be transferred from the material to the body proteins.[12]

Uncontrolled release of Au^{3+} ions in the body could cause long-term adverse effects or be lethal because they could bind to proteins and DNA.[4] Even though most of the Au^{3+} ions in the gel network are reduced and formed AuNPs, there could be some unreacted Au^{3+} ions present in the material. To detect the presence of gold at different oxidation states (Au^{3+}, Au^{+}, and Au^{0}) in the material, X-ray photoelectron spectroscopy (XPS) could be used. An example of an XPS spectrum of a material containing gold is shown in Figure 6.2.

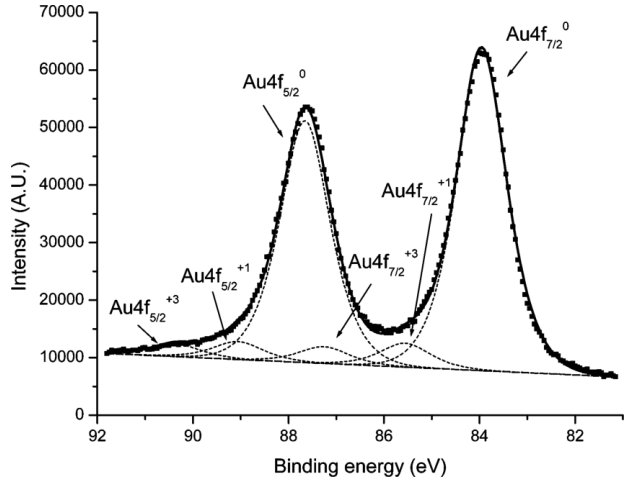

Figure 6.2 Example of a high-resolution Au4f XPS spectrum with different gold oxidation states, copied from ref. 16.

With XPS, the intensity of the Au $4f_{7/2}$ and $4f_{5/2}$ core levels and binding energy values are measured. Based on the position and shift of the binding energy, the oxidation state of gold can be determined. The different oxidation states of gold, with their corresponding binding energy are: Au^{0} (84 eV, 87.8 eV), Au^{+} (85 eV, 89.1 eV), and Au^{3+} (87.3 eV, 90.4 eV).[13-16]

If there are still unreacted Au^{3+} ions detected in the material, a reducing agent could be added to the material to reduce all the Au^{3+} ions and synthesize AuNPs. Examples of mild reducing agents include citrate,[17] single amino acids,[18] or carbohydrates.[19] AuNPs are considered to be inert, compared to Au^{3+} ions. However, there is very few information available about the short and long term health effects of AuNPs in organisms, which should also be considered.[20]

6.3.2 Au^{3+} reduction and AuNPs synthesis by proteins

Au^{3+} ions are strong oxidative agents[4] and can form AuNPs through reduction of Au^{3+} to Au^{+} and Au^{0}. Proteins have been reported as reducing and stabilizing agents for the formation of AuNPs.[14] However, only a few reports acknowledge that the exposure of proteins to Au^{3+} ions leads to changes in the protein structure, such as cross-linking, through oxidation.[21] In fact, much research has been focused on using proteins for the synthesis of AuNPs.[22] In addition to using Au^{3+} ions for the formation of

protein gel networks, we also explored different pH conditions for HDL and Au^{3+} ions to synthesize AuNPs with different shapes.

Synthesis of hexagonal- and/or triangular-shaped AuNPs

We found that protein concentrations below 1.5% (w/v) and/or adding below 150 molar equivalents of Au^{3+} ions did not result into a protein gel network. To synthesize AuNPs using HDL, we used lower protein concentrations (0.1% (w/v)) to avoid protein gel network formation.

When proteins are at acidic conditions (pH 1-4), amino acids with carboxylic acid side groups, such as aspartic and glutamic acid, are involved in Au^{3+} reduction.[23] It has been reported that aspartic acid not only acts as reducing agent, but also as shape-directing agents for the formation of hexagonal and triangular gold nanoplates.[24] To study the effect of acidic conditions (pH 1-4) on the AuNPs shapes, by using HDL, UV-Vis absorbance and TEM was used. In Figure 6.3, the UV-Vis absorbance spectra of the AuNPs synthesized with HDL at pH 1-4 are shown.

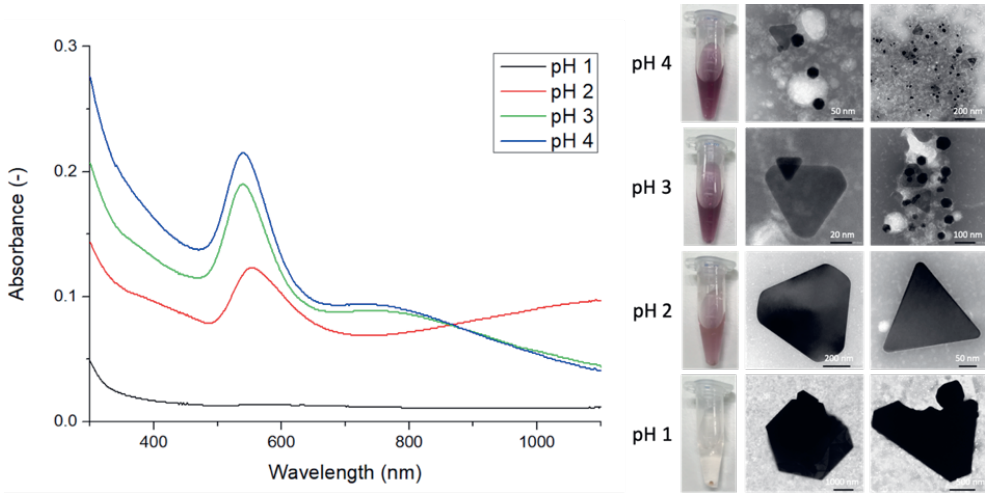

Figure 6.3 UV-Vis absorbance spectra, pictures, and TEM images of 0.1% (w/v) HDL in deionized water with 250 equivalents of Au^{3+} ions, at pH 1-4, after 2 weeks of preparation.

The UV-Vis spectra detects the surface plasmon resonance absorbance of the AuNPs, which is strongly dependent on the AuNPs size, shape, surface, and aggregation state.[25] The UV-Vis spectra show absorbance peaks at λ = 550 nm (pH 2-4), and at λ = 780 nm (pH 3-4), and an increase in absorbance at λ = 1100 nm (pH 2). However, the UV-Vis absorbance spectrometer in our lab cannot measure absorbance above λ = 1100 nm, so the absorbance peak could not be determined. At pH 1, no absorbance was observed because the AuNPs were sedimented. The absorbance at λ = 550 nm corresponds to surface plasmon resonance of spherical AuNPs.[26] The absorbance at λ = 780 nm and around λ = 1100 nm corresponds to in-plate dipole and quadrupole plasmon resonance of gold nanoplates, for example triangular shaped.[27] The peaks are broadened because the particles are > 100 nm in size and due to the presence of transversal and longitudinal surface plasmon resonances.[25] To

analyze the shapes of the synthesized AuNPs at pH 1-4, TEM was used. In Figure 6.3, the TEM images of the AuNPs synthesized at pH 1-4 (from bottom to top) are shown. When the AuNPs were synthesized using HDL, at pH 1, hexagonal-like and triangular-like AuNPs structures, with sizes between 2-5 µm were observed. In the sample prepared at pH 2, AuNPs with triangular structures with rounded and sharp corners, of 200-500 nm, were observed. At pH 3-4 mixtures of triangular and spherical shaped AuNPs with different sizes 20-50 nm were observed. A possible growth process of the hexagonal and triangular shaped AuNPs was proposed as three distinctive stages: reduction of Au^{3+} ions to gold nuclei, induction process for formation of hexagonal- and/or triangular-shaped seeds, and the growth of the seeds into nanoplates.[28] The proteins may aid in directing the growth of the hexagonal- and/or triangular-shaped seeds, according to the "surface wrapping" mechanism.[29] With increasing pH, the AuNPs decrease in size and have a different shape (hexagonal and/or triangular at low pH and spherical at higher pH). These trends could be related to changes in the conformation of HDL structure with pH. The pH has an effect on the charges on the proteins, which could affect the strength of interaction between the proteins and the gold seeds. This could then lead to AuNPs shapes at different pH.

Synthesis of fluorescent AuNPs

When proteins are at alkaline conditions (pH 10-13), amino acids with aromatic side groups, such as tyrosine, tryptophan, and phenylalanine, are involved in Au^{3+} reduction.[30] It has been reported that the strong reducing properties of the tyrosine results in the formation of fluorescent AuNPs, which have sizes below 3 nm. However, when Au^{3+} ions are at alkaline conditions, they hydrolyze to hydrated gold oxides, which are less reactive. Therefore, to synthesize fluorescent AuNPs, by using HDL, the Au^{3+} ions were first added under acidic conditions, before addition of NaOH to increase the pH to 12. To analyze the optical properties of the AuNPs, obtained with HDL, the solutions were put under visible (tube light, TL) and UV (λ = 365 nm) light. In Figure 6.4, the images of the AuNPs solutions under TL and UV light are shown.

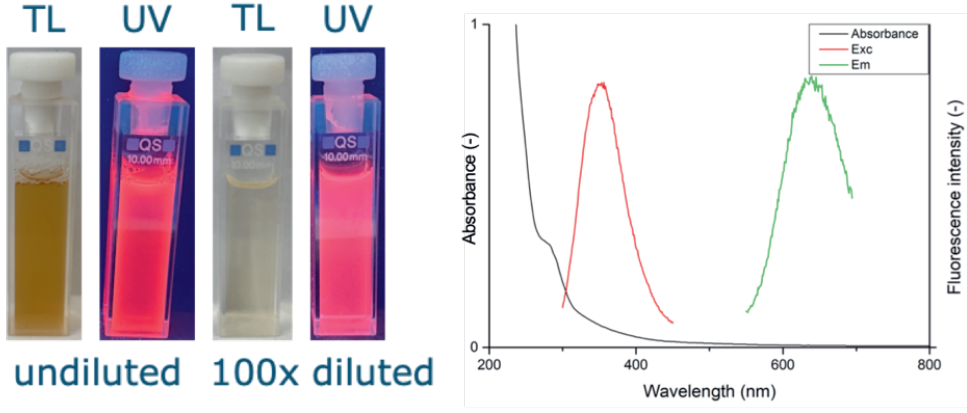

Figure 6.4 Pictures of the Au-HDL aqueous solutions under TL and UV light. UV-Vis absorbance (black line), excitation (λ_{em} = 640 nm, red line) and emission (λ_{ex} = 380 nm, green line) spectra of the Au-HDL aqueous solutions. The solutions were prepared as 2% (w/v) HDL in deionized water with ~84.5 molar equivalents of Au^{3+} ions, at pH 12. The images and spectra were taken 1 day after preparation.

The color of the AuNPs solution turned from yellow to light brown under visible. When under UV light, the light brown solution of the AuNPs emitted an intense red fluorescence. The fluorescence was still detected when the solution was diluted 100 times with deionized water. The red fluorescence indicates the presence of AuNPs with sizes <3 nm (proteins only exhibit blue fluorescence due to the presence of aromatic side groups of amino acids). To confirm the optical properties, UV-Vis absorption, and fluorescence excitation and emission spectra were measured, which are shown in Figure 6.4. The UV-Vis spectrum showed an absorption at λ = 280 nm. However, there was no surface plasmon resonance absorbance detected in the region of λ = 550 nm. This suggests that the AuNPs are <3 nm, which have no surface plasmon resonance absorbance. The fluorescence spectra show excitation and emission peaks at λ = 380 nm and λ = 640 nm, respectively. The wavelength of fluorescent AuNPs depends on the size of the AuNPs, where smaller and larger AuNPs emit at shorter and longer wavelengths, respectively. This red emission wavelength was close to the reported red emission from AuNPs synthesized with BSA[14] and pepsin,[30] which consisted of 25 gold atoms. Therefore, it was assumed that HDL synthesized AuNPs with ~25 atoms.

By using HDL at acidic or alkaline conditions, different AuNPs were synthesized. At acidic conditions, a mixture of large hexagonal and/or triangular shaped AuNPs were obtained, while small, red fluorescent AuNPs were obtained at alkaline conditions. Therefore, it is of apparent interest to investigate the synthesis of AuNPs, using proteins, at different concentrations and pH values.

6.3.3 Hollow particles

In the general introduction (**Chapter 1**), we categorized the protein gels based on their dimensions as macrogels, microgels and microparticles. The majority of the microgels and microparticles have a spherical shape because it is consistent and has a predictable surface area.[31] However, we found in **Chapter 3 and 4** that further classification can be done on the core densities, such as solid (uniform matrix) and hollow (empty core). The hollow particles offer advantageous properties over their solid counterparts due to their low density and large internal voids.[32] Therefore, the most important applications of hollow particles is the storage of compounds inside, coatings, as nanoreactors for confined reactors, and fillers.[33] There are various methods available to construct hollow particles, which we will address below. Additionally, alternative (bio)polymers for constructing hollow particles, as described in **Chapter 3 and 4**, will be discussed.

Methods for constructing hollow particles

Hollow particles can be obtained through different methods, which are illustrated in Figure 6.5:

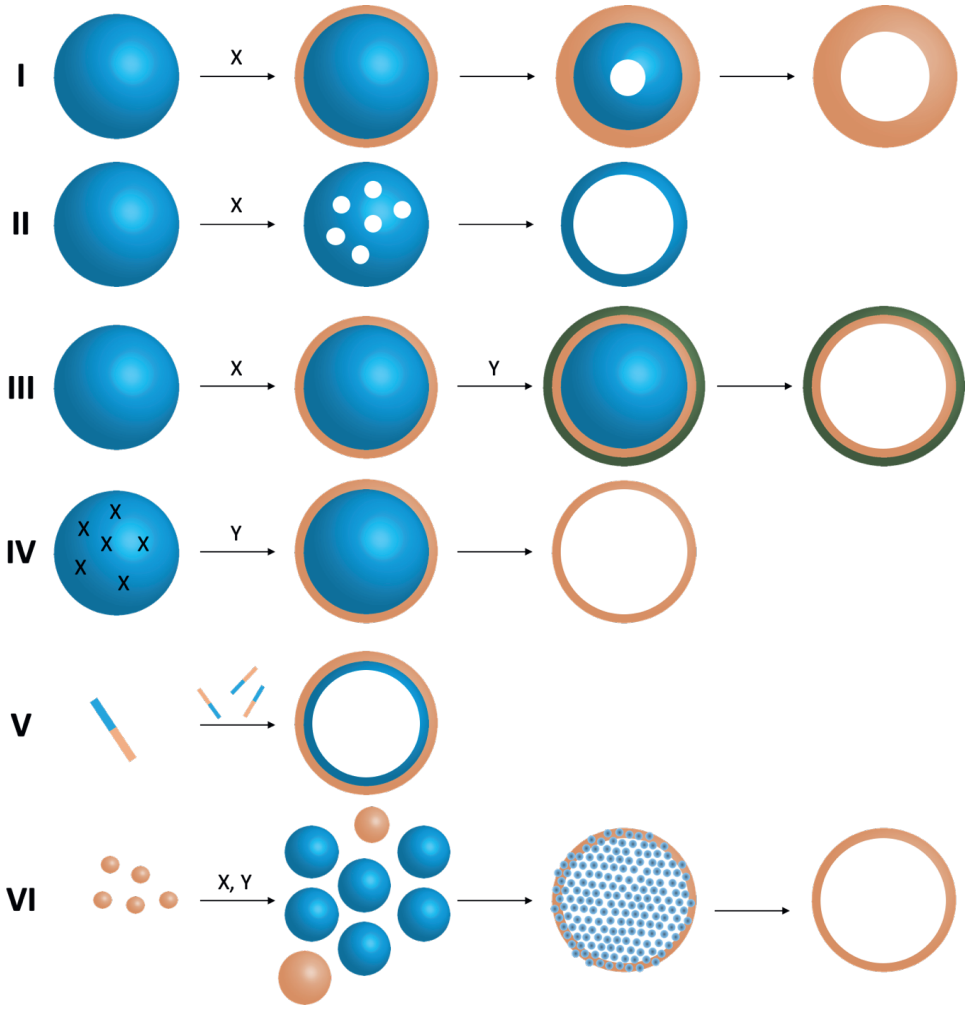

Figure 6.5 Schematic representation of different methods for the formation of hollow particles. (I) The Kirkendall effect, (II) Osmogen-mediated, (III) layer-by-layer assembly, (IV) interfacial polymerization, (V) self-assembly, (VI) and through co-precipitation of aggregates during template synthesis.

1. The Kirkendall effect

A solid particles and reactant (in solution or gas phase) react at their interface, which leads to outward diffusion of the core elements of the solid particle towards the growing composite, and leaving a cavity inside the particle.[34]

2. Osmogen-mediated

Water diffuses into the solid particle and the core elements of the solid particle migrate towards the particle edges, leaving water in the core.[35]

3. Layer-by-layer assembly

Deposition, or coating, of (bio)polymers onto the template, followed by selective removal of the template.[36]

4. Interfacial polymerization

Polymerization of two types of monomers at the interface of two immiscible phases (such as oil-water and water-water systems) in droplet reactors.[37]

5. Self-assembly

The polymers spontaneously assemble, without external driving forces, into hollow structures.[38]

In **Chapter 3 and 4**, we describe a new method for forming hollow particles:

6. Through co-precipitation of aggregates during template synthesis

The template is synthesized in presence of large aggregates, which results in accumulation of the aggregates on the template edges, leaving a cavity inside the particle.

However, not all of the above mentioned methods are directly applicable for the (bio)polymers to construct hollow particles. The choice of an appropriate method is dependent on the physical and chemical properties of the used (bio)polymeric materials.[39] For example, self-assembly is limited to polymers which have the property of directional exchanges, such as cyclodextrin-conjugated PEG.[38]

Alternative (bio)polymers for constructing hollow particles

In our method described in **Chapter 4**, we found that small aggregate, soluble proteins (BSA and β-lac) resulted in the formation of solid microparticles and large aggregated, poorly soluble proteins (caseins and HDL) hollow protein microparticles. Caseins and HDL contain phosphoserine amino acids, of which the phosphate group strongly binds with the Ca^{2+} ions. In this case, the Ca^{2+}, from the template precursor solution, induces aggregation of the proteins. We expect that proteins, assembled into large aggregates through different methods, could also form hollow protein microparticles through the use of $CaCO_3$ templates.

In this thesis, animal-derived proteins are used. As an alternative, plant proteins, such as from soy, pea, lentils, are of interest due to their lower environmental impact. For isolating proteins from plant sources, the proteins are exposed to harsh conditions, such as high temperatures, alkaline or acidic conditions.[40] This could lead to protein unfolding and the formation of small soluble aggregates[41] and large insoluble aggregates.[40] The full fraction of plant protein isolates is a polydisperse dispersion of soluble and insoluble proteins. A soluble fraction can be obtained by centrifugation of the plant protein dispersion.[42] It has been reported that the soluble fraction of soy protein isolate resulted in the formation of solid protein microparticles.[43] It would be interesting to investigate whether the use of the polydisperse plant protein dispersion (with sizes >100 nm) would result into the formation of hollow protein microparticles.

Next to proteins, starch could be used as biopolymer because it is commercially available from low-cost and renewable resources,[44] and is present as large aggregates (ranging from 0.4-53 µm) in aqueous solutions.[45] It has been reported that the starch affects the crystallization of $CaCO_3$ and different morphologies of $CaCO_3$ could be obtained, such as ring-like, cone-like structures, by changing the starch concentrations.[46] This study was only focused on the morphology of the synthesized starch/$CaCO_3$ complexes. Therefore, it would be interesting to investigate whether starch would form solid or hollow microparticles after template removal.

We only discussed two suggestions as alternative polymers for casein and HDL. However, we expect more different types of synthetic, semi-synthetic, and biobased polymers should be explored for constructing hollow protein microparticles through the use of $CaCO_3$ templates.

6.3.4 Alternative cross-linking methods

In this thesis, the focus was on using Au^{3+} ions to initiate protein oxidation and subsequently cross-linking to construct protein-based materials. However, for constructing macrogels, microgels and microparticles, other cross-linking methods could be used as well. We also explored the use of other metal ions and chemical cross-linkers, such as glutaraldehyde.

Alternative metal ions for initiating protein oxidation and cross-linking

In addition to Au^{3+} ions, also other metal ions could be used for directly initiating protein oxidation. Platinum(IV) (Pt^{4+}) and palladium(II) (Pd^{2+}) are similar to Au^{3+} because they are noble metals and have large positive reduction potentials.[47, 48] Additionally, Pt^{4+} and Pd^{2+} can also be reduced to form nanoparticles. Both Pt and Pd nanoparticles are widely used as catalysts and in biomedical applications.[49] Therefore, it is hypothesized that Pt^{4+} and Pd^{2+} could be used as alternative metal ions for Au^{3+} ions to initiate protein cross-linking and gel network formation through a similar mechanism.

Next to noble metal ions, transition metal ions, such as iron or copper, also have oxidative properties. However, their reduction potentials are lower compared to those of noble metals. Transition metals can react with hydrogen peroxide and generate reactive oxygen species through the Fenton reaction:[50]

$$Fe^{2+} + H_2O_2 \rightarrow Fe^{3+} + OH^- + {}^{\bullet}OH$$

The formed reactive oxygen species can subsequently attack proteins either by addition or hydrogen abstraction,[51] or the production of carbonyls on amino acid residues.[52] Several reducing amino acids (e.g. tyrosine, aspartic acid) and agents (e.g. ascorbate, superoxide anions) can reduce Fe^{3+} back to Fe^{2+}.[53]

Some preliminary experiments were done by using Pt^{2+}, Pd^{2+}, Fe^{2+}, Fe^{3+}, and Cu^{2+} for cross-linking proteins. We found that the addition of Pt^{2+} to proteins did not result into a protein gel network. We assumed that Pt^{2+} is an intermediate and is less reactive than Pt^{4+}. The addition of Pd^{2+} resulted in the formation of a protein gel network. Some spots in the gel network were brown colored, which was due to the poor solubility of $PdCl_2$ in water. Fe^{2+} forms a mixture of iron oxides and oxide-hydroxides, when exposed to air and water, which was not reactive towards the proteins. When using Fe^{3+} or Cu^{2+}, higher amounts (>1500 molar equivalents to HDL) were required for the formation of protein gel networks

compared to Au^{3+} (250 molar equivalents) at room temperature. Additionally, when the Fe^{3+}- and Cu^{2+}-HDL mixtures were incubated at 40-80 °C, there was no gel network formation. This suggests that transition metal ions form protein gel networks through a different mechanism compared to Au^{3+} ions. Further investigations are required for using metal ions for the formation of protein gel networks.

Chemical cross-linking by glutaraldehyde

Only the use of metal ions is discussed for constructing protein-based materials. However, proteins can be cross-linked through their primary amines, carboxylic acids and sulfhydryls groups with chemical cross-linkers, such as N-hydroxysuccinimide esters, maleimide, carbodiimide, and glutaraldehyde.[54] We also explored the use of glutaraldehyde as cross-linker to construct protein microparticles through the use of $CaCO_3$ templates. Glutaraldehyde reacts with amine groups of amino acids, such as lysine, and generates an imine (Schiff base).[55] We added glutaraldehyde to β-lac, BSA, casein, and HDL-encapsulated $CaCO_3$ templates to investigate whether we still formed solid and hollow protein microparticles. To confirm whether the protein microparticles kept their solid and hollow structures, after template removal, the proteins were labelled with FITC and visualized with CLSM. In Figure 6.6 A-D, the images of the obtained protein microparticles are shown.

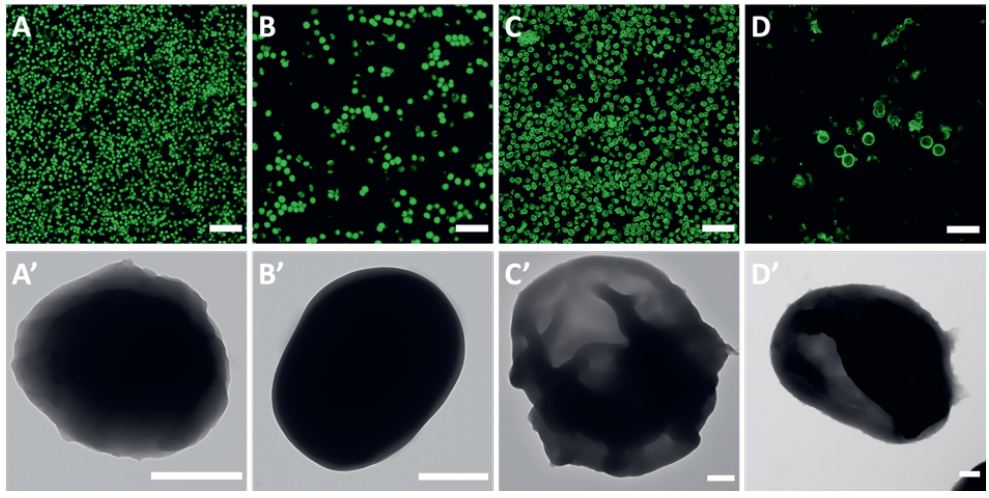

Figure 6.6 (A-D) CLSM and (A'-D') TEM images of (A) β-lac, (B) BSA, (C) casein, and (D) HDL microparticles. The proteins were covalently labelled with FITC for CLSM imaging, scale bars are 25 μm. The scale bars in the TEM images are 0.5 μm.

The CLSM images of the β-lac and BSA microparticles demonstrate the presence of spherical particles with a uniform fluorescence density (Figure 6.6 A,B). On the other hand, the CLSM images of casein and HDL microparticles show the presence of spherical particles with an empty core (Figure 6.5 C,D). Similar fluorescence distribution was observed in the protein microparticles obtained with Au^{3+} ions in **Chapter 4**. To investigate their morphology and density, TEM imaging was done on the protein microparticles. The TEM images of the protein microparticles are shown in Figure 6.6 A'-D'. In the TEM images of β-lac and BSA microparticles, dense and spherical protein matrices are observed (Figure 6.6

A', B'). The casein and HDL microparticles had areas with light grey color and darker shades (Figure 6.6 C',D'). Similar results were obtained with protein microparticles cross-linked through the use of Au^{3+} ions. However, no additional spherical nano-sized particles were observed due to the absence of AuNPs. These results show that the hollow and solid particle formation is not limited to the use of cross-linkers and it is expected that other cross-linking methods could also be used.

6.4 Summarizing main concluding remarks

We discussed that use of Au^{3+} ions provided a dual functionality to the design of protein-based materials, by initiating oxidation and subsequent cross-linking of proteins, and formation of AuNPs, embedded in the gel network. The Au^{3+} ions react rapidly with the proteins (seconds after addition), which allowed to construct protein-based materials at short time scales (minutes to 1 day). We used egg yolk HDL as a model protein, but we also showed that the cross-linking could be applied to other proteins (e.g. β-lac, BSA, and casein). Considering these advantages, the prospect for implementing Au^{3+} ions, or other metal ions, in the design of controlled gel networks is promising, especially after carrying out future work in follow-up projects.

We also showed that we can construct macrogels, microgels, and microparticles through the use of Au^{3+} ions. We did not only obtain spherical-shaped, solid protein-based materials, but we could also form hollow protein microparticles and branched, urchin-like microgels. As a next step, other (bio)polymers should be explored, which would open new perspectives to the formation of highly functional particles for a broad range of applications, such as hosting guest molecules, multimodal bio-imaging, nanoreactors for confined reactors, and many more.

References

1. I. Hammami and N.M. Alabdallah, Gold nanoparticles: Synthesis properties and applications, *Journal of King Saud University-Science*, 2021, **33**, 7, 101560.
2. I. Fratoddi, R. Matassa, L. Fontana, I. Venditti, G. Familiari, C. Battocchio, E. Magnano, S. Nappini, G. Leahu, and A. Belardini, Electronic properties of a functionalized noble metal nanoparticles covalent network, *The Journal of Physical Chemistry C*, 2017, **121**, 33, 18110-18119.
3. W. Zhang, S. Xiao, and D.U. Ahn, Protein oxidation: basic principles and implications for meat quality, *Critical reviews in food science and nutrition*, 2013, **53**, 11, 1191-1201.
4. C. Gabbiani, A. Casini, and L. Messori, Gold (III) compounds as anticancer drugs, *Gold Bulletin*, 2007, **40**, 1, 73-81.
5. A.I. Petrov, D.V. Volodkin, and G.B. Sukhorukov, Protein—calcium carbonate coprecipitation: a tool for protein encapsulation, *Biotechnology progress*, 2005, **21**, 3, 918-925.
6. A. Totosaus, J.G. Montejano, J.A. Salazar, and I. Guerrero, A review of physical and chemical protein-gel induction, *International journal of food science & technology*, 2002, **37**, 6, 589-601.
7. A. Clark, G. Kavanagh, and S. Ross-Murphy, Globular protein gelation—theory and experiment, *Food Hydrocolloids*, 2001, **15**, 4-6, 383-400.
8. K. Oda, New families of carboxyl peptidases: serine-carboxyl peptidases and glutamic peptidases, *The Journal of Biochemistry*, 2012, **151**, 1, 13-25.
9. M.-L. Bax, L. Aubry, C. Ferreira, J.-D. Daudin, P. Gatellier, D. Rémond, and V. Santé-Lhoutellier, Cooking temperature is a key determinant of in vitro meat protein digestion rate: investigation of underlying mechanisms, *Journal of agricultural and food chemistry*, 2012, **60**, 10, 2569-2576.
10. S. Wiezorek, P. Lamers, and C. Bolm, Conversion and degradation pathways of sulfoximines, *Chemical Society Reviews*, 2019, **48**, 21, 5408-5423.
11. K.J. Rodgers and N. Shiozawa, Misincorporation of amino acid analogues into proteins by biosynthesis, *The international journal of biochemistry & cell biology*, 2008, **40**, 8, 1452-1466.
12. M. Hellwig, The chemistry of protein oxidation in food, *Angewandte Chemie International Edition*, 2019, **58**, 47, 16742-16763.
13. D.V. Yakimchuk, V.D. Bundyukova, J. Ustarroz, H. Terryn, K. Baert, A.L. Kozlovskiy, M.V. Zdorovets, S.A. Khubezhov, A.V. Trukhanov, and S.V. Trukhanov, Morphology and microstructure evolution of gold nanostructures in the limited volume porous matrices, *Sensors*, 2020, **20**, 16, 4397.
14. J. Xie, Y. Zheng, and J.Y. Ying, Protein-directed synthesis of highly fluorescent gold nanoclusters, *Journal of the American Chemical Society*, 2009, **131**, 3, 888-889.
15. K. Chaudhari, P.L. Xavier, and T. Pradeep, Understanding the evolution of luminescent gold quantum clusters in protein templates, *ACS nano*, 2011, **5**, 11, 8816-8827.
16. J.-P. Sylvestre, S. Poulin, A.V. Kabashin, E. Sacher, M. Meunier, and J.H. Luong, Surface chemistry of gold nanoparticles produced by laser ablation in aqueous media, *The Journal of Physical Chemistry B*, 2004, **108**, 43, 16864-16869.
17. J. Turkevich, P.C. Stevenson, and J. Hillier, A study of the nucleation and growth processes in the synthesis of colloidal gold, *Discussions of the Faraday Society*, 1951, **11**, 55-75.
18. T. Maruyama, Y. Fujimoto, and T. Maekawa, Synthesis of gold nanoparticles using various amino acids, *Journal of colloid and interface science*, 2015, **447**, 254-257.
19. Z. Shervani and Y. Yamamoto, Carbohydrate-directed synthesis of silver and gold nanoparticles: effect of the structure of carbohydrates and reducing agents on the size and morphology of the composites, *Carbohydrate research*, 2011, **346**, 5, 651-658.
20. A. Sani, C. Cao, and D. Cui, Toxicity of gold nanoparticles (AuNPs): A review, *Biochemistry and biophysics reports*, 2021, **26**, 100991.
21. L. Su, T. Shu, J. Wang, Z. Zhang, and X. Zhang, Hidden dityrosine residues in protein-protected gold nanoclusters, *The Journal of Physical Chemistry C*, 2015, **119**, 21, 12065-12070.
22. N. Basu, R. Bhattacharya, and P. Mukherjee, Protein-mediated autoreduction of gold salts to gold nanoparticles, *Biomedical Materials*, 2008, **3**, 3, 034105.

23. J. Xie, J.Y. Lee, and D.I. Wang, Synthesis of single-crystalline gold nanoplates in aqueous solutions through biomineralization by serum albumin protein, *The Journal of Physical Chemistry C*, 2007, **111**, 28, 10226-10232.
24. Y.N. Tan, J.Y. Lee, and D.I. Wang, Aspartic acid synthesis of crystalline gold nanoplates, nanoribbons, and nanowires in aqueous solutions, *The Journal of Physical Chemistry C*, 2008, **112**, 14, 5463-5470.
25. V. Amendola, R. Pilot, M. Frasconi, O.M. Maragò, and M.A. Iatì, Surface plasmon resonance in gold nanoparticles: a review, *Journal of Physics: Condensed Matter*, 2017, **29**, 20, 203002.
26. H. Wei, Z. Wang, J. Zhang, S. House, Y.-G. Gao, L. Yang, H. Robinson, L.H. Tan, H. Xing, and C. Hou, Time-dependent, protein-directed growth of gold nanoparticles within a single crystal of lysozyme, *Nature nanotechnology*, 2011, **6**, 2, 93.
27. Y. Huang, A.R. Ferhan, Y. Gao, A. Dandapat, and D.-H. Kim, High-yield synthesis of triangular gold nanoplates with improved shape uniformity, tunable edge length and thickness, *Nanoscale*, 2014, **6**, 12, 6496-6500.
28. J. Xie, J.Y. Lee, D.I. Wang, and Y.P. Ting, Identification of active biomolecules in the high-yield synthesis of single-crystalline gold nanoplates in algal solutions, *small*, 2007, **3**, 4, 672-682.
29. J. Feng and H.C. Zeng, Size-controlled growth of Co3O4 nanocubes, *Chemistry of materials*, 2003, **15**, 14, 2829-2835.
30. H. Kawasaki, K. Hamaguchi, I. Osaka, and R. Arakawa, ph-Dependent synthesis of pepsin-mediated gold nanoclusters with blue green and red fluorescent emission, *Advanced Functional Materials*, 2011, **21**, 18, 3508-3515.
31. K. Midha, M. Nagpal, and S. Arora, Microspheres: a recent update, *Int. J. Recent. Sci. Res., l (8)*, 2015, 5859-67.
32. J. Sharma, D.A. Cullen, G. Polizos, K. Nawaz, H. Wang, N. Muralidharan, and D.B. Smith, Hybrid hollow silica particles: Synthesis and comparison of properties with pristine particles, *RSC Advances*, 2020, **10**, 38, 22331-22334.
33. W. Wichaita, D. Polpanich, and P. Tangboriboonrat, Review on synthesis of colloidal hollow particles and their applications, *Industrial & Engineering Chemistry Research*, 2019, **58**, 46, 20880-20901.
34. A. Cabot, M. Ibáñez, P. Guardia, and A.P. Alivisatos, Reaction regimes on the synthesis of hollow particles by the Kirkendall effect, *Journal of the American Chemical Society*, 2009, **131**, 32, 11326-11328.
35. S. Kharel, W.L. Lee, X.Y. Lee, and S.C.J. Loo, Osmogen-Mediated One-Step Technique of Fabricating Hollow Microparticles for Encapsulation and Delivery of Bioactive Molecules, *Macromolecular bioscience*, 2017, **17**, 4, 1600328.
36. D. Volodkin, A. Skirtach, and H. Möhwald, Bioapplications of light-sensitive polymer films and capsules assembled using the layer-by-layer technique, *Polymer international*, 2012, **61**, 5, 673-679.
37. M.J. Raaijmakers and N.E. Benes, Current trends in interfacial polymerization chemistry, *Progress in polymer science*, 2016, **63**, 86-142.
38. W. Ha, X.-W. Meng, Q. Li, M.-M. Fan, S.-L. Peng, L.-S. Ding, X. Tian, S. Zhang, and B.-J. Li, Self-assembly hollow nanosphere for enzyme encapsulation, *Soft Matter*, 2010, **6**, 7, 1405-1408.
39. M.G. Bah, H.M. Bilal, and J. Wang, Fabrication and application of complex microcapsules: A review, *Soft Matter*, 2020, **16**, 3, 570-590.
40. M. Chen, J. Lu, F. Liu, J. Nsor-Atindana, F. Xu, H.D. Goff, J. Ma, and F. Zhong, Study on the emulsifying stability and interfacial adsorption of pea proteins, *Food Hydrocolloids*, 2019, **88**, 247-255.
41. J.R. Wagner, D.A. Sorgentini, and M.C. Añón, Relation between solubility and surface hydrophobicity as an indicator of modifications during preparation processes of commercial and laboratory-prepared soy protein isolates, *Journal of Agricultural and Food Chemistry*, 2000, **48**, 8, 3159-3165.
42. C.E. Gumus, E.A. Decker, and D.J. McClements, Formation and stability of ω-3 oil emulsion-based delivery systems using plant proteins as emulsifiers: Lentil, pea, and faba bean proteins, *Food Biophysics*, 2017, **12**, 2, 186-197.

43. Y. Dong, T. Lan, X. Wang, Y. Zhang, L. Jiang, and X. Sui, Preparation and characterization of soy protein microspheres using amorphous calcium carbonate cores, *Food Hydrocolloids*, 2020, **107**, 105953.
44. H. Yang, Y. Yang, B.-Z. Li, B. Adhikari, Y. Wang, H.-L. Huang, and D. Chen, Production of protein-loaded starch microspheres using water-in-water emulsion method, *Carbohydrate polymers*, 2020, **231**, 115692.
45. D. Zhong-Min, Y. Yan-Ping, M. ZHANG, L. Wen-Yang, Y. Su-Hui, C. Rui-Guo, and W. Zhen-Lin, Distribution of starch granule size in grains of wheat grown under irrigated and rainfed conditions, *Acta Agronomica Sinica*, 2008, **34**, 5, 795-802.
46. W. Wei, G.-H. Ma, G. Hu, D. Yu, T. Mcleish, Z.-G. Su, and Z.-Y. Shen, Preparation of hierarchical hollow CaCO3 particles and the application as anticancer drug carrier, *Journal of the American Chemical Society*, 2008, **130**, 47, 15808-15810.
47. T. Lazarević, A. Rilak, and Ž.D. Bugarčić, Platinum, palladium, gold and ruthenium complexes as anticancer agents: Current clinical uses, cytotoxicity studies and future perspectives, *European journal of medicinal chemistry*, 2017, **142**, 8-31.
48. S. Medici, M. Peana, V.M. Nurchi, J.I. Lachowicz, G. Crisponi, and M.A. Zoroddu, Noble metals in medicine: Latest advances, *Coordination Chemistry Reviews*, 2015, **284**, 329-350.
49. M.S. Akhtar, J. Panwar, and Y.-S. Yun, Biogenic synthesis of metallic nanoparticles by plant extracts, *ACS Sustainable Chemistry & Engineering*, 2013, **1**, 6, 591-602.
50. J.J. Pignatello, E. Oliveros, and A. MacKay, Advanced oxidation processes for organic contaminant destruction based on the Fenton reaction and related chemistry, *Critical reviews in environmental science and technology*, 2006, **36**, 1, 1-84.
51. M. Lund and C. Baron, *Protein oxidation in foods and food quality*, in *Chemical deterioration and physical instability of food and beverages*. 2010, Elsevier. p. 33-69.
52. Y.L. Xiong and A. Guo, Animal and plant protein oxidation: Chemical and functional property significance, *Foods*, 2020, **10**, 1, 40.
53. B. Morgan and O. Lahav, The effect of pH on the kinetics of spontaneous Fe (II) oxidation by O2 in aqueous solution–basic principles and a simple heuristic description, *Chemosphere*, 2007, **68**, 11, 2080-2084.
54. X. Tang and J.E. Bruce, *Chemical cross-linking for protein–protein interaction studies*, in *Mass Spectrometry of Proteins and Peptides*. 2009, Springer. p. 283-293.
55. I. Migneault, C. Dartiguenave, M.J. Bertrand, and K.C. Waldron, Glutaraldehyde: behavior in aqueous solution, reaction with proteins, and application to enzyme crosslinking, *Biotechniques*, 2004, **37**, 5, 790-802.

Summary

Chapter 1 provides the general introduction and outline of this thesis. In this chapter, we discuss the use of proteins for constructing protein-based materials. Proteins are biopolymers with a complex three-dimensional structure and consist of amino acids as monomeric units. The sequence of amino acids (especially their functional residual groups) and the ordered protein structure can be used as building blocks for assembling protein-based materials. Combining templates and cross-linking allows to control the assembly of proteins into their final structure.

This thesis was focused on:

- Using Au^{3+} ions for cross-linking proteins, through oxidation
- Constructing hollow and solid protein microparticles through the use of solid, $CaCO_3$ templates
- Constructing spherical and urchin-like microgels inside fully aqueous droplet reactors

In **Chapter 2**, an alternative methodology for cross-linking proteins through Au^{3+} initiated oxidation is presented. Currently, proteins are cross-linked through changing environmental conditions (e.g. temperature, pH, ionic strength) or using enzymatic or chemical cross-linking agents. Proteins can also be cross-linked through oxidation, which can be initiated by reactive oxygen species, radicals, radiation, or metal ions. However, protein cross-linking through oxidation is much less studied and the mechanisms are only partly elucidated. Therefore, we investigated the interactions of Au^{3+} ions with amino acids, and used it to create covalent bonds between proteins (egg yolk high-density lipoprotein) in an aqueous dispersion. Adding $\geq$ 150 molar equivalents of Au^{3+} to HDL resulted in the formation of a gel network, while lower amounts only formed protein aggregates. The gel networks did not only form at room temperature, but also at 4 °C. Additionally, at higher temperatures (T = 40-80 °C), the time for gel network formation was decreased to less than 15 minutes. The gel network formation was revealed by vial tilting method, rheology, optical density measurements, and confocal laser scanning microscopy (CLSM) imaging. The interactions between Au^{3+} ions and amino acids were further characterized by Fourier-Transform Infrared Spectroscopy (FTIR), gel electrophoresis, and fluorescence spectroscopy, showing that disulfide bonds and dityrosine cross-links were formed. Next to the formation of gel networks, the soft material obtained a red color. By using UV-Vis absorbance and TEM, we confirmed that the red color was derived from the formation of gold nanoparticles (AuNPs). Using Au^{3+} ions for covalently cross-linking proteins and formation of gel networks may contribute to the design and construction of novel protein-based materials.

In **Chapter 3**, cross-linking proteins through the use of Au^{3+} ions was combined with $CaCO_3$ templates to construct protein microparticles. $CaCO_3$ templates were synthesized by direct mixing of equimolar $CaCl_2$ and Na_2CO_3 solutions to initiate precipitation at supersaturation. HDL was encapsulated into the $CaCO_3$ templates by capturing the proteins during $CaCO_3$ synthesis. The obtained HDL/$CaCO_3$ complexes are spherical and have sizes of around 5 µm. HDLs interact in the pores of the $CaCO_3$ template through hydrophobic forces and are predominantly concentrated at the edges of the template. After template removal, the spherical structure of the template and the protein distribution were conserved. However, the protein microparticles collapse under dry conditions. Additionally, the particles were not stable against pH, in terms of aggregation. The hydrophobic forces were not enough to sustain the structure of the hollow protein microparticles. To enhance the rigidity of the hollow

protein microparticles, Au^{3+} ions were added to the HDL/$CaCO_3$ complexes, before template removal. The Au^{3+} ions form covalent cross-links between amino acids, such as cysteine and tyrosine, which stabilizes the spherical structure of the protein microparticles. Additionally, amino acids, such as tryptophan and aspartic acid, act as reduction sites of Au^{3+} ions and synthesize AuNPs. After cross-linking and template formation, the protein distributions were conserved. Under dry conditions, the protein microparticles were flattened, but contained folds and creases structures. When under different pH conditions, the protein microparticles did not show aggregation. The AuNPs were observed at the protein surface of the protein microparticles. The design of the stable hollow protein microparticles, through the use of Au^{3+} ions, opens new avenues for constructing hollow particles in simple steps, using biobased molecules. Additionally, the presence of AuNPs, embedded on the protein particle surface, allows new possibilities for carrying functional molecules and multimodal imaging.

In **Chapter 4**, we constructed solid and hollow protein microparticles by using proteins with a different tendency to aggregate in an aqueous environment and their subsequent reduced solubility inside $CaCO_3$ templates. The protein microparticles were fabricated by encapsulation through co-precipitation and cross-linking by using Au^{3+} ions. β-lactoglobulin (β-lac) and Bovine Serum Albumin (BSA) are approximately 7 nm in size and fit inside the 20-60 nm pore sizes of the $CaCO_3$ templates. Synthesizing $CaCO_3$ templates in presence of β-lac or BSA resulted in the formation of spherical protein/$CaCO_3$ complexes with a smooth surface and uniform protein distribution inside the templates. Caseins and HDL form large aggregates (30-5000 nm) during the $CaCO_3$ synthesis, due to the interactions between Ca^{2+} and phosphoserine amino acids. The protein/$CaCO_3$ complexes, by using casein or HDL, have a rough surface and the proteins are accumulated at the template edges. Protein microparticles were then obtained after cross-linking the proteins, using Au^{3+} ions, and template removal. The protein microparticles formed of β-lac or BSA conserved their uniform protein distribution and were solid-like. Under dry conditions, the particles appeared dense and spherical. Protein microparticles formed of caseins or HDL also conserved their protein distribution and were hollow-like. Due to their hollow core, the particles flattened and had a wrinkled structure under dry conditions. Finally, the protein microparticles had spherical, nano-sized particles present on their surfaces. By using SEM-EDX, it was found that those particles were not carbon-based, but based on gold. The AuNPs were formed by Au^{3+} reduction by protein amino acids and were spread over the protein microparticle surfaces. The method suggested for the formation of solid and hollow protein microparticles, based on the sizes of the protein aggregates, opens new paths on the design of biocompatible, functional particles. The protein microparticles can find applications as carriers of therapeutics or imaging agents, while the embedded AuNPs provides an attractive platform as multimodal imaging agent.

In **Chapter 5**, cross-linking proteins through the use of Au^{3+} ions was applied to proteins compartmentalized in a fully aqueous droplet reactor (FADR) to construct protein microgels. FADRs are composed of transient aqueous two-phase systems (ATPS), of which one aqueous phase is dispersed into the other aqueous phase. HDL was compartmentalized in an ATPS of Na_2SO_4 as droplet phase and polyethylene glycol (PEG) as continuous phase. The FADRs were prepared at different concentrations of HDL (5-40 mg/mL) and pH values (5-7). At pH 5, close to the point of zero charge,

HDL formed aggregates in the droplet phase, while at pH 7-9, HDL was evenly confined and homogeneously distributed. Au^{3+} ions were then added as an aqueous solution to the FADRs to cross-link the proteins and obtain microgels. The shapes of the microgels were affected by reaction conditions of the FADRs. At low HDL concentration, and low pH, random aggregates were obtained. The proteins already formed aggregates at pH 5, which hindered the formation of a stable protein gel network. Additionally, when the protein concentrations are too low, no stable gel network could be formed. At medium HDL concentration, and medium pH, the addition of the aqueous Au^{3+} ions solution creates a concentration gradient in the FADR. After reaching a new equilibrium, HDL and water diffuse from the droplets to the PEG-rich phase, as branches, while getting cross-linked through the Au^{3+} ions. At high HDL concentration, high pH, the FADR was stable against the addition of the aqueous Au^{3+} ions solution, and spherical microgels were obtained. The use of FADRs for microgel preparation can be used and implemented for generating biocompatible spherical and urchin-like structures, which may find applications different fields, such as catalysis, optical switches, or sensors.

Chapter 6 provides a general discussion on the most important experimental outcomes of this thesis and shows some results of other additional experiments. An outlook and suggestions for future research are provided, ending with a general conclusion.

Acknowledgements

And that's it, these last few pages will mark the end of this thesis. It was a moving era, in which I dealt with ups and downs, but mostly I learned a lot as a scientist and as a person. Along the way, I was accompanied by many different people, which were very important to me and -directly and indirectly- helped and motivated me to finalize the thesis.

First, I would like to thank my supervisors, and I would like to start with **Aldrik Velders**. Our journey actually didn't start at the beginning of the PhD, but already in 2015. I followed the minor and did both my BSc and MSc thesis at the BioNanoTechnology (BNT) group. Even though I was already known as the "sticky gum" of BNT, you wanted me to grow further as a scientist and suggested me this PhD project. Thank you for all our discussions and pushing me to the limits. Our ways now will finally (finely) part, but my heart will stay in nanotechnology. **Costas Nikiforidis**, you were my daily supervisor and we started on a completely different topic for the PhD. On the way, we found that the topic did not work as expected and we came up with a new topic, which is now described in this thesis. I really enjoyed our bi-weekly meetings, where you were always able to calm me down and inspired me to continue. I will remember the "chaos" and try to improve it for the next steps in my future career. Thank you so much for supporting me during this PhD project, the many meetings, flexibility and creativity. **Harry Bitter**, thank you for welcoming me in the Biobased Chemistry & Technology (BCT) group and pushing me to look at the broader picture of my research. I will always keep the "facts for fiction" in my mind. But mostly, thank you for sharing your fancy dinner experiences, I still need to finish the list. Hallo **Vittorio Saggiomo**, how are you? You were playing many different roles in my PhD project: you provided me chocolate when needed, we had many coffees together, we were temporarily office buddies, we shared interests in Harry Potter and Scrubs. I really admire your creativity in the lab, and I will definitely miss your personality around. After all this time, I am leaving BNT, always.

My project was part of different (sub)groups, which all played an important role for my PhD.

The Biobased Soft Materials group (BioSoM):

Even though my topic was not connected to oleosomes and plant proteins, I really enjoyed the discussion during the BioSoM meetings and the trip to Strasbourg. But overall, thank you for discussing mostly about the Bettersizer. **Eleni Ntone** and **Simha Sridharan**, we started our PhD together with at BCT and I really enjoyed spending time with you. I would like to thank you for your help in the lab, with the CLSM and AFM, and the fruitful discussions. **Umay Vardar-Kule**, you joined us one year later and I enjoyed listening to your stories and experiences. Thank you for the small plants you gave me. **Mingzhao Han** and **Zhaoxiang Ma**, I had a lot of fun with you in the lab and during the trip in Strasbourg. **Kübra Ayan**, thank you for your kindness and interest in my protein particles project. **Lorenz Plankensteiner**, thank you for suggesting me to buy a carrot (which I did not) and sharing your

extraordinary passion for oleosomes. I hope you will meet the nestle guy soon again. **Jack Yang**, thank you for being my office mate. You were always there to cheer me up after meetings and you were very useful during the final steps. And the former member, **Christos Fryganas**, thank you for your discussions and the beers and dinner we had together.

Biobased Chemistry and Technology:

Elinor Scott, thank you for always warning us when the coffee/tea/lemonade or lunch breaks were starting. I liked our conversations during those breaks, ranging from scientific brainstorms to inappropriate jokes. **Akbar Asadi Tashvigh**, thank you that "the next time wasn't me" and for having us for dinner. **Tomas van Haasterecht**, **Guanna Li**, **Lars Kiewit** thank you for the conversations during the breaks. **Nazila Masoud**, thank you for your kindness and interests, but mostly for your suggestion to add the gold ions directly to the proteins. Without you, I would not have made this shift in the PhD research.

Marlene Führer, **Cynthia Klostermann**, **Sanne de Smit**, thank you for organizing many events at and outside BCT, without you the group would not have been the same. **Dmitry Pirgach**, thank you for being my chemistry lab buddy and organizing the BCT Christmas online activity together. My former office mates **Xinhua Windt** and **Gerben Wierda**, thank you for the support and taking care of my plants. **Roxani Chatzipanagiotou**, **Matthijs van der Ham**, **Tim Hoogstad**, **Frits van der Klis**, **Roel Bisselink**,**Tunan Gao**, **Raghavendra Meena**, **Ivo van Luijk**, **Torin de Groot**, **Freek Karacoban**, **Xiaojie Qin**, thank you for the discussions during the PhD meetings and having beers together.

BioNanoTechnology:

Julia Krug, **Namita Sharma**, **Tatiana Nikolaeva**, **Fatemeh Azadi Chegeni**, **Merlin Cotessat** thank you for the conversations during the breaks. Olaaa **Anton Bunschoten**, thank you for arranging everything in the labs and organizing food and activities for the group. I really liked our discussions during the MSc thesis and it was a shame you were not that involved in my PhD project anymore. Hallo **Sander**(s) **Baas**, thank you for arranging the coffee at BNT. **Rebecca Kaup**, thank you for welcoming me temporarily in the dendrimers and micelles sub-group. **Keqing Hu**, thank you for our collaboration and your kindness, I wish you all the best with finalizing the project. **Yurdanur Yilmaz** and **Zahra Mohammadi**, my apologies for bothering you every time I had discussions with Keqing in your office. It was nice to see you enjoyed your time together. And former members: **Jan Bart ten Hove**, you started as my BSc thesis supervisor, you were my office mate during my MSc thesis, and we published my first paper together during my PhD. I also had the honor to be your paranymph during your PhD defense and to enjoy your "bachelor party" when you left the BNT group. Thank you for teaching me and all the fun we had together. **Koen Martens**, thank you for sharing your knowledge about microscopes and the conversations. **Camilla Facciotti**, thank you for arranging my MSc internship at your former university in Verona. I really had a great time over there and this would not have happened without you. **Ashkan Madadlou**, thank you for your inspiration for constructing protein microparticles and the collaboration with Keqing's project.

In particular I would like to thank the people who were involved in the background: **Daniëlle Bollebakker**, **Banu van Moerkerk**, **Gerda Bos**, thank you for arranging all the administrative tasks and scheduling meetings. **Susan Witte**, **Nadine Dieterman**, **Annemarie Hage,** the muses of the BCT lab, thank you for making sure that the chemicals were available, the lab equipment was working properly, and that the labs were extraordinary clean and tidy.

I would also like to thank the BSc and MSc thesis students, which were around in the BCT or BNT group. It was very inspiring for me to see you working passionately on your projects. **Laurine Yoe, Patrick Kreft**, thank you for providing me insides in small parts of my research. **Daniël Klaassen**, thank you for your enthusiasm during your thesis, it was very nice having you around. **Tamara Fikke**, thank you for being such an enthusiastic thesis student. I really enjoyed our time together and after that we also became good friends. **Thomas Vogelaar**, thank you for your help with the third chapter of this thesis, which we published together. I learned a lot from our collaboration. I would like to wish all of my thesis students the best of luck in their future career.

Next to Wageningen University, I was allowed to spend some time of my research at the Nanomaterials Research Group, Verona University. I would like to thank **Adolfo Speghini** for arranging this collaboration and the fruitful discussions and **Giacomo Lucchini** and **Lorenzo Rolla** for their support in the lab.

During the PhD, I joined the OBK Bennekom harmony orchestra, in which I played the clarinet. I would like to thank the clarinettists for improving my skills. I would like to thank the conductor for his calm attitude and patience. But most of all, I would like to thank **Kim**, **Timo**, **Vincent**, **Hans** (2x), **Erik**, **Jan**, the three musketeers: **Dick**, **Jan** and **Jan Willem**, the other people from the drum band for the beers and conversations.

Next, I would like to thank my family. **Frank Schijven**, you were always my inspiration and you pushed me into this career, thank you for always believing in me. **Diana Schijven**, thank you for always supporting me with good conversations or distractions, like shopping. **René Schijven**, even though you like to tease your little sister, I am happy that you are always proud of me. Please know that I am proud of you too! And my family-in-law, **Guido Willems**, **Lucie Pashuyzen**, **Nathalie Willems**, **Eve Lake**, **Katrien Willems**, thank you for spending the weekends, celebrations and holidays together. In addition, I would like to thank you for all the discussions we had during these times, sometimes it is good to refresh your memory about the carbon cycle and inefficient solar cells.

And last, but definitely not least, my friend, supervisor, colleague, boyfriend, fiancé, husband-to-be **Stan Willems**. You were definitely the most important part for my PhD. Without you, I would not have been able to finish this. Before I started the PhD, you supported me to do a PhD, but when I started you had to deal with all my frustrations. I am happy this also resulted in a published paper we worked on together. Thank you for your support, advice, endless patience, love and care. I am looking forward to our next adventures as a married couple.

About the Author

Laura Maria Irene was born on January 10th 1994 in Roosendaal & Nispen, the Netherlands. She obtained her Gymnasium diploma in Nature & Health in 2012 at Gertrudis college, Roosendaal. She then moved to Wageningen and started her Bachelor of Science in Molecular Life Sciences at Wageningen University in 2012. She obtained her bachelor's degree in 2015, for which she completed a BSc thesis in the BioNanoTechnology group under the supervision of Dr J.B. ten Hove, Dr J. Wang, and Prof. Dr A.H. Velders, working on the synthesis of gold nanoparticles. She then obtained her master's degree in Molecular Life Sciences at Wageningen University in 2017, with a specialization in Physical Chemistry. She completed her MSc thesis in the BioNanoTechnology group under the supervision of Dr S.B.J. Willems, Dr A. Bunschoten, and Prof. Dr A.H. Velders, where she worked on immobilizing bacterial cells on nickel-NTA glass surfaces. For her master's internship, she did research at the Nanomaterials Research Group at Verona University in lanthanide-based upconversion metal-organic frameworks under the supervision of Prof. Dr A. Speghini and Dr G. Lucchini. After obtaining her MSc degree, she joined Biobased Chemistry and Technology and BioNanoTechnology, Wageningen University, to work on her PhD project. Her PhD work was carried out under the supervision of Dr C.V. Nikiforidis, Dr V. Saggiomo, Prof. Dr A.H. Velders and Prof. Dr J.H. Bitter. The results of her PhD work are presented in this thesis. From September 2022, she will be working as a chemist in nanomedicines at Ardena, Oss.

List of Publications

This thesis

L.M.I. Schijven, V. Saggiomo, A.H. Velders, J.H. Bitter, & C.V. Nikiforidis. (2021). Au 3+-Induced gel network formation of proteins. *Soft Matter*, *17*(42), 9682-9688.

L.M.I. Schijven, T.D. Vogelaar, S. Sridharan, V. Saggiomo, A.H. Velders, J.H. Bitter, & C.V. Nikiforidis. (2022). Hollow protein microparticles formed through cross-linking by an Au 3+ initiated redox reaction. *Journal of Materials Chemistry B*, 10, 6267-6295.

L.M.I. Schijven, V. Saggiomo, A.H. Velders, J.H. Bitter, & C.V. Nikiforidis. (2022). On the influence of protein aggregate sizes for the formation of solid and hollow protein microparticles. *Submitted.*

L.M.I. Schijven,[*] K. Hu,[*] A. Madadlou, V. Fogliano, J.H. Bitter, C.V. Nikiforidis, A.H. Velders, & V. Saggiomo. Formation of protein microgels with spherical and urchin-like shapes within a fully aqueous droplet reactor. *In preparation.*

Other publications

J.B. Ten Hove,[*] **L.M.I. Schijven**,[*] J. Wang, & A.H. Velders. (2018). Size-controlled and water-soluble gold nanoparticles using UV-induced ligand exchange and phase transfer. *Chemical communications*, *54*(95), 13355-13358.

S.B.J. Willems, **L.M.I. Schijven**, A. Bunschoten, F.W.B. van Leeuwen, A.H. Velders, & V. Saggiomo. (2019). Covalently bound monolayer patterns obtained by plasma etching on glass surfaces. *Chemical Communications*, *55*(53), 7667-7670.

[*] The authors have contributed equally to this work and share first authorship

Overview of completed training activities

Discipline specific activities		
NWO CHAINS conference	NWO, Veldhoven, the Netherlands	2017
Basic TEM operation	WEMC, Wageningen, the Netherlands	2017
1st international conference on oil bodies	WUR, Wageningen, the Netherlands	2018
Food proteins: functionality, modifications and analysis	VLAG, Wageningen, the Netherlands	2018
NWO CHAINS conference[1]	NWO, Veldhoven, the Netherlands	2018
Nanomedicine 2019	Nanomib, Milano, Italy	2019
COOPERINT exchange project	Verona University, Verona, Italy	2019
NWO CHAINS conference	NWO, Veldhoven, the Netherlands	2019
NWO CHAINS conference	NWO, online	2020
2nd international conference on lipid droplets & oleosomes[1]	WUR/IBMP, Strasbourg, France	2021
General courses		
VLAG PhD week	VLAG, Baarlo, the Netherlands	2017
Scientific Artwork – Vector graphics + images	WUR, Wageningen, the Netherlands	2018
Scientific writing	WGS, Wageningen, the Netherlands	2018
Presenting with impact	WGS, Wageningen, the Netherlands	2018
Career Perspectives	WGS, Wageningen, the Netherlands	2021
Other activities		
Preparation of research proposal	Wageningen, the Netherlands	2017
PhD study tour[2]	Copenhagen, Lund, Aarhus, Denmark and Sweden	2018
BCT weekly group meetings	Wageningen, the Netherlands	2017-2022
BNT weekly group meetings	Wageningen, the Netherlands	2017-2022

[1] poster presentation, [2] oral presentation

The research described in this thesis was financially supported by the Graduate School VLAG (Advanced studies in Food Technology, Agrobiotechnology, Nutrition and Health Sciences), the Netherlands.

Financial support from Wageningen University for printing this thesis is gratefully acknowledged.

Cover design by the author

Printed by ProefschriftMaken on FSC-certified paper